Enhanced Multicarrier Techniques for Professional Ad-Hoc and Cell-Based Communications

(EMPhAtiC)

Document Number D3.2

Adaptive equalization and Successive self-Interference Cancellation (SIC) methods

Contractual date of delivery to the CEC:	28/02/2014
Actual date of delivery to the CEC:	12/05/2014
Project Number and Acronym:	318362 EMPhAtiC
Editor:	Slobodan Nedic (UNS)
Authors:	Slobodan Nedic (UNS), Sladjana Jošilo (UNS), Vladimir Stanivuk (UNS), Milan Narandzic (UNS), Markku Renfors (TUT), Juha Yli-Kaakinen (TUT), Eleftherios Kofidis (CTI), Antonis Beikos (CTI), Rostom Zakaria (CNAM)
Participants:	UNS, TUT, CTI, CNAM
Workpackage:	WP3
Security:	Public (PU)
Nature:	Report
Version:	1.1
Total Number of Pages:	91

Abstract:

Interference reduction for FBMC/OQAM waveforms is addressed in the context of Widely Linear Filtering (WLF) MMSE estimation-based per-subchannel equalization, by taking the input correlation matrix pertaining to the kindred co-channel interference into account. Furthermore, several adaptive multi-tap configurations are developed and evaluated for both frequency-selective and time-variant subchannel transfer functions, in particular considering the sparseness of the overall channel impulse response and devoting special attention to the PMR environment in the interference free scenarios. In addition to the channel estimation methods reported in D3.1, this deliverable elaborates a specific form

of channel estimation that relies on direct utilization of a pair of (real-valued) pilots, as an alternative to using auxiliary pilots for controlling the intrinsic interference.

Based on the real-domain FBMC/OQAM orthogonality conditions, a real-domain successive interference cancellation (SIC) framework is proposed and an attempt is bmade to take advantage of the redundant information contained in the received signal quadrature. Furthermore, due to the fact that the received noise samples at T/2 separation are correlated in the complex domain, the block-wise processing nature of the SIC approach is used to perform a suitable noise prediction and cancellation.

This deliverable also contains progress in carrier synchronization incorporated within the FC-FB framework, thus supplementing the symbol-synchronization and “per sub-bin” one-tap equalization considered and reported within the deliverable D3.1.

Keywords: Channel equalization, channel estimation, CFO, CP, DFE, FBMC, FMT, interference, IPNLMS , LMS, NLMS, NPC, OQAM, OFDM, pilots, preamble, PMR, TEDS, WLF

Document Revision History

Version	Date	Author	Summary of main changes
0.1	01.10.2014	Slobodan Nedic	Initial structure of the document
0.2	06.03.2014	Eleftherios Kofidis	Incorporation of the CTI's contribution (Chapter 4 Adaptive Equalization of Doubly Dispersive Channels)
0.3	17.03.2014	Juha Yli-Kaakinen	Added 8th chapter "Progress with the unified frequency-domain synchronization concept"
0.4	22.03.2014	Eleftherios Kofidis	Inclusion of some results in Chapter 3
0.5	28.03.2014	Rostom Zakaria	Added 5th chapter "Channel Estimation"
0.6	29.03.2014	Milan Narandžić	Merging of contributions and cross-referencing
0.7	05.4.2014	Slobodan Nedic	Abstract, introduction and conclusion
0.8	15.4.2014	Juha Yli-Kaakinen	Some minor corrections and suggestions
0.9	16.04.2014	Eleftherios Kofidis	Corrections and suggestions throughout
1.0	24.04.2014	Milan Narandžić	Integration of corrections from different document versions. Fixing of cross-referencing and formatting
1.1	25.04.2014	Slobodan Nedić	Rewriting of abstract and other changes, including the Conclusion in the WLF part.

Table of Contents

1. Introduction

Compensation of linear distortions introduced in the subchannels of an FBMC/OQAM signal by wireless channel was the first challenge towards making it competitive to the traditional CP-OFDM multicarrier waveform. This and related problems are studied in this deliverable. Both (strictly) linear and decision-feedback equalization, (S)LE and DFE, structures will be introduced, based on the intrinsic quasi-complex T/2-spaced PAM signaling in FBMC/OQAM and the effective restoration of the system's orthogonality through the inversion of the channel transfer function within the bandwidth of a particular subchannel.

A large part of this document is devoted to applying the in recently actualized widely linear filtering (WLF) framework in FBMC/OQAM equalization. This has brought to the forefront the inherent robustness of the staggered formats against kindred co-channel interference. It has turned out that if the co-channel interference is properly accounted for through its correlation and (in complex-domain formulation) pseudo-correlation matrices, the per-channel equalizer becomes - to a certain extent - able to suppress the interferer's impact simultaneously with the compensation of the useful signal's linear distortions. These results may have important implications on the selection of the mostly suitable form of FBMC-like waveforms.

Of a great practical interest is also to be able to compensate for linear distortions for doubly dispersive channels, that is, channels exhibiting both time- and frequency-selectivity. The aim of Chapter 4 is to provide a concise picture of the adaptive equalization problem in such scenarios. This contribution is split into three parts. First, the possible gains from using a diversity enhancing precoder at the transmitter are evaluated. As an example, a Walsh-Hadamard transformation (WHT) is tested, in view of its proven success in OFDM systems and the low additional computational cost it entails. The second part is concerned with channel estimate-based design of the equalizers and relies on pilot-assisted channel tracking to deal with the fast fading nature of the channel. The role of the scattered pilots, designed to follow an LTE format while also taking the intrinsic interference into account, is made apparent in this part. Finally, adaptive algorithms for *direct* per-subcarrier equalization are evaluated in the third part of this chapter. Here, the sparse structure that the subchannel responses often exhibit is exploited through the application of a computationally efficient yet highly performing adaptive algorithm, designed so as to speed up the adaptation of equalizer filters that are themselves of a sparse nature.

This deliverable covers also pilot-based channel estimation method, which alleviates the problem of intrinsic interference, and is applicable in channels of low frequency selectivity. This comes in contrast to earlier methods that rely on the auxiliary pilot idea and has important relative advantages over those. Chapter 5 is devoted to this problem. First, the general Maximum Likelihood (ML) estimator is derived, disregarding the complexity issue. The study starts from calculating the Cramer-Rao lower bound of the optimal estimator, over the various forms of estimator optimizations, and goes on with developing the estimator the under assumption of a Gauss distributed interference.

In the realm of the nonlinear data (symbols) detection approaches, such as the maximum likelihood sequence estimation (MLSE) and the maximization of a-posteriori (MAP) (MAP), the I/Q staggered nature of the FBMC/OQAM type of signaling waveforms offers the

possibility of purely real-domain processing in the successive interference cancellation (SIC) sense. Together with estimated real-valued subchannels' impulse responses, this contributes to a potential reduction in the implementation complexity beyond the mere use of two instead of four real multiplications per QAM data symbol interval. MLSE, in combination with the minimum mean squared error (MMSE) estimation, is elaborated in the EMPhAtiC deliverable D4.1 in the MIMO context. In the present deliverable, only the MAP approach in the context of the successive self-interference cancellation is exposed. In addition to that, since the noise samples on in-phase (I) and quadrature (Q) components of subchannel outputs are independent, the apparent possibility to effectuate some inherent 'noise-diversity' gain by independently processing the two components with the corresponding SIC method and with their outputs properly combined is investigated in Chapter 6. On the other hand, since the subchannel noise is correlated (in the complex-domain) and the SIC operated at the level of an entire block (frame) of received samples, it is temptous to include the prediction and cancellation of the noise samples without any causality constraint, both in MLSE and in the SIC framework, and this is evaluated in Chapter 7 of this report.

Besides the symbols synchronization and subchannel equalization embedment within the fast convolution filter bank (FC-FB) framework, which was reported within the deliverable D3.1, one of the main targets of the synchronization studies under EMPhAtiC WP3 is to move the time and frequency synchronization functions from the time-domain processing side to frequency domain, to be implemented through subcarrier processing. The related method and its versatility have been elaborated on in Chapter 8.

Chapter 1 provides the FBMC/OQAM transceiver and transmission channel system models to be used throughout the document. Finally, a summary of the main conclusions of this report as a whole is provided in Chapter 9.

2. The adopted transmission scheme

2.1 System model

The block diagram of a linear, time invariant FBMC transceiver is shown in Fig. 2.1. It comprises the following stages: input QAM data stream de-multiplexing (serial-to-parallel conversion), I/Q staggering, transmit synthesis filter bank (SFB), transmission channel, AWGN source, receiver analysis filter-bank (AFB), detector, I/Q de-staggering, and de-multiplexing (parallel-to-serial) conversion – not shown. In this section, the corresponding overall transmission system model is introduced, with representations in complex- and real-valued domains.

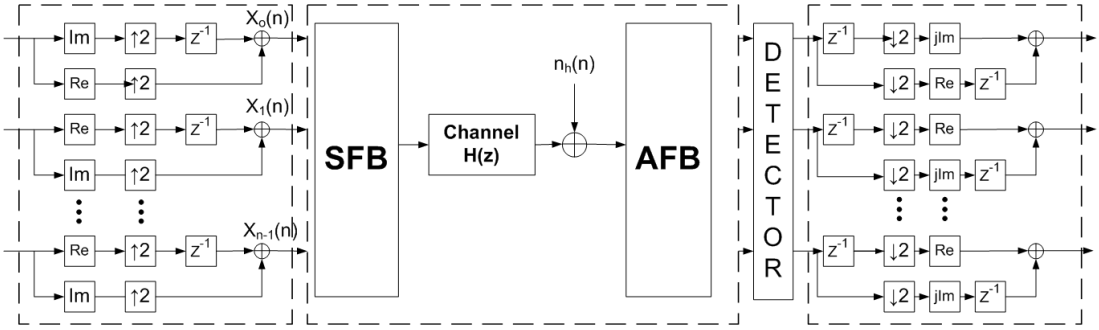

Fig. 2.1 MIMO representation of the FBMC/OQAM configuration.

In this system, at the transmitter side, the discrete-time FBMC/OQAM signal is written as follows

$$s[n] = \sum_{k=0}^{M-1} \sum_{m \in Z} d_{k,m} g[n - mM/2] e^{j\frac{2\pi}{M}k(m-\frac{D}{2})} e^{j\varphi_{k,m}} \quad (2.1)$$

where M is the (even) number of subcarriers, $g[n]$ is the prototype filter impulse response (taking real values), and $\frac{D}{2}$ is the delay term, which depends on the length (L_g) of $g[n]$. We have $D = KM - 1$ and $L_g = KM$, where K is the overlapping factor. The transmitted symbols $d_{k,m}$ are real-valued symbols corresponding to the real or the imaginary parts of the QAM symbols. The additional phase term is given by

$$\varphi_{k,m} = \frac{\pi}{2}(m+k) - \pi mk \quad (2.2)$$

We can rewrite (2.1) in a simple manner as

$$s[n] = \sum_{k=0}^{M-1} \sum_{m \in Z} d_{k,m} g_{k,m}[n] \tag{2.3}$$

where $g_{k,m}[n]$ are the shifted versions of $g[n]$ in time and frequency, the form of which can be infered from (2.1). In the absence of channel-induced linear distortions, the demodulated symbol over the k' th subcarrier and the n' th instant, with conveniently changed indexes, is determined using the inner product of $s[m]$ and $g_{k',n'}[m]$:

$$r_{k',n'} = \left\langle s, g_{k',n'} \right\rangle = \sum_{m=-\infty}^{+\infty} s[m] g^{*}_{k',n'}[m] = \sum_{m=-\infty}^{+\infty} \sum_{k=0}^{M-1} \sum_{n \in Z} d_{k,n} g_{k,n}[m] g^{*}_{k',n'}[m], \tag{2.4}$$

The trans-multiplexer impulse response can be derived assuming null data except at one time-frequency position (k_0, n_0), where a unit impulse is applied. Then, the equation above becomes

$$\begin{aligned} r_{k',n'} &= \sum_{m=-\infty}^{+\infty} g_{k_0,n_0}[m] g^{*}_{k',n'}[m] \\ &= \sum_{m=-\infty}^{+\infty} g[m] g[m - \Delta n M/2] e^{j\frac{2\pi}{M}\Delta k(\frac{D}{2}-m)} e^{j\pi(\Delta k + k_0)\Delta n} e^{-j\frac{\pi}{2}(\Delta k + \Delta n)}, \end{aligned} \tag{2.5}$$

where $\Delta n = n' - n_0$ and $\Delta k = k' - k_0$. We notice that the impulse response of the transmultiplexer depends on k_0. Indeed, the sign of some impulse response coefficients depends on the parity of k_0. Various pulse shaping prototype filters $g[m]$ of essentially Nyquist square root raised-cosine designs can be used according to their properties. In this document, we consider the pulse shape referred to as the PHYDYAS prototype filter. Their transmultiplexer impulse response, with *K*=4, is given in the table below.

Table 2.1 Transmultiplexer impulse response of the FBMC/OQAM using PHYDYAS filter.

	$n-3$	$n-2$	$n-1$	n	$n+1$	$n+2$	$n+3$
$k-1$	$0.043j$	$0.125j$	$0.206j$	$0.239j$	$0.206j$	$0.125j$	$0.043j$
k	$-0.067j$	0	$-0.564j$	1	$0.564j$	0	$0.067j$
$k+1$	$0.043j$	$-0.125j$	$0.206j$	$-0.239j$	$-0.206j$	$-0.125j$	$0.043j$

All the prototype filters $g[m]$ are designed to satisfy the real orthogonality condition given by

$$\mathrm{Re}\{\sum_{m=-\infty}^{\infty} g_{k',n'}[m] g^{*}_{k,n}[m]\} = \delta_{k,k'} \delta_{n,n'} \tag{2.6}$$

After passing through the radio channel and adding noise contribution $b[m]$, equation (2.4) becomes

$$r_{k',n'} = h_{k',n'} d_{k',n'} + \underbrace{\sum_{(k,n)\neq(k',n')} h_{k,n} d_{k,n} \sum_{m-\infty}^{+\infty} g_{k,n}[m] g^*_{k',n'}[m]}_{I_{k',n'}} + \underbrace{\sum_{m-\infty}^{+\infty} b[m] g^*_{k',n'}[m]}_{\gamma_{k',n'}}, \quad (2.7)$$

where $h_{k',n'}$ is the channel coefficient at subcarrier k' and time index n', and the term $I_{k',n'}$ is defined as an intrinsic interference. The autocorrelation of the noise sample $\gamma_{k',n'}$ is given by

$$E\left\{\gamma_{k',n'}\gamma^*_{k,n}\right\} = \sigma^2 \sum_{m=-\infty}^{+\infty} g_{k',n'}[m] g^*_{k,n}[m] \quad (2.8)$$

where σ^2 is the variance of the noise $b[m]$.

The energy of the impulse response is mostly localized in a restricted time-frequency set around the considered symbol position. Consequently, for the mere MMSE equalization, and specifically for the zero-forcing (ZF) equalizer coefficients adaptation, conceptually useful is the factorisation of the subchannel transfer function as the product of the back-to-back transceiver transfer function and the equivalent (base-band) transfer function of the channel pertaining to the particular subchannel. The T/2-spaced FIR filter coefficients of an equalizer will then target the inversion of the latter response. For utilization of the known direct- and cross-subchannel impulse responses in deriving the WLF MMSE equalizer coefficients, the structured system model, as used in D3.1 for estimating the (sub)channel impulse response, is very useful. According to this model, input of N-tap equalizer is the vector $\mathbf{y}_k[n] = [r_{k,n}\ r_{k,n-1}\ r_{k,n-2}\ \cdots\ r_{k,n-N+1}]^T$, consisting of the N T/2-spaced k-th subchannel received samples, is expressed as

$$\mathbf{y}_k[n] \approx \mathbf{G}_k \cdot \mathbf{x}_k[n] + \mathbf{M}_k \cdot \mathbf{x}_{k-1}[n] + \mathbf{N}_k \cdot \mathbf{x}_{k+1}[n] + \mathbf{\Gamma}_k \cdot \boldsymbol{\eta}[n], \quad (2.9)$$

with the (Toeplitz) convolution matrices $\mathbf{G}_k \in \mathbb{C}^{\mathrm{NxL}}$, $\mathbf{M}_k \in \mathbb{C}^{\mathrm{NxL}}$ and $\mathbf{N}_k \in \mathbb{C}^{\mathrm{NxL}}$ defined by the downsampled) subchannel impulse response from, respectively, the *k*-th, (k-1)-st and (k+1)-st subchannel input to the *k*-th subchannel output, $\mathbf{x}_k[n]$, $\mathbf{x}_{k-1}[n]$ and $\mathbf{x}_{k+1}[n]$ being the vectors of the three subchannels quasi-complex data symbols (in accordance with the I/Q staggering of QAM symbols), $\mathbf{\Gamma}_k \in \mathbb{C}^{\mathrm{NxR\ bb}}$representing a matrix defined by the receiver (AFB) impulse response, and $\boldsymbol{\eta}[n]$ standing for the vector of the sum of the AWGN and interference signal samples at the AFB input [1].[1]

The downsampled subchannel impulse responses $g_k(n)$, $m_k(n)$ and $n_k(n)$ which define the convolution matrices G_k, M_k and N_k, respectively, are given by:

$$\begin{aligned} g_k(n) &= [h_k(n) * h_{ch}(n) * h_k(n)]_{\downarrow M/2}, \\ m_k(n) &= [h_{k-1}(n) * h_{ch}(n) * h_k(n)]_{\downarrow M/2}, \\ n_k(n) &= [h_{k+1}(n) * h_{ch}(n) * h_k(n)]_{\downarrow M/2} \end{aligned} \quad (2.10)$$

[1] It might be useful to note that in the case that the broadband transmission channel impulse response is available instead, for example with the aid of the methods reported in D3.1, the subchannel impulse responses can easily be computed from it and the filter bank employed.

h_k(n), h_{k-1}(n) and h_{k+1}(n) denote prototype filters of length L_g for *k*-th, (*k*-1)-th and (*k*+1)-th subchannels respectively and h_{ch}(n) denotes the channel impulse response, of length L_{ch}. Notice that the first of the dimensions of convolution matrices, *N* , represents the number of equalizer coefficients, while the other dimension of matrices G_k, M_k and N_k is *L*=*N*+*Q*-1, and $Q = \lceil (2*\mathrm{Lg} + \mathrm{L_{ch}} - 2)/(\mathrm{M}/2) \rceil$ is the length of downsampled impulse responses $g_k(n)$, $m_k(n)$ and $n_k(n)$. The second dimension of the downsampled noise-filtering convolution matrix Γ_k is $R=M/2 \cdot N + L_g$. It is also important to mention that the matrix Γ_k is not Toeplitz because it contains downsampling by *M*/2, where *M* is the number of subchannels.

2.1.2 Real-domain formulation

A slightly different representation (starting with continuous time and, occasionally, somewhat differing notations) of the transmit FBMC/OQAM modulated signal is defined by

$$x(t) = \sum_{k=k_1}^{k_2} \sum_{m=0}^{2M-1} j^{k+m} d_m^k \cdot g(t - mT/2) e^{j2\pi k \frac{t-mT/2}{T}} \tag{2.11}$$

where the symbols d_n^k are (again) the real valued (Real or Imaginary parts of QAM symbols, belonging to a block of transmitted data). The index of the *K* subcarriers are denoted with numbers between k_1 and k_2. The function $g(t)$ is a real, even, square root Nyquist function of norm 1, with the low-pass bandwidth $B_g = (1+\alpha)/T$, where α is the roll off factor. It has finite time duration $[-L_g T, L_g T]$, with *T* denoting the QAM signaling interval.

As a modulation, with real valued symbols, of an orthogonal basis

$$\phi_m^k(t) = g(t - mT/2) e^{2j\pi k \frac{t-mT/2}{T}} \tag{2.12}$$

and (2.11) becomes

$$x(t) = \sum_{k=k_1}^{k_2} \sum_{m=0}^{2M-1} j^{k+m} d_m^k \phi_m^k(t) \tag{2.13}$$

After a transmission over an AWGN channel, the maximum likelihood, ML, receiver is obtained by the real part of the scalar product between the received signal $r(t) = x(t) + b(t)$ and the basis functions $\phi_m^k(t)$, with

$$r_m^k = \mathrm{Re}\left\{ \int_{-L_g T}^{L_g T} r(mT/2 + t) \overline{\phi_m^k(mT/2 + t)} dt \right\} \tag{2.14}$$

where the over-bar denotes complex conjugation. By using orthonormality of basis functions, the sampled version of (2.14) becomes $r_m^k = d_m^k + b_m^k$. It should be clear from the context, that index *m* corresponds to *T/2* instants, as the index *m* in(2.11).

Transmission over a dispersive channel

The time-dispersive channel is defined by a finite impulse response $h(t)$ for $t \in [-L_h T, L_h T]$ with an AWGN noise at the FIR filter output. The received signal is represented by

$$r(t) = \int_{-L_h T}^{L_h T} x(t - \xi) h(\xi) d\xi + b(t), \tag{2.15}$$

or

$$r(t)=\sum_{k=k_1}^{k_2}\sum_{m=0}^{2M-1} j^{k+m} d_m^k g_k(t-mT/2) e^{j2\pi k\frac{t-mT/2}{T}} + b(t) \tag{2.16}$$

Here

$$g_k(t)=\int_{t+L_gT-mT/2}^{t-L_gT-mT/2} g(\xi) e^{-j2\pi k\frac{t-\xi}{T}} h(t-\xi)d\xi \tag{2.17}$$

is a function of time with duration over the interval $t\in\left[-\left(L_h+L_g\right)T,\left(L_h+L_g\right)T\right]=\left[-\left(L_{g+h}\right)T,\left(L_{g+h}\right)T\right]$ and has bandwidth $B_g=(1+\alpha)/T$. Projection of the received signal over the orthogonal basis $\phi_m^k(t)$ is defined by(2.12).

With

$$\phi_m^k\left(mT/2+t\right)=j^{k+m}g\left(t\right)e^{2j\pi k\frac{t}{T}}, \tag{2.18}$$

$$r_m^k=\mathrm{Re}\left\{\int_{-L_gT}^{L_gT}\sum_{k'=k_1}^{k_2}\sum_{n'=0}^{2M-1} j^{k'+n'}d_{n'}^{k'}g_{k'}\left(t+\left(m-n'\right)T/2\right)\cdot e^{j2\pi k'\frac{t+(m-n')T/2}{T}} j^{-k-m}g(t)\cdot e^{-j2\pi k\frac{t}{T}}dt\right\} \tag{2.19}$$

whereby is temporarily taken $b(t)=0$, and by using $k'=k+k''$ and $n'=m-n''$

$$r_m^k=\sum_{k''-1}^{1}\sum_{n''=m}^{m-(2M-1)} d_{m-n''}^{k+k''}\mathrm{Re}\left\{j^{k''-n''}\int_{-L_gT}^{L_gT} g_{k+k''}\left(t+n''T/2\right)\cdot e^{j2\pi(k+k'')\frac{t+n''T/2}{T}} g(t)\,e^{-j2\pi k\frac{t}{T}}dt\right\} \tag{2.20}$$

Due to the finite length duration in time and frequency of the impulse functions of the modulator and the channel, the received signal is the output of a linear matrix filter represented by real valued samples plus a white Gaussian noise, not accounted for after equation (2.4). The 3x1 MISO model of adjacent subchannels interference is described by the following relation (*m* replaced by *n*)

$$r_n^k=\sum_{k''=-1}^{1}\sum_{n''=-2L_{g+h}}^{2L_{g+h}} d_{n-n''}^{k+k''}h_{n''}^{k,k''}+b_n^k, \tag{2.21}$$

with reinserting (uncorrelated) noise samples, where $h_{n''}^{k,k''}$ are the three impulse responses of the global filters. $h_{n''}^{k,0}$ is the impulse response on the subchannel k, $h_{n''}^{k,1}$ represents the interferences from the upper sub carrier of index $k+1$ and $h_{n''}^{k,-1}$ interferences from the lower subchannel of index $k-1$. It should be noted that the samples $h_{n''}^{k,k''}$ and the data d_n^k are all real-valued. Also, it should be kept in mind that although the noise samples in the real-domain formulation are independent due to their quadrature relationship, the complex samples at T/2 separation are correlated – the fact that will be used later on for its prediction and partial cancellation. If the duration of the transmitter impulse were fixed to 4*T,* and the duration of the channel impulse response is less than *T*, then the size of the matrix *H* is 3 times 10. Due to the very notation used in (2.9) same filters are used for even and odd *T*/2 instants, since their definition does not depend on index *n*.

The 3x1 MISO form of channel model pertinent to the FBMC/OQAM format in SISO configuration, the complex samples of which in back-to-back connection case were shown in

Table 3-1, is shown in Fig. 2.2 .

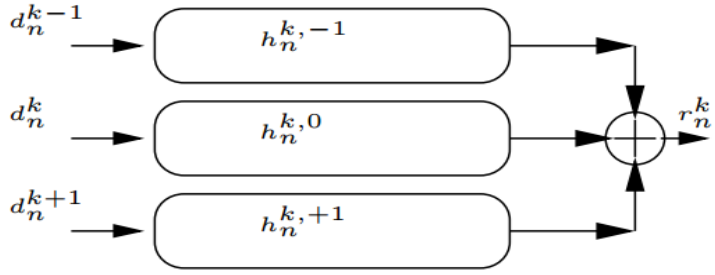

Fig. 2.2 3x1 MISO representation for one FBMC/OQAM subchannel

For the subchannels impulse response identification, the sum of squared noise terms from (2.22) is minimized over a training period of length *N*, which by re-reshuffling $\hat{h}^k_{3n"+k"} = \hat{h}^{k,k"}_{n"}$ and $d^k_{3(n-n")-k"} = d^{k+k"}_{n-n"}$, becomes the one dimension vector form

$$\sum_{n=1}^{N}\left(r_n^k - \sum_{n'=n}^{n-3L} d^k_{n-n'}\hat{h}^k_{n'}\right)^2 . \qquad (2.22)$$

Then by applying this method for each sub carrier of index *k*, the $\hat{H}_k$ matrices of size 3x(*L* +1), *L*=2L_{g+h}, with impulse responses representing the inter-subchannel (1st and 3rd raw) and intersymbol interferences (2nd raw) can be estimated by product of the inverse data autocorrelation matrix and the signal-data cross-correlation vector, in line with conventional least-squares (LS) criterion for minimization of metric in (2.22).

For illustrative purpose, below are shown a set of estimated, real-valued subchannel and cross-subchannel impulse responses for the flat Rayleigh fading case, and the reference system impulse response of length 4T, as per the optimization methodology in [2].

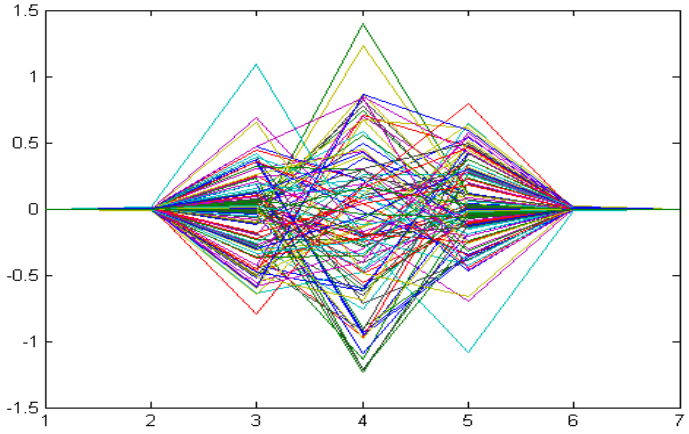

Fig. 2.3 Real-domain impulse responses of k-th sub-channel and flat Rayleigh channel realizations marked by different colours.

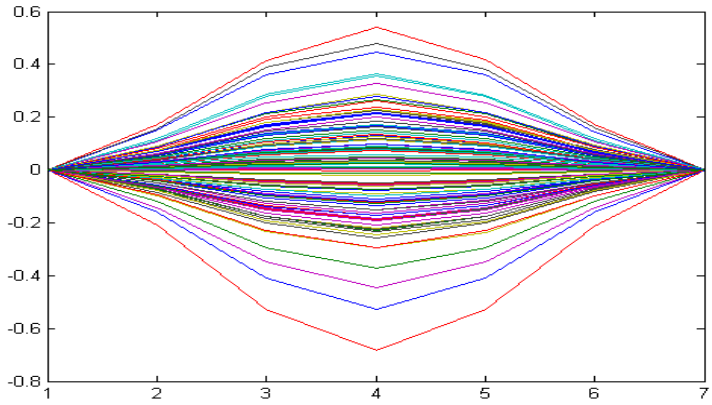

Fig. 2.4 Real-domain impulse responses between k-th and (k+1)-st sub-channels for flat Rayleigh channel realizations marked by different colours.

In case that the complex (sub)channel impulse responses are provided in another fashion, for example by some of the methods proposed in D3.1 which are efficient regarding the required transmission overhead, it is to expect that the real-valued impulse responses needed for the SIC procedure be produced by just taking their real parts. Regarding the plausibility of the real-valued FBMC system model, it might be worth stating that in the case of the even-spaced subchannel arrangement (subchannel positioned at the odd multiples of frequency 1/2T), the staggering pattern is such that on each of the subchannels purely real or purely imaginary data symbols are modulated interchangeably on adjacent subchannels, so that with respect to central frequencies of the even-spaced arrangement the subchannel modulations take the form of the vestigial sub-band pulse amplitude modulations. Please note that in general, even for the frequency flat transmission channels the impulse responses of real-valued system model have multiple coefficients, determined by the length of the filterbank referent impulse response. Of course, if the flat channel impulse response can be represented by just one complex number at the sub-channel level, and as such used in appropriately defined configurations for successive interference cancelation and/or for the subchannel correlated noise prediction and cancellation, the approaches for the FBMC performance enhancements over the CP-OFDM case by the end of this section.

For both complex- and real-valued system models, extension to the time-limited orthogonal (TLO) multi-carrier waveforms is quite straightforward: only the number of mutually interfering, that is, spectrally overlapping subchannels is increased, while the impulse response lengths are decreased, at least in the flat fading case, by the factor of K(=4).

3. MMSE Widely Linear Filtering Equalization (WLFE)

With exception of the firstly proposed equalization of the FBMC/OQAM signal [3], where the I/Q de-staggering is performed before the equalizer (detector), all other proposals, for both single-carrier [4, 5], and multi-carrier context [6, 7], rely on intrinsic signalling by purely real or purely imaginary components of the complex QAM data signals. Consequently, the per-subchannel equalizer has a complete freedom in producing the complementary quadrature parts. In presence of additive noise impairment with circular statistics, it has been shown that the conventional, strictly linear processing, whereby merely the complex signal at the output of the AFB is used, these degrees of freedom are used to effectively produce the inversion of the subcahannel's equivalent transfer function by adequately adapting the equaliser's feed-forward filter (FFF) coefficients [6, 8, 9], while the feed-back filter (FBF) filter part in case of the DFE provide some increase in degrees of freedom to, for example better cope with the presence of narrow-band interference (NBI), provided that the effect of decision errors propagation is not too much pronounced to offset the advantages.

In the last two decades we have witnessed an increased awareness of the potentials of simultaneous processing of both the complex signal and its complex-conjugated version in situations where the additive impairments have non-circular statistics, typical for the wireless networks with reuse factor one, and related co-channel interferers. The difference between the two equalizer configurations has been analysed in [10], and the difference in behaviour of the two equalizer configurations in case of rectilinear BPSK modulations and the MMSE-based coefficients synthesis is shown in the following figure.

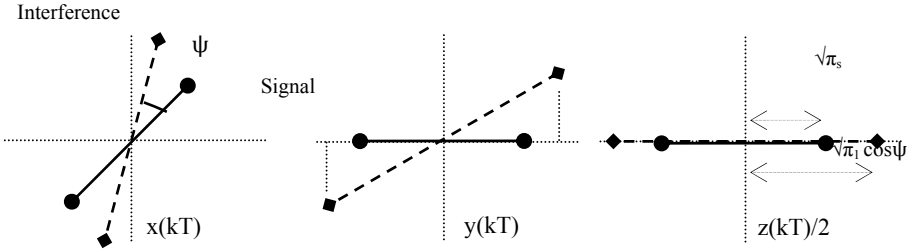

Fig. 3.1 BPSK useful signal and interference for CIR-ML receiver input and output.

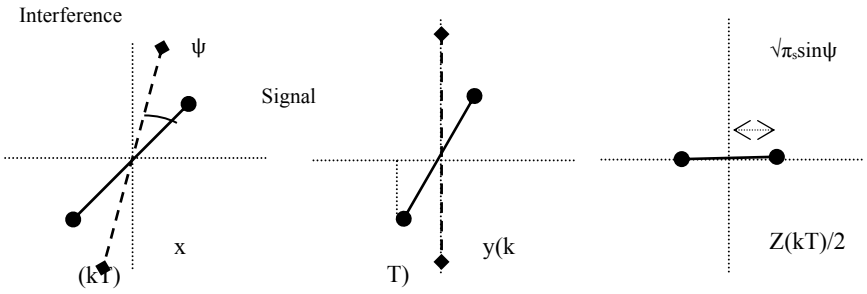

Fig. 3.2 Constellation of BPSK useful signal and interference for the NCIR-MLE case.

While the SLF-based linear equalizer, in the considered case of channel transfer function given by a complex number (frequency-flat fading) aligns the useful signal to the real axis irrespectively of the phase of the interfering signal, thus the former being mostly (even for the relatively high signal-to-interference power ration, SIR) corrupted by the latter one, the WLF-based equalizer approximately aligns the phase of the interference on the imaginary axis, bringing the considerable interference suppression, in particular for the relatively high SIRs. The (one-tap) equalizer thus tends to suppress the real part of the interference and thus its contribution in the output, while the useful signal's SNR becomes partly degraded.

Differently to the rectilinear, generally pulse amplitude modulations (PAM), in the case of the OQAM format the signal constellation at the output of AFB in the case of ideal channel is not composed from only two points, but consists of two lines, with the points along them actually representing the interpolated values of data bearing transmitted symbols. This is illustrated in Figs. 3-3, 3-4, and 3-5, for ideal channel and the particular realization of the one-tap frequency-flat channel.

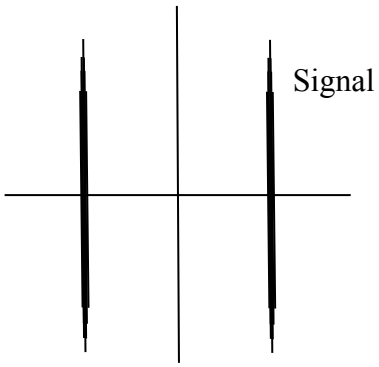

Fig. 3.3 Constellation of a FBMC/OQAM subchannel signal for BPSK and ideal transmission channel.

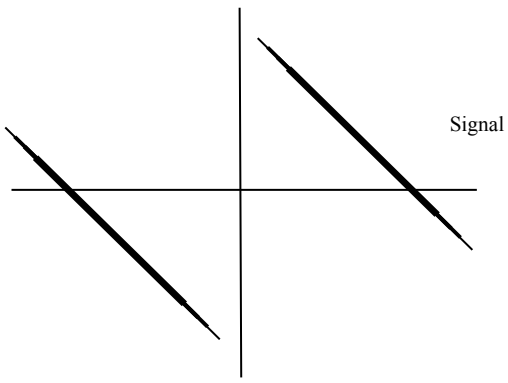

Fig. 3.4 Constellation of OQAM useful signal at the frequency-flat channel output.

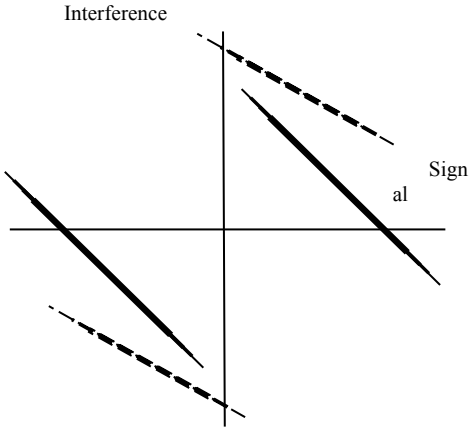

Fig. 3.5 Constellation of OQAM useful signal and interference for flat fading channel.

Obviously, for the case of I/Q staggered (both single-carrier and multi-carrier) modulation formats it then becomes obvious that the one-tap equalizer now can not align the interferer on the imaginary axis without inflicting a heavy corruption of the useful signal through the interfering signal's projection on the real-axis. As suggested in [10] generally more than one tap equalizer structures will be needed, even in the frequency-flat channel case. The reasonable expectation will then be for the multi-tap equalizer to effectuate the alignment of the interfering signal to the imaginary axis in the frequency-selective fashion, within the effect of overlapping around the frequencies ±1/T.

In the following, the focus will be on the specialization of the general WLF-based equalization framework to account for the presence of the interfering signals along the additive (Gaussian) noise, and the exploration of conditions under which it can be effective.

3.1 Analytical derivation of equalizer coefficients

In [1] there has been made a profound analysis of the WLF-based linear and DFE MMSE equalization of the FBMC system in all generality, from the even- and odd-spaced subchannels stacking, to the receive additive noise statistical features. By starting from the combined processing of the complex subchannel signals and their complex conjugate versions, it has been shown that the MMSE equalizer is time-invariant, and that the complex T/2 spaced FR filter being same for the even and odd multiples of T/2 intervals, whereby only the relevant quadrature components being extracted, as illustrated in Fig. 3-6.

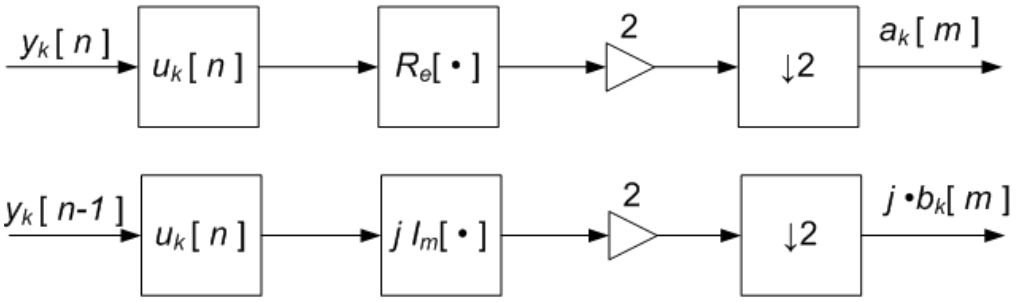

Fig. 3.6 Widely linear equalization: real and imaginary parts.

Thereby, this turns out to be identical with the previously heuristically derived equalizer configuration targeting only the relevant (data bearing) quadrature components, proposed in [6]. However, besides many other relevant aspects, the most important contribution of the Waldhauser's thesis, regarding the task of this deliverable, is the analytical derivation of the equalizer coefficients based on the availability of subchannels (direct and adjacent cross-talk) transfer functions, to be briefly outlined bellow.

However, this applies only to the case when the statistical features of additive interference is circular, in which case its pseudo-correlation matrix becomes identical to zero. Since in this deliverable of prime interest is the exploration of the WLF-based equalizer structure in the case when besides the AWGN there is present an interferer of the same kind (that is – kindred) as the useful FBMC, we used the relevant steps of the derivations in the Waldhauser's thesis [1] to arrive at the solution that implies and specifies the time-invariant equalizer coefficients set-up.

By looking for the WLF-equalized subchannel output sample at the (say, for the particular subchannel index k) even n-th T/2 time-instant (*n=2m*, and *m* the subchannel's QAM symbol index) in the form

$$\overline{a}_k[m] = \mathbf{u}_k^H[n] \cdot \mathbf{y}_k[n] + \mathbf{v}_k^H[n] \cdot \mathbf{y}^*{}_k[n] \tag{3.1}$$

Instead of the conventional, strictly linear formulation

$$\overline{a}_k[m] = \mathbf{w}_k^H[n] \cdot \mathbf{y}_k[n] \tag{3.2}$$

the vector of N equalizer coefficients is produced in the form of

$$\mathbf{u}_k[n] = \mathbf{v}_k^*[n] = (\mathbf{R}_{y_k} - \mathbf{P}_{y_k}[n] \cdot \mathbf{R}_{y_k}^{-1,*} \cdot \mathbf{P}^*{}_{y_k}[n])^{-1} \cdot (\mathbf{r}_k - \mathbf{P}_{y_k}[n] \cdot \mathbf{R}_{y_k}^{-1,*} \cdot \mathbf{s}^*{}_k[n]) \tag{3.3}$$

where $\mathbf{R}_{y_k}$ and $\mathbf{P}_{y_k}$ are respectively the input signal (comprising the useful signal and the generally combined additive noise and co-channel interference signals) correlation and pseudocorrelation (without the row-vector conjugation in the correlation matrix definition) matrices, while $\mathbf{r}_k$ and $\mathbf{s}_k$ respectively are the cross-correlation and the pseudo cross-correlation vectors between the input signal vector (observation vector) and the transmit data that corresponds to the data to be estimated at particular moment (delayed from actual transmission instant by $v \cdot T/2$), defined by $0.5 \cdot \sigma_k^2 \cdot \mathbf{g}_{k,2v}$, with $\mathbf{g}_{k,2v}$ being the $2v-th$ column-vector of the matrix $\mathbf{G}_k$. (It is noted here that the sings of $\mathbf{P}_{y_k}$ and $\mathbf{s}_k$ are changed every other index *n*, that for its even and odd values, but since they appear in products, the equalizer coefficients remain time-invariant, as defined for say even indexes.)

By using the complex-valued, or complex-domain subchannel-level transmission system model of (2.9), the two matrices take the forms

$$\mathbf{R}_{y_k}[n] = \mathbf{G}_k \cdot \mathbf{R}_{x_k}[n] \cdot \mathbf{G}_k^H + \mathbf{M}_k \cdot \mathbf{R}_{x_{k-1}}[n] \cdot \mathbf{M}_k^H + \mathbf{N}_k \cdot \mathbf{R}_{x_{k+1}}[n] \cdot \mathbf{N}_k^H + \mathbf{\Gamma}_k \cdot \mathbf{R}_\eta \cdot \mathbf{\Gamma}_k^H \tag{3.4}$$

$$\mathbf{P}_{y_k}[n] = \mathbf{G}_k \cdot \mathbf{P}_{x_k}[n] \cdot \mathbf{G}_k^T + \mathbf{M}_k \cdot \mathbf{P}_{x_{k-1}}[n] \cdot \mathbf{M}_k^T + \mathbf{N}_k \cdot \mathbf{P}_{x_{k+1}}[n] \cdot \mathbf{N}_k^T + \mathbf{\Gamma}_k \cdot \mathbf{P}_\eta \cdot \mathbf{\Gamma}_k^T \tag{3.5}$$

with $\mathbf{R}_{x_k} \in \mathbb{C}^{\mathrm{LxL}}$ and $\mathbf{P}_{x_k} \in \mathbb{C}^{\mathrm{LxL}}$ the correlation and pseudo-correlation matrices of the input data samples, respectively, and the correlation and pseudo-correlation matrices of interference plus noise $\mathbf{R}_\eta \in \mathbb{C}^{\mathrm{RxR}}$ and $\mathbf{P}_\eta \in \mathbb{C}^{\mathrm{RxR}}$, respectively.

Due to generally valid assumption about independence of the transmitted data samples, the latter two correlation matrices are defined as

$$\mathbf{R}_{x_k}[n] = \frac{1}{2}\sigma_{d_k}^2 \cdot \mathbf{I}_L,\ \mathbf{P}_{x_k}[n] = (-1)^k \cdot \frac{1}{2} \cdot \sigma_{d_k}^2 \cdot \mathbf{J}_L, \text{ and } \mathbf{P}_{x_k}[n+2m+1] = -\mathbf{P}_{x_k}[n], \tag{3.6}$$

where $\mathbf{I}_L$ is identity matrix, and $\mathbf{J}_L = diag[(-1)^1, (-1)^2, \cdots, (-1)^L]$.

The assumed circularity of additive interference, i.e. $\mathbf{R}_\eta = E[\boldsymbol{\eta}[l] \cdot \boldsymbol{\eta}^H[l]] = \sigma_\eta^2 \mathbf{I}_R$ and $\mathbf{P}_\eta = \mathbf{0}$, based on the subsequent analysis in the Thesis, with the assumption of circular noise, leads

to the final expressions of the direct and the pseudo-correlation matrices to be used in (3.3).

$$\mathbf{R}_{y_k}[n] = 0.5 \cdot (\sigma_k^2 \cdot \mathbf{G}_k \cdot \mathbf{G}_k^H + \sigma_{k-1}^2 \cdot \mathbf{M}_k \cdot \mathbf{M}_k^H + \sigma_{k+1}^2 \cdot \mathbf{N}_k \cdot \mathbf{N}_k^H + \sigma_\eta^2 \cdot \mathbf{\Gamma}_k \cdot \mathbf{\Gamma}_k^H) \quad (3.7)$$

$$\mathbf{P}_{y_k}[n] = 0.5 \cdot (\sigma_k^2 \cdot \mathbf{G}_k \cdot \mathbf{J}_L \cdot \mathbf{G}_k^T - \sigma_k^2 \cdot \mathbf{M}_k \cdot \mathbf{J}_L \cdot \mathbf{M}_k^T - \sigma_k^2 \cdot \mathbf{N}_k \cdot \mathbf{J}_L \cdot \mathbf{N}_k^T) \quad (3.8)$$

Similarly, for the odd n-th T/2 time-instant, *n-1=2m-1*, the corresponding WLF formulation is

$$j \cdot \overline{b}_k[m] = \mathbf{g}_k^H[n] \cdot \mathbf{y}_k[n-1] + \mathbf{h}_k^H[n] \cdot \mathbf{y}^*{}_k[n-1], \quad (3.9)$$

leading in the general case, without any assumptions regarding the statistics of additive disturbance, to

$$\mathbf{g_k} = -\mathbf{h}_k^* \quad (3.10)$$

and thus, through arguments given in the Thesis and not repeated here, to the utilization of just one filter $\mathbf{g_k}$, which further, with circular interference assumption, was shown to be same as $\mathbf{u_k}$, so that the scheme in Fig. 3-6 applies.

But this equivalence between the FIR filters to be used for the even and for the odd multiples of T/2 spaced WLF (linear) equalizer outputs is produced based on the equations

$$\mathbf{R}_{y_k}[n-1] = \mathbf{R}_{y_k}[n], \ \mathbf{P}_{y_k}[n-1] = -\mathbf{P}_{y_k}[n] \quad \text{and} \quad \mathbf{s}_k^*[n-1] = -\mathbf{s}_k^*[n] \quad (3.11)$$

whereby the second one comes out from using (3.6) in (3.5) for $\mathbf{P}_\eta \equiv \mathbf{0}$ (zero matrix).
In general then the expression for the input signal pseudocorrelation matrix will be

$$\mathbf{P}_{y_k}[n-1] = 0.5 \cdot (-\sigma_k^2 \cdot \mathbf{G}_k \cdot \mathbf{J}_L \cdot \mathbf{G}_k^T + \sigma_k^2 \cdot \mathbf{M}_k \cdot \mathbf{J}_L \cdot \mathbf{M}_k^T + \sigma_k^2 \cdot \mathbf{N}_k \cdot \mathbf{J}_L \cdot \mathbf{N}_k^T + \mathbf{\Gamma}_k \cdot \mathbf{P}_\eta \cdot \mathbf{\Gamma}_k^T), \quad (3.12)$$

while the related signal (direct) correlation matrix is same as in (3.4), that is

$$\mathbf{R}_{y_k}[n] = 0.5 \cdot (\sigma_k^2 \cdot \mathbf{G}_k \cdot \mathbf{G}_k^H + \sigma_{k-1}^2 \cdot \mathbf{M}_k \cdot \mathbf{M}_k^H + \sigma_{k+1}^2 \cdot \mathbf{N}_k \cdot \mathbf{N}_k^H + \sigma_\eta^2 \cdot \mathbf{\Gamma}_k \cdot \mathbf{\Gamma}_k^H), \quad (3.13)$$

so that the expression for the calculation of the WLF equalizer for odd-spaced T/2 instants is

$$\mathbf{g}_k[n-1] = (\mathbf{R}_{y_k} - \mathbf{P}_{y_k}[n-1] \cdot \mathbf{R}_{y_k}^{-1,*} \cdot \mathbf{P}^*{}_{y_k}[n-1])^{-1} \cdot (\mathbf{r}_k - \mathbf{P}_{y_k}[n-1] \cdot \mathbf{R}_{y_k}^{-1,*} \cdot \mathbf{s}^*{}_k[n-1]) \quad (3.14)$$

Taking into account the time variance of pseudocorrelation matrix and pseudocorrelation vector, illustrated in the second and third equations from (3.11), expression (3.14) can be written in the same form as the equalizer coefficients vector for even index *n* in (3.3), that is

$$\mathbf{g}_k[n-1] = (\mathbf{R}_{y_k} - \mathbf{P}_{y_k}[n] \cdot \mathbf{R}_{y_k}^{-1,*} \cdot \mathbf{P}^*{}_{y_k}[n])^{-1} \cdot (\mathbf{r}_k - \mathbf{P}_{y_k}[n] \cdot \mathbf{R}_{y_k}^{-1,*} \cdot \mathbf{s}^*{}_k[n]) \quad (3.15)$$

It should be noted that besides for the circular noise, this applies as well in presence of kindred co-channel interference which is of the primary interest in this section. However, in

general case, and in particular for example when the co-channel interference is a STBC-coded FBMC signal, although for circular AWGN disturbance $\mathbf{P}_\eta \equiv \mathbf{0}$ still applies, the middle and/or the part on the left side of (3.11) might not stand anymore, producing the time-variant equalization structure, with the equalizer filters different for even and odd T/2 instants.

The same author has tackled the WLF in the context of entirely real-domain formulation of complex signal processing in [1] and the production of the time-invariant equalizer structure based on the interference circularity.

While the difference between the two seemingly equivalent WLF equalization structures – the independent processing of complex signal and its complex-conjugated version, and such a processing of the signals' in-phase and quadrature components, in terms of sensitivity/robustness to/against the error propagation effect in DFE configurations [11, 12] has been found, we explore their equivalence or possible differences in both the SISO case, and in presence of kindred co-channel interference.

Using here somewhat modified notation to better relate to [1], in [8] the vector composed of real and imaginary parts of a subchannel equalizer $\mathbf{u}_k^{'T} = [\mathbf{u}_k^{(R),T} \;\; \mathbf{u}_k^{(I),T}]$ is derived as

$$\mathbf{u}_k^{'T} = \left[\mathbf{H}_k \cdot \mathbf{R}_x \cdot \mathbf{H}_k^T + \mathbf{F}_k \cdot \hat{\mathbf{R}}_x \cdot \mathbf{F}_k^T + \mathbf{R}_{\eta,k}^{'}\right]^{-1} \cdot \mathbf{H}_k \cdot \mathbf{R}_x \cdot \mathbf{e}_\nu \,, \tag{3.16}$$

with $\mathbf{H}_k \in \mathbb{C}^{2\mathrm{N}\times\mathrm{L}}$ and $\mathbf{F}_k \in \mathbb{C}^{2\mathrm{N}\times 2\mathrm{L}}$ defined by

$$\mathbf{H}_k = \begin{bmatrix} \mathbf{G}_k^{(R)} \\ \mathbf{G}_k^{(I)} \end{bmatrix} \text{ and } \mathbf{F}_k = \begin{bmatrix} \mathbf{M}_k^{(R)} & \mathbf{N}_k^{(R)} \\ \mathbf{M}_k^{(I)} & \mathbf{N}_k^{(I)} \end{bmatrix}, \tag{3.17}$$

(It is important to mention that every second column of matrices $\mathbf{G}_k$, $\mathbf{M}_k$ and $\mathbf{N}_k$ is multiplied by *j*, before taking real and imaginary parts (R and I) in (3.17). This is done in order to shift-out *j* from imaginary entry of transmitted sequence (which contains real and imaginary parts of symbols alternately) in matrices $\mathbf{H}_k$, $\mathbf{M}_k$ and $\mathbf{N}_k$.)

Correlation matrix $\mathbf{R}_x = \frac{1}{2}\sigma_d^2 \cdot \mathbf{I}_L$, representing also sub-matrix of signal correlation matrix $\hat{\mathbf{R}}_x \in \mathbb{C}^{2\mathrm{L}\times 2\mathrm{L}}$

$$\hat{\mathbf{R}}_x = \begin{bmatrix} \mathbf{R}_x & \mathbf{0}_L \\ \mathbf{0}_L & \mathbf{R}_x \end{bmatrix} \tag{3.18}$$

The interference correlation matrix $\mathbf{R}_{\eta,k}^{'} \in \mathbb{C}^{2\mathrm{N}\times 2\mathrm{N}}$ in the real-domain formulation then is

$$\mathbf{R}_{\eta,k}^{'} = \mathbf{\Gamma}^{'}{}_k \cdot \mathbf{R}_\eta \cdot \mathbf{\Gamma}_k^{'T} = \begin{bmatrix} \mathbf{R}_{\eta,k,1}^{'} & \mathbf{R}_{\eta,k,2}^{'} \\ -\mathbf{R}_{\eta,k,2}^{'} & \mathbf{R}_{\eta,k,1}^{'} \end{bmatrix}, \tag{3.19}$$

where by $\mathbf{\Gamma}'_k \in \mathbb{C}^{2N\times 2R}$ denotes down-sampled interference convolution matrix Γ_k in the real-domain formulation

$$\mathbf{\Gamma}'_k = \begin{bmatrix} \mathbf{\Gamma}_k^{(R)} & -\mathbf{\Gamma}_k^{(I)} \\ \mathbf{\Gamma}_k^{(I)} & \mathbf{\Gamma}_k^{(R)} \end{bmatrix} \tag{3.20}$$

From (3.19) and (3.20) it follows

$$\mathbf{R}'_{\eta,k,1} = 0.5\cdot\left(\mathbf{\Gamma}_k^{(R)}\cdot\mathbf{R}_\eta\cdot\mathbf{\Gamma}_k^{(R),T} + \mathbf{\Gamma}_k^{(I)}\cdot\mathbf{R}_\eta\cdot\mathbf{\Gamma}_k^{(I),T}\right) \tag{3.21}$$

and

$$\mathbf{R}'_{\eta,k,2} = 0.5\cdot\left(\mathbf{\Gamma}_k^{(R)}\cdot\mathbf{R}_\eta\cdot\mathbf{\Gamma}_k^{(I),T} - \mathbf{\Gamma}_k^{(I)}\cdot\mathbf{R}_\eta\cdot\mathbf{\Gamma}_k^{(R),T}\right) \tag{3.22}$$

If in the TUM's simulator the interference correlation function is taken as $\mathbf{R}_\eta = E[\boldsymbol{\eta}[l]\cdot\boldsymbol{\eta}^H[l]] = \sigma_\eta^2\mathbf{I}_R$, (3.22) becomes equal to zero, and (3.19) is a diagonal matrix. The modification in the MATLAB code then is the evaluation by calculation (or estimation in the practical situation) of the noise plus interference correlation matrix and its adequate insertion into the sub-matrices of (3.19).

As for the availability of calculation of the interference (joint noise and the co-channel parts) in the realistic operation of a FBMC type transceiver, the elimination of cyclic prefix (CP), while keeping the same packet structure in FBMC as in the CP-OFDM case, can be used to allow for a proportional section of the transmitted packet to be idle, as it has been conceived by the EMPhAtiC cross-workpackage group and published as the MS4 document. It might be also useful to note that in (open-loop) MIMO configurations the transmitted streams can be considered as co-channel interfering signals the transfer function of which are known, so that their correlation matrices are known and can be used as part of overall interference correlation matrices to possibly directly extend the SISO MMSE equalization as an alternative to the method used in Lipardi's thesis [13]. (Although here we consider the co-channel interference scenario only, we still rely on availability of the interferers transfer functions as seen by the actual receiver.)

3.2. Comparison between analytical derivation of equalizer coefficients in complex domain and real domain notation

In the text bellow we discuss relation between the two above mentioned solutions in the case of absence of kindred co-channel interference. This relation is also confirmed through simulation in Figs. 3-7 and 3-8. Latter we will proceed with addition of co-channel interference as a part of noise, with appropriate definitions of related matrices.

In [1] it is mentioned that in the case of exponentially modulated subcarrier filters and identical weighting of subcarriers *k*, *k*-1, *k*+1, pseudocorrelation matrix $\mathbf{P}_{y_k}$ is equal to zero matrix. The result of this is a wide-sense stationary and circular subcarrier signal. In this case the one of degrees of freedom is lost, which can be important for the case of presence of

kindred co-channel interference signal. This, however, applies only for essentially 100% roll-off sub-channel signals, and it is not the case for smaller roll-off factors, use of the time-limited orthogonal (TLO) FBMC waveforms, and I/Q staggered filtered multi-tone (FMT – non-staggered FMT form has been considered in [14]), that is the frequency-division multiple of spectrally non-overlapping sub-carriers, as it has been the case with (linearized form of) GMSK modulation in 2G GSM standard. For that reason, in this deliverable the situations with non-zero pseudo-correlation matrix are emulated through the single-carrier case, that is the FBMC configuration with every second subchannel active.

WLF-based linear equalization for zero-valued matrix $\mathbf{P}_{y_k}$ yields to SLF-based linear equalization, because the additional degree of freedom, which comes from processing complex-conjugated version of received complex signal, through pseudocorrelation matrix $\mathbf{P}_{y_k}$, is lost. In that case substituting (3.4) into (3.3), expression (3.3) is simplified to

$$\mathbf{u}_k[n] = \mathbf{v}_k^*[n] = (\mathbf{G}_k \cdot \mathbf{R}_{x_k}[n] \cdot \mathbf{G}_k^H + \mathbf{M}_k \cdot \mathbf{R}_{x_{k-1}}[n] \cdot \mathbf{M}_k^H + \mathbf{N}_k \cdot \mathbf{R}_{x_{k+1}}[n] \cdot \mathbf{N}_k^H + \mathbf{\Gamma}_k \cdot \mathbf{R}_\eta \cdot \mathbf{\Gamma}_k^H)^{-1} \cdot (\mathbf{r}_k) \quad (3.23)$$

Comparing (3.23) and (3.16), it can be seen that these expressions are similar. Also, from (3.17) and (3.20), it can be seen that the transition from complex to real-domain notation is not done in the same way. In comparison with (3.20), it appears that in (3.17) the second column is omitted.

In the following we considered the case when 6 out of 8 subchannels are active and the case when 4 out of 8 subchannels (every second subchannel) are active.
In the case when every second subchannel is active, pseudocorrelation matrix is not equal to zero matrix and it is expected to give additional degree of freedom for certain level of suppression of kindred co-channel interference, which will be discussed in the section bellow. In the case when every second subchannel is active, expression (3.16) can be simplified to

$$\mathbf{u}_k^{'T} = \left[\mathbf{H}_k \cdot \mathbf{R}_x \cdot \mathbf{H}_k^T + \mathbf{R}_{\eta,k}^{'}\right]^{-1} \cdot \mathbf{H}_k \cdot \mathbf{R}_x \cdot \mathbf{e}_\nu \,. \quad (3.24)$$

Also, in that case expressions (3.4) and (3.5) are simplified to

$$\mathbf{R}_{y_k}[n] = \mathbf{G}_k \cdot \mathbf{R}_{x_k}[n] \cdot \mathbf{G}_k^H + \mathbf{\Gamma}_k \cdot \mathbf{R}_\eta \cdot \mathbf{\Gamma}_k^H \quad (3.25)$$

$$\mathbf{P}_{y_k}[n] = \mathbf{G}_k \cdot \mathbf{P}_{x_k}[n] \cdot \mathbf{G}_k^T + \mathbf{\Gamma}_k \cdot \mathbf{P}_\eta \cdot \mathbf{\Gamma}_k^T \quad (3.26)$$

Expression (3.23), which corresponds to the SLF-based equalization, in the case when every second subchannel is active can be additionally simplified to

$$\mathbf{u}_k[n] = \mathbf{v}_k^*[n] = (\mathbf{G}_k \cdot \mathbf{R}_{x_k}[n] \cdot \mathbf{G}_k^H + \mathbf{\Gamma}_k \cdot \mathbf{R}_\eta \cdot \mathbf{\Gamma}_k^H)^{-1} \cdot (\mathbf{r}_k) \quad (3.27)$$

For both cases (the case with overlapped subchannels and the case when every second subchannel is active) we compared BER performances obtained for WLF-based linear equalization in the complex-domain notation, WLF-based linear equalization in the real-domain notation and SLF-based linear equalization in the complex-domain notation (which corresponds to the case when pseudo-correlation matrix is not included in expression for calculating equalizer's coefficients).

For 6 out of 8 active subchannels (the case with overlapped subchannels), equivalence of WLF-based linear equalization in complex-domain notation (expression (3.3) with R_{yk} and P_{yk} defined according to (3.4) and (3.5)) and WLF-based linear equalization in real-domain notation (expression (3.16) with H_k and F_k defined according to (3.17)) is proven through comparison of the final values of coefficients as well as through BER performance, which is illustrated in Fig. 3-7. The same BER performances and final values of coefficients are obtained in the case of SLF-based linear equalization in the complex-domain notation (expression (3.23)) which is also illustrated in Fig. 3-7. Simulations are given for flat Rayleigh fading case and 4-QAM modulation.

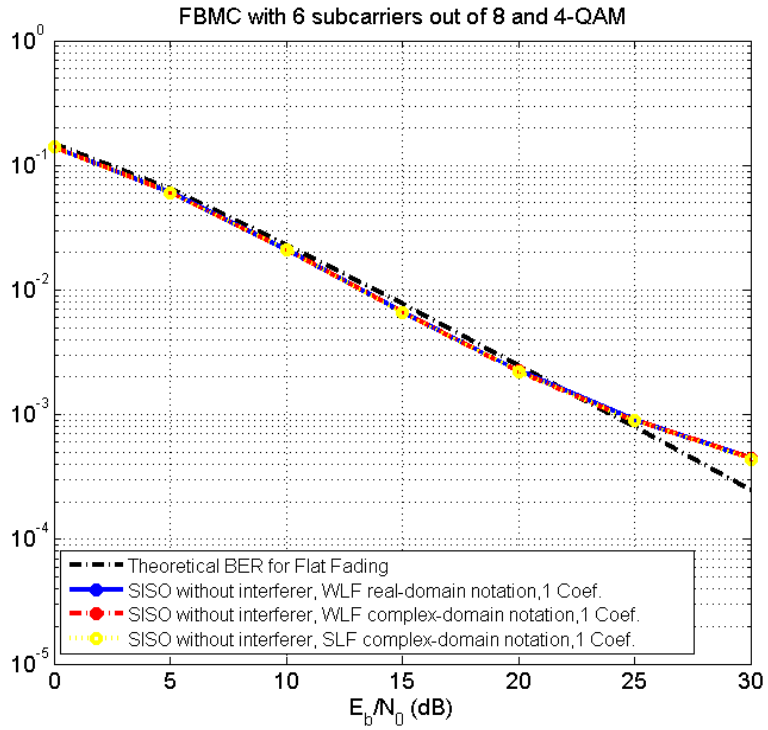

Fig. 3.7 Comparison between BER performances obtained using WLF processing in complex-domain notation -red, WLF processing in real-domain notation -blue; SLF processing in complex-domain notation –yellow; the case with overlapped subchannels and one-tap equalizer.

For the case of 4 out of 8 active subchannels (every second active subchannel), equivalence of WLF-based linear equalization in complex-domain notation (expression (3.3) with R_{yk} and P_{yk} defined according to (3.25) and (3.26)) and WLF-based linear equalization in real-domain notation (expression (3.24) with H_k defined according to (3.17)) is proven through comparison of the final values of coefficients as well as through BER performance, which is illustrated in Fig. 3-8. The same BER performances are obtained in the case of SLF-based linear equalization in the complex-domain notation (expression (3.27)), which is also illustrated in Fig. 3-8, but for differing values of coefficients which indicates expected different mechanism depending on the effectively acting constraints. Simulations are given for flat Rayleigh fading case and 4-QAM modulation.

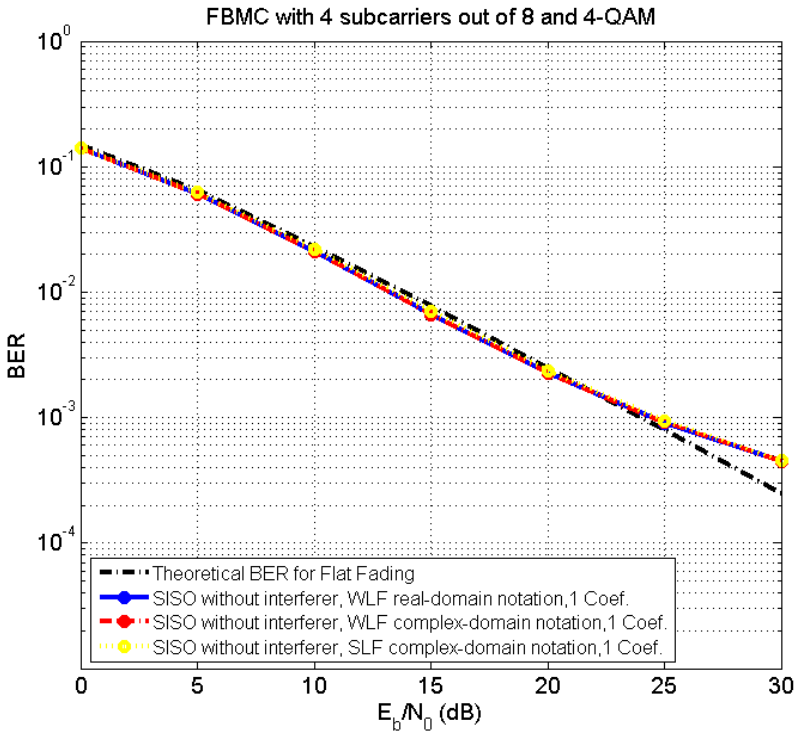

Fig. 3.8 Comparison between BER performances obtained using WLF processing in complex-domain notation -red, WLF processing in real-domain notation -blue; SLF processing in complex-domain notation – yellow; for the case with every second active subchannel; one-tap equalizer.

When we compare results from Figs. 3-7 and 3-8, it can be seen that in the considered case when there is no kindred co-channel interference, no essential difference in BER performance is noticeable, and all results fall close to the theoretical curve. It is important to say though, that the equivalence in the context of final values of coefficients, for case when every second subchannel is active, is present only between WLF-based equalization in complex-domain notation and WLF-based equalization in real-domain notation, but this equivalence is not present between WLF-based equalization and SLF-based equalization, although all results are equivalent in the context of BER performances. In the case with overlapped subchannels, WLF-based equalization yields to SLF-based equalization, because matrix $\mathbf{P}_{y_k}$ is zero-valued, and as the consequence of that all results depicted in Fig. 3-7 are same in context of final values of coefficients as well as in context of BER performances. This indicates that the "mechanism" by which the equalizer "operate" might be substantially different, depending on presence absence of adjacent subchannel interference, and/or accounting or not for the pseudocorrelation matrix in the complex-domain and one or the other form of correlation matrix in real-domain formulation. (Notably, when adjacent subchannels are present, the equalizer transfer function tends to invert the subchannel equivalent transfer function, while in the case of non-overlapped subchannels there are more degrees of freedom for coefficients adaptation, including the tendency to reconstruct the ideal rectangular transfer function by spectral overlapping around -1/2T and 1/2T; this increased degree of freedom can be also indicative of the co-channel interference cancellation potential.)

3.3. Analytical derivation of equalizer coefficients in the presence of kindred co-channel interference signal

Starting from the above given expressions for calculating equalizers coefficients in case of absence of co-channel interference signal, here are derived expressions for the case when kindred co-channel interference signal is present. We continue with the case when every second subchannel is active because in that way, as was discussed in the section above, the pseudo-correlation matrix is non-zero, ensuring the non-circular statistics of both the useful and its co-channel interfering signal. The case with overlapped subchannels will be treated bellow and the case with TLO FBMC configuration will be treated at some later date, which apparently may have the non-zero pseudo-correlation matrix.

First, we start from expression (3.24) given in real-domain notation with matrix H_k defined, by (3.17). By including the convolution matrix of interference signal $\mathbf{H}_k^{'}$ in (3.24), newly obtained expression is given with

$$\mathbf{u}_k^{'T} = \left[\mathbf{H}_k \cdot \mathbf{R}_x \cdot \mathbf{H}_k^T + \mathbf{R}_{\eta,k}^{'}\right]^{-1} \cdot \mathbf{H}_k \cdot \mathbf{R}_x \cdot \mathbf{e}_\nu \tag{3.28}$$

where $\mathbf{R}_{\eta,k}^{'}$ is interference correlation matrix given by

$$\mathbf{R}_{\eta,k}^{'} = \mathbf{\Gamma}^{'}{}_k \cdot (\mathbf{R}_\eta + \mathbf{H}_k^{'} \cdot \mathbf{R}_x \cdot \mathbf{H}_k^{'T}) \cdot \mathbf{\Gamma}_k^{'T} \tag{3.29}$$

$\mathbf{H}_k^{'} \in \mathbb{C}^{2R \times L'}$ is real-valued convolution matrix of interference signal in which is included the impact of transmitted prototype filter $h_k(n)$ and channel impulse response $h_{ch}(n)$ only (impact of received prototype filter $h_k(n)$ is included through interference convolution matrix $\mathbf{\Gamma}^{'}{}_k$).

$$\mathbf{H}_k^{'} = \begin{bmatrix} \mathbf{G}_k^{'(R)} \\ \mathbf{G}_k^{'(I)} \end{bmatrix} \tag{3.30}$$

where $\mathbf{G}_k^{'} \in \mathbb{C}^{R \times L'}$ is the down-sampled convolution matrix of interference signal in complex-domain, formed from impulse response $g_k^{'}(n) = [h_k(n) * h_{ch}(n)]$

$$\mathbf{G}_k^{'} = \begin{bmatrix} g_k^{'}(n) & \mathbf{0} & \cdots & \mathbf{0} & \mathbf{0} \\ \mathbf{0} & g_k^{'}(n) & & & \\ \vdots & \vdots & \ddots & \vdots & \vdots \\ & & & g_k^{'}(n) & \mathbf{0} \\ \mathbf{0} & \mathbf{0} & \cdots & \mathbf{0} & g_k^{'}(n) \end{bmatrix}_{\downarrow M/2} \tag{3.31}$$

Every second column of matrix $\mathbf{G}_k^{'}$ is multiplied by *j* as well as it was done with matrices in (3.17), and the number of rows after decimation in is $L^{'} = \lceil (Lg + L_{ch} + R - 2)/(M/2) \rceil$.

In the following are given expressions for equalizers coefficients in complex-domain notation. Starting from (3.3), new expression which takes into account presence of interference signal is obtained as

$$\mathbf{u}_k[n] = \mathbf{v}_k^*[n] = (\mathbf{R}'_{y_k} - \mathbf{P}'_{y_k}[n] \cdot \mathbf{R}'^{-1,*}_{y_k} \cdot \mathbf{P}'^{*}_{y_k}[n])^{-1} \cdot (\mathbf{r}_k - \mathbf{P}'_{y_k}[n] \cdot \mathbf{R}'^{-1,*}_{y_k} \cdot \mathbf{s}^*{}_k[n]) \quad (3.32)$$

where $\mathbf{R}'_{y_k}$ and $\mathbf{P}'_{y_k}$ represent correlation and pseudo-correlation matrices which take into account presence of interference signal, so that they are given with

$$\mathbf{R}'_{y_k}[n] = \mathbf{G}_k \cdot \mathbf{R}_{x_k}[n] \cdot \mathbf{G}_k^H + \mathbf{\Gamma}_k \cdot (\mathbf{R}_\eta + \mathbf{G}'_k \cdot \mathbf{R}_{x_k}[n] \cdot \mathbf{G}'^H_k) \cdot \mathbf{\Gamma}_k^H \quad (3.33)$$

$$\mathbf{P}'_{y_k}[n] = \mathbf{G}_k \cdot \mathbf{P}_{x_k}[n] \cdot \mathbf{G}_k^T + \mathbf{\Gamma}_k \cdot (\mathbf{P}_\eta + \mathbf{G}'_k \cdot \mathbf{P}_{x_k}[n] \cdot \mathbf{G}'^T_k) \cdot \mathbf{\Gamma}_k^T \quad (3.34)$$

$\mathbf{G}'_k \in \mathbb{C}^{R \times L'}$ is down-sampled convolution matrix of interference signal given with (3.31).

In the case of SLF-based linear equalization expression for calculating of equalizer's coefficients is given with

$$\mathbf{u}_k[n] = \mathbf{v}_k^*[n] = (\mathbf{G}_k \cdot \mathbf{R}_{x_k}[n] \cdot \mathbf{G}_k^H + \mathbf{\Gamma}_k \cdot (\mathbf{R}_\eta + \mathbf{G}'_k \cdot \mathbf{R}_{x_k}[n] \cdot \mathbf{G}'^H_k) \cdot \mathbf{\Gamma}_k^H)^{-1} \cdot (\mathbf{r}_k) \quad (3.35)$$

In Fig. 3-9, are presented BER performances obtained using expression (3.28) (WLF-based equalization in real-domain notation) and expression (3.32) (WLF-based equalization in complex-domain notation). Results are given for three different values of signal to interference ratio (SIR=-10 dB, SIR=0 dB and SIR=10 dB) and for the flat Rayleigh fading case and 4-QAM modulation.

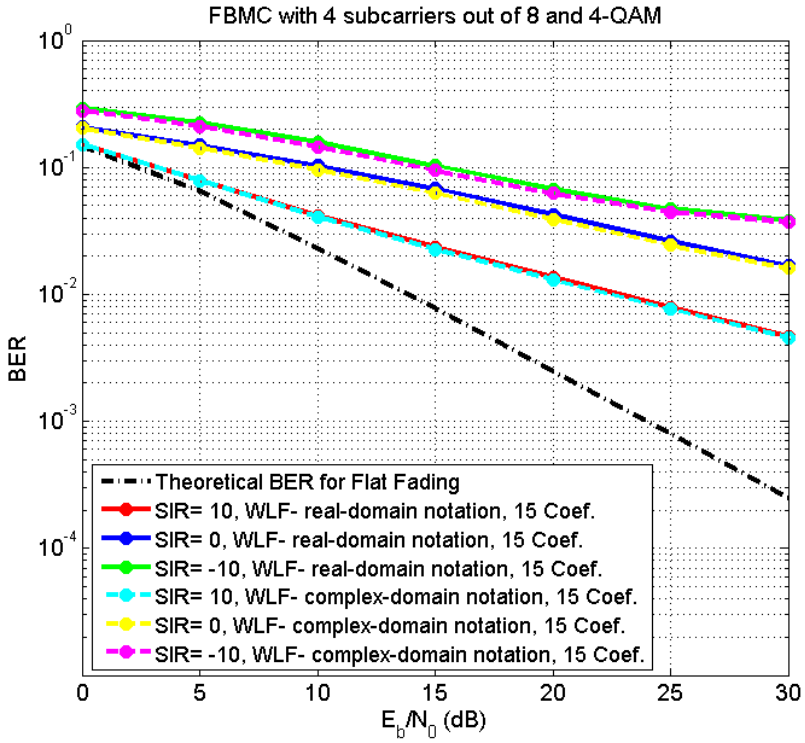

Fig. 3.9 Comparison between BER performances obtained using WLF-based equalization in real-domain notation (solid lines) and using WLF-based equalization in complex-domain notation (dashed lines) for SIR=-10 dB-green, SIR=0 dB-blue and SIR=10 dB-red; the case with every second active subchannel; 15-tap equalizer.

For further comparison for the sake of checking, in Fig. 3-10 **¡Error! No se encuentra el origen de la referencia.** for SIR = 0 dB are presented BER performances obtained using expression (3.32) (red line - WLF-based equalization in complex-domain notation), expression (3.32) for the case when the correlation and pseudo-correlation matrices of interference signal are omitted from expressions (3.33) and (3.34). (The blue line- WLF-based equalization in complex-domain notation which does not take into account correlation and pseudo-correlation matrices of interference signal-in figure denotes an incomplete WLF-based equalization in complex-domain notation), and the expression (3.35) (green line - SLF-based equalization in complex-domain notation). Results are also given for the flat Rayleigh fading case and 4-QAM modulation.

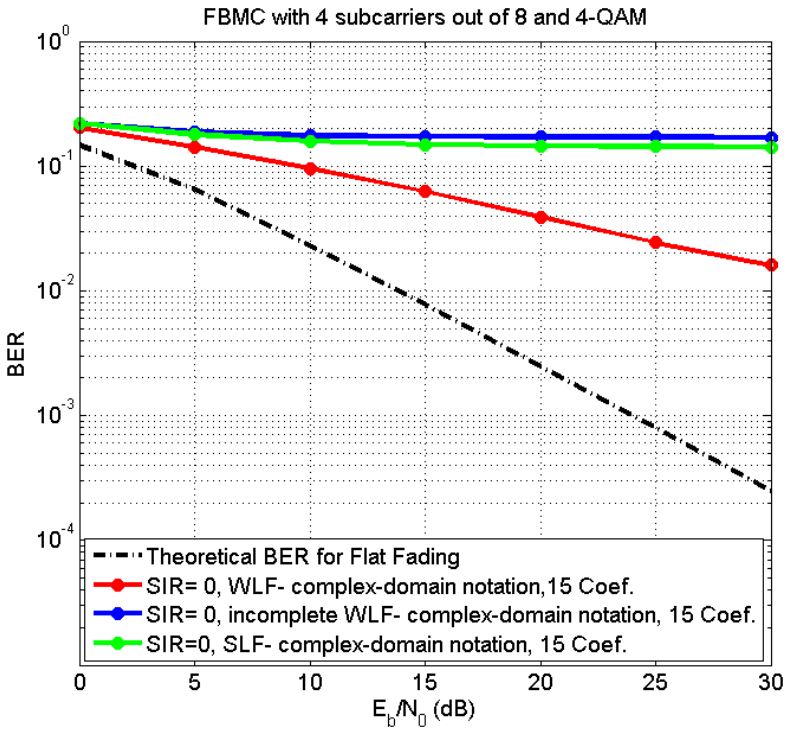

Fig. 3.10 Comparison between BER performances obtained using WLF-based equalization in complex-domain notation (red line), using incomplete WLF-based equalization in complex-domain notation (blue line) and using SLF-based equalization in complex-domain notation (green line) for SIR= 0 dB; the case with every second active subchannel; 15-tap equalizer.

From Fig. 3-9, it is noticeable that the results obtained in the real-domain are same as results obtained in the complex-domain, i.e. equivalence between those two notations is same as it was the case when interference signal was not present. From Fig. 3-10, it can be seen that the WLF-based equalization which takes into account correlation and pseudo-correlation matrices of interference signal gives significantly better result than WLF-based equalization which does not take in account correlation and pseudo-correlation matrices of interference signal and SLF-based equalization.

In the following, we will be presenting expressions and accompanying results for the case with overlapped subchannels, when - due to the essentially 100% roll-off factor used - the pseudo-correlation matrix is zero-valued. In this case in real-domain notation expression for equalizer's coefficients is given with

$$\mathbf{u}_k^{'T} = \left[\mathbf{H}_k \cdot \mathbf{R}_x \cdot \mathbf{H}_k^T + \mathbf{F}_k \cdot \hat{\mathbf{R}}_x \cdot \mathbf{F}_k^T + \mathbf{R}_{\eta,k}^{'}\right]^{-1} \cdot \mathbf{H}_k \cdot \mathbf{R}_x \cdot \mathbf{e}_v \tag{3.36}$$

where $\mathbf{R}_{\eta,k}^{'}$ is interference correlation matrix given by

$$\mathbf{R}_{\eta,k}^{'} = \mathbf{\Gamma}^{'}{}_k \cdot (\mathbf{R}_\eta + \mathbf{H}_k^{'} \cdot \mathbf{R}_x \cdot \mathbf{H}_k^{'T} + \mathbf{S}_k^{'} \cdot \hat{\mathbf{R}}_{x-1} \cdot \mathbf{S}_k^{'T} + \mathbf{T}_k^{'} \cdot \hat{\mathbf{R}}_{x+1} \cdot \mathbf{T}_k^{'T}) \cdot \mathbf{\Gamma}^{'T}_k \tag{3.37}$$

$\mathbf{S}_k^{'} \in \mathbb{C}^{2R \times L'}$ is real-valued convolution matrix which contains interference from (k-1)-th to k-th subcarrier of interference signal and $\mathbf{T}_k^{'} \in \mathbb{C}^{2R \times L'}$ is real-valued convolution matrix which contains interference from (k+1)-th to k-th subcarrier of interference signal. As it was case with $\mathbf{H}_k^{'}$, in matrices $\mathbf{S}_k^{'}$ and $\mathbf{T}_k^{'}$ are included the impact of transmitted prototype filter $h_{k-1}(n)$ (for $\mathbf{S}_k^{'}$) and $h_{k+1}(n)$ (for $\mathbf{T}_k^{'}$) and channel impulse response $h_{ch}(n)$ only (impact of received prototype filter $h_k(n)$ is included through interference convolution matrix $\mathbf{\Gamma}^{'}_k$).

$$\mathbf{S}_k^{'} = \begin{bmatrix} \mathbf{M}_k^{'(R)} \\ \mathbf{M}_k^{'(I)} \end{bmatrix} \mathbf{T}_k^{'} = \begin{bmatrix} \mathbf{N}_k^{'(R)} \\ \mathbf{N}_k^{'(I)} \end{bmatrix} \tag{3.38}$$

where $\mathbf{M}_k^{'} \in \mathbb{C}^{R \times L'}$ and $\mathbf{N}_k^{'} \in \mathbb{C}^{R \times L'}$ are the down-sampled convolution matrices of (k-1)-th and (k+1)-th subchannel's of interference signal in complex-domain, formed from impulse responses $m_k^{'}(n) = [h_{k-1}(n) * h_{ch}(n)]$ and $n_k^{'}(n) = [h_{k+1}(n) * h_{ch}(n)]$, respectively

$$\mathbf{M}_k^{'} = \begin{bmatrix} m_k^{'}(n) & \mathbf{0} & \cdots & \mathbf{0} & \mathbf{0} \\ \mathbf{0} & m_k^{'}(n) & & & \\ \vdots & \vdots & \ddots & \vdots & \vdots \\ & & & m_k^{'}(n) & \mathbf{0} \\ \mathbf{0} & \mathbf{0} & \cdots & \mathbf{0} & m_k^{'}(n) \end{bmatrix}_{\downarrow M/2} \quad \mathbf{N}_k^{'} = \begin{bmatrix} n_k^{'}(n) & \mathbf{0} & \cdots & \mathbf{0} & \mathbf{0} \\ \mathbf{0} & n_k^{'}(n) & & & \\ \vdots & \vdots & \ddots & \vdots & \vdots \\ & & & n_k^{'}(n) & \mathbf{0} \\ \mathbf{0} & \mathbf{0} & \cdots & \mathbf{0} & n_k^{'}(n) \end{bmatrix}_{\downarrow M/2} \tag{3.39}$$

Each second column of matrices $\mathbf{M}_k^{'}$ and $\mathbf{N}_k^{'}$ is multiplied by *j* as well as it was done with matrices in (3.17), and the number of rows after decimation is $L^{'} = \lceil (Lg + L_{ch} + R - 2)/(M/2) \rceil$.

In complex-domain notation expression for equalizers coefficients is same as one defined with (3.32), but with different definition of matrices $\mathbf{R}_{y_k}^{'}$ and $\mathbf{P}_{y_k}^{'}$.

$$\mathbf{R}_{y_k}^{'}[n] = \mathbf{G}_k \cdot \mathbf{R}_{x_k}[n] \cdot \mathbf{G}_k^H + \mathbf{M}_k \cdot \mathbf{R}_{x_{k-1}}[n] \cdot \mathbf{M}_k^H + \mathbf{N}_k \cdot \mathbf{R}_{x_{k+1}}[n] \cdot \mathbf{N}_k^H + \mathbf{\Gamma}_k \cdot (\mathbf{R}_\eta + \mathbf{G}_k^{'} \cdot \mathbf{R}_{x_k}[n] \cdot \mathbf{G}_k^{'H} + \mathbf{M}_k^{'} \cdot \mathbf{R}_{x-1_k}[n] \cdot \mathbf{M}_k^{'H} + \mathbf{N}_k^{'} \cdot \mathbf{R}_{x_k+1}[n] \cdot \mathbf{N}_k^{'H}) \cdot \mathbf{\Gamma}_k^H \tag{3.40}$$

$$\mathbf{P}_{y_k}^{'}[n] = \mathbf{G}_k \cdot \mathbf{P}_{x_k}[n] \cdot \mathbf{G}_k^T + \mathbf{M}_k \cdot \mathbf{P}_{x_{k-1}}[n] \cdot \mathbf{M}_k^T + \mathbf{N}_k \cdot \mathbf{P}_{x_{k+1}}[n] \cdot \mathbf{N}_k^T + \mathbf{\Gamma}_k \cdot (\mathbf{P}_\eta + \mathbf{G}_k^{'} \cdot \mathbf{P}_{x_k}[n] \cdot \mathbf{G}_k^{'T} + \mathbf{M}_k^{'} \cdot \mathbf{P}_{x_k-1}[n] \cdot \mathbf{M}_k^{'T} + \mathbf{N}_k^{'} \cdot \mathbf{P}_{x_k+1}[n] \cdot \mathbf{N}_k^{'T}) \cdot \mathbf{\Gamma}_k^T \tag{3.41}$$

$\mathbf{M}_k^{'} \in \mathbb{C}^{RxL'}$ and $\mathbf{N}_k^{'} \in \mathbb{C}^{RxL'}$ are down-sampled convolution matrices given with (3.39). It is important to mention that the pseudo-correlation matrix $\mathbf{P}_{y_k}^{'}$ in (3.41) will be reduced only to pseudo-correlation matrix of noise because the pseudo-correlation matrices of desired and interference signal are zero valued.

In the case of SLF-based linear equalization and case with overlapped subchannels, expresbsion for calculating the equalizer's coefficients is given with

$$\mathbf{u}_k[n] = \mathbf{v}_k^*[n] = (\mathbf{R}_{y_k}^{'})^{-1} \cdot (\mathbf{r}_k) \tag{3.42}$$

where $\mathbf{R}_{y_k}^{'}$ is given with (3.40).

In Fig. 3-11, are presented BER performances obtained using expression (3.36) (WLF-based equalization in real-domain notation) and expression (3.32) with matrices $\mathbf{R}_{y_k}^{'}$ and $\mathbf{P}_{y_k}^{'}$ defined with (3.40) and (3.41) (WLF-based equalization in complex-domain notation). Results are given for three different values of signal to interference ratio (SIR=-10 dB, SIR=0 dB and SIR=10 dB) and for the flat Rayleigh fading case and 4-QAM modulation.

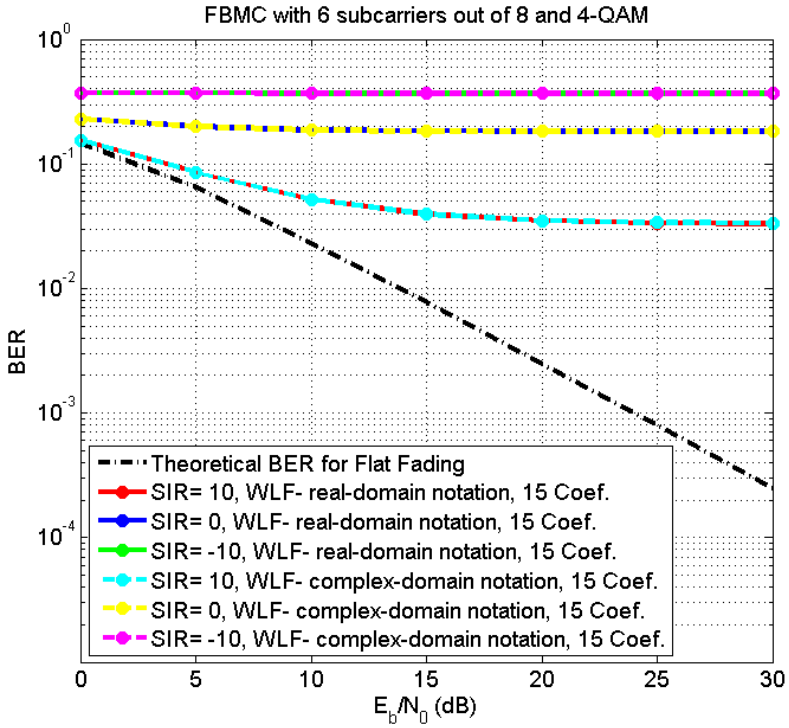

Fig. 3.11 Comparison between BER performances obtained using WLF-based equalization in real-domain notation (solid lines) and using WLF-based equalization in complex-domain notation (dashed lines) for SIR=-10 dB-green, SIR=0 dB-blue and SIR=10 dB-red; the case with overlapped subchannels; 15-tap equalizer.

For the purpose of comparison and further checking, in Fig. 3-12 for SIR = 0 dB are presented BER performances obtained using expression (3.32) with matrices $\mathbf{R}_{y_k}^{'}$ and $\mathbf{P}_{y_k}^{'}$ defined with (3.40) and (3.41) (solid line- WLF-based equalization in complex-domain notation), expression (3.32) for the case when the correlation and pseudo-correlation

matrices of interference signal are omitted from expressions (3.40) and (3.41) (dashed line- WLF-based equalization in complex-domain notation which does not take in account correlation and pseudo-correlation matrices of interference signal) and expression (3.42) (dotted line- SLF-based equalization in complex-domain notation). Results are also given for the flat Rayleigh fading case and 4-QAM modulation.

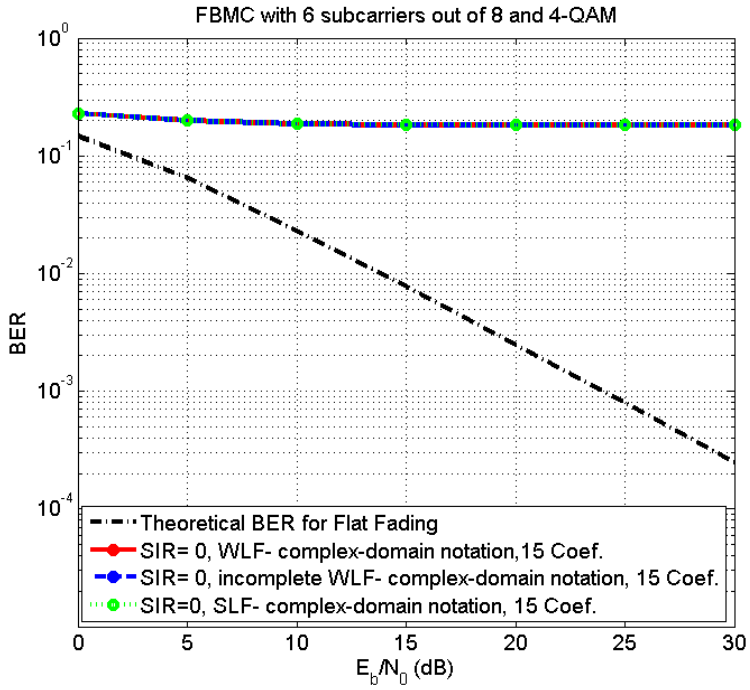

Fig. 3.12 Comparison between BER performances obtained using WLF-based equalization in complex-domain notation (red line), using incomplete WLF-based equalization in complex-domain notation (blue line) and using SLF-based equalization in complex-domain notation (green line) for SIR= 0 dB; the case with overlapped subchannels; 15-tap equalizer.

From Fig. 3-11, it is noticeable that the results obtained in the real-domain are same as results obtained in the complex-domain as it was the case with every second active subchannel (Fig. 3-9). But, when we compare performances in Figs. 3-11 and 3-9 results are significantly worse for the case of overlapped subchannels, as a consequence of the loss of additional degree of freedom, which WLF equalization provides for non-circular statistics for which applies that the pseudo-correlation matrix is non-zero.

From Fig. 3-12, it can be seen that the all BER performances are same and very poor. There are no difference between WLF-based equalization in complex-domain notation, incomplete WLF-based equalization in complex-domain notation, and SLF-based equalization in complex-domain notation.

In all the considered cases the number equalizer coefficients is substantially larger that in the case without presence of co-channel interference, when just one-tap equalizer is sufficient. From that reason in Table 3-1 (and Fig. 3-13) are given BER values for SNR = 30 dB in function of different numbers of equalizer's coefficients. Results are given for the case of SIR = 0 dB, for WLF-based equalization in complex domain. In the same table (figure) are given BER values for the case when every second subchannel is active and the case with overlapped subchannels. It should be noted that for the case with two coefficients actually corresponds to just one, since the other one is essentially zero, and this had to be done

because of unavailability of option to define just one coefficient in the simulation set-up used.

Table 3.1 BER performances for SNR = 30 dB and SIR = 0 dB in function of number of equalizer's coefficients for every second active subchannel and overlapped subchannels.

	Every second active subchannel	Overlapped subchannels
Number of equalizer's coefficients	BER[SNR=30 dB, SIR=0 dB]	BER[SNR=30 dB]
2	0.1551	0.1821
3	0.0408	0.1818
5	0.0338	0.1819
7	0.0215	0.1818
9	0.0190	0.1816
11	0.0174	0.1821
13	0.0168	0.1823
15	0.0159	0.1812
17	0.0160	0.1818

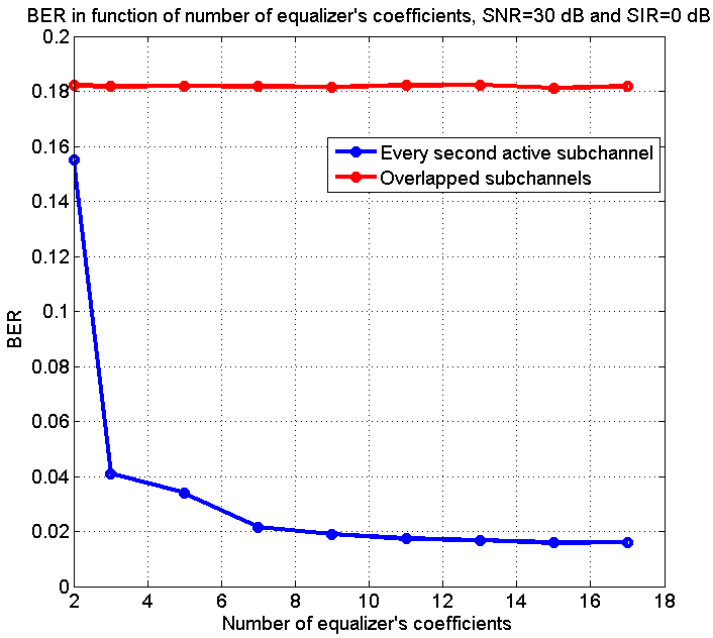

Fig. 3.13 BER performances for SNR = 30 dB and SIR = 0 dB in function of number of equalizer's coefficients for every second active subchannel (blue line) and overlapped subchannels (red line)

As can be seen for Table 3.1 (or Fig. 3-13), in presence of interference signal, the one-tap equalizer is not sufficient and BER performances are steadily improving with increasing the number of equalizer's coefficients for the case when every second subchannel is active. For the case of overlapped subchannels, BER values are approximately same for the all numbers of equalizer's coefficients.

3.4. Conclusion

This rather comprehensive treatment of the co-channel interference resilience of the FBMC/OQAM format with the use of MMSE WLF clearly indicates certain gain in comparison with the strictly linear MMSE EQL approach, attained when the circular statistics was imposed by the avoidance of spectral overlapping among subchannels. This leads to the need to revisit the classical FBMC waveforms as studied so far. On the other side, it motivates the striving to similar SNR gains for overlapped subchannels with relatively small roll-off factors, FMT subchannels configuration with I/Q staggering, and particularly the fully overlapped TLO FB-MC subchannels (documented in D2.1). While the latter option offers an appealing trade-off between spectral efficiency and the transmission latency, it actually – at least for the case of 4-QAM constellation, and of course can be used for higher constellation sizes – represents the linearized form of the GMSK modulation format having been the basis for the 2G GSM wireless cellular system. The staggered FMT format would also "fall" close to it.

We will explore the impact of spectral overlapping of subchannels with roll-off factors smaller than one, as well as the case where sunchannels overlap among several consecutive subchannels, a it is the case in the time-limited (TLO) multi-carrier waveform case, including also the non-overlapping subchannels with relatively small roll-off factors to trade-off spectral efficiency and the so-channel interference suppression capability.

4. Adaptive Equalization of Doubly Dispersive Channels

Early studies of channel equalization in FBMC/OQAM systems include [3, 16], where rather simple methods were considered, to cope with channels of limited time- and frequency-selectivity. The special nature of staggered QAM (OQAM) and its role in the design of a (decision feedback) equalizer was first considered in [5]. The latter work emphasized the obvious yet very important fact that the equalizer design should not consider recovering the interference (imaginary) part of the FBMC signal. This saves degrees of freedom, allowing the designer to concentrate on the useful signal part and hence achieve higher equalization performance. More work on FBMC/OQAM equalization, exploiting its special nature, was reported in [17, 18, 19]. The time-frequency selectivity of the channel was more explicitly taken into account in works including [7, 20, 21, 22]. Recently, the correlation statistics of the intrinsic interference was analyzed, giving rise to an equalization scheme that shows performance gain over more classical equalizers not exploiting this characteristic of the interference component [23]. In [9], a simple yet quite effective technique of designing per-subcarrier multi-tap equalizers was developed. It relies on samples of the channel frequency response (CFR), assumed known. A *frequency sampling* approach was also followed in [24], where the equalizer is designed using geometric interpolation. Explicit input/output models that take the specifics of the filter bank system into account and make no assumption on the frequency selectivity of the subchannels (thus requiring multi-tap equalizers) were developed in [8] and [25], for minimum mean squared error (MMSE) linear and decision feedback equalizers, respectively. Similar but less straightforward approaches were reported in [26, 27, 28].

Adaptive equalization algorithms, able to cope with *doubly* selective channels, were developed and tested in [7, 29, 30]. In all of these works, initial channel information is assumed to be available and used to appropriately initialize the equalizer filters (see [1] for a detailed overview). A rather simplistic adaptive FBMC/OQAM equalizer (based on a straightforward application of the least mean squares (LMS) algorithm) was recently tested in [31]] and brings nothing new to our knowledge of this area.

The aim of this chapter is to provide a concise picture of the adaptive equalization problem in FBMC/OQAM-based systems characterized by highly time- and/or frequency-selective channels such as those encountered in PMR scenarios. Our contribution is split into three parts. First, the possible gains from using a diversity enhancing precoder at the transmitter are evaluated. As an example, a Walsh-Hadamard transformation (WHT) is tested, in view of its proven success in OFDM systems and the low additional computational cost it entails. To simplify the presentation and avoid the extra complexity (associated with the need to use forward and inverse transformations) that an adaptive algorithm would imply, only time invariant (but highly frequency selective) channels are assumed in this first part. Time varying channels are considered in the second and third parts. The former is concerned with channel estimate-based design of the equalizers and relies on pilot-assisted channel tracking to deal with the fast fading nature of the channel. The role of the scattered pilots, designed to follow an LTE format while also taking the intrinsic interference into account, is made

apparent in thish part. Finally, adaptive algorithms for *direct* per-subcarrier equalization are evaluated in the third part of the chapter. Here, the sparse structure that the subchannel responses often exhibit is exploited through the application of a computationally efficient yet highly performing adaptive algorithm, designed so as to speed up the adaptation of equalizer filters that are themselves of a sparse nature.

4.1 FBMC/OQAM equalization using Walsh-Hadamard transformation

That the use of a WHT precoder (with a corresponding postcoder at the receiver) can considerably improve the performance of OFDM equalization, particularly in channels of low coherence bandwidth that exhibit deep nulls in the frequency domain, was demonstrated in [32], among others. The reason behind the positive effect of such a precoder is that it effectuates an increase in frequency diversity (through the "spreading" of the subcarriers in frequency). Recently, this idea was also applied in an FBMC/OQAM system [33] and significant gains in bit error rate (BER) over the classical non-precoded system were reported. A schematic diagram of the WHT-based system is shown in Fig. 4.1 . Note that the WHT is very cheap in terms of computational cost as it only involves additions/subtractions, and there are widely available fast algorithms for its implementation (which, moreover, can be applied jointly with (I)FFT [32]).

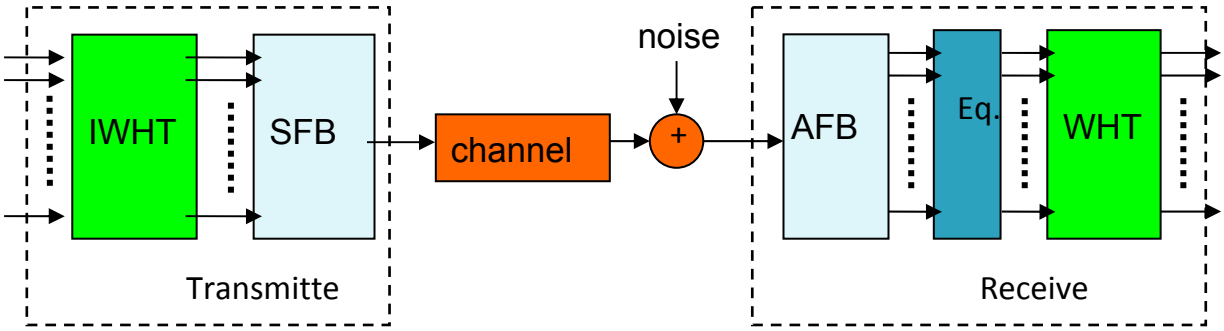

Fig. 4.1 WHT-based multicarrier system [32].

In this section, we report some illustrative results from comparing WHT-based with classical systems, including the CP-OFDM in the comparison. Fig. 4.2 shows the BER performances of *single*-tap minimum mean squared error (MMSE) per-subcarrier equalizers for both CP-OFDM and FBMC/OQAM systems with and without WHT. The PHYDYAS filter bank [34] was employed, with $M = 128$ and $K = 3$. Two channel models, of (a) moderate (ITU-VehA) and (b) high (3GPP-HT) frequency selectivity were considered. The subcarrier spacing was chosen as it is common in LTE, namely $\Delta f = 15\,\mathrm{kHz}$. In both cases, the CP length in CP-OFDM was chosen equal to $M/4$. In this and all of the experiments reported in this chapter, QPSK symbols were transmitted. One can see that the WHT-based schemes greatly outperform the conventional ones, with the FBMC/OQAM system to be somewhat better than CP-OFDM in low to moderate signal to noise ratio (SNR) values. At higher SNRs, the well known error floors of FBMC/OQAM manifest themselves. The latter effect is more severe as the flat subchannel assumption (underlying the adoption of a single-tap equalizer)

becomes less accurate (see Fig. 4.2 (b)). The error floors in the CP-OFDM schemes in Fig. 4.2 (b) are due to the inadequacy of the CP duration in this case. The result is residual intersymbol (ISI) and intercarrier interference (ICI) that the simple per-subcarrier equalizer is unable to deal with.

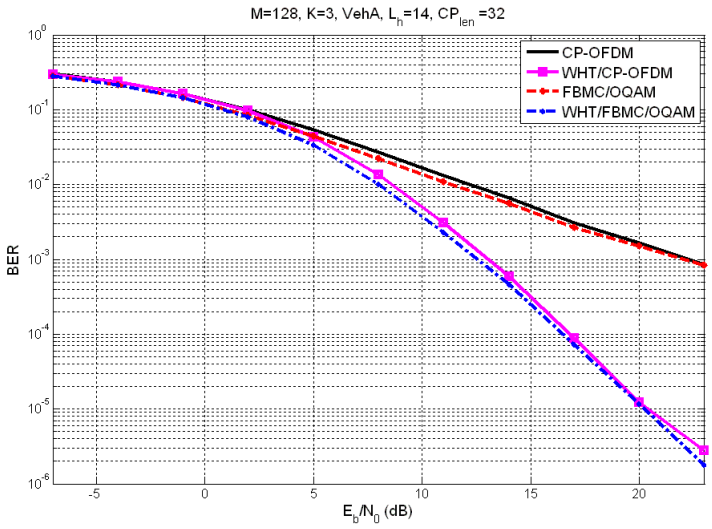

(a)

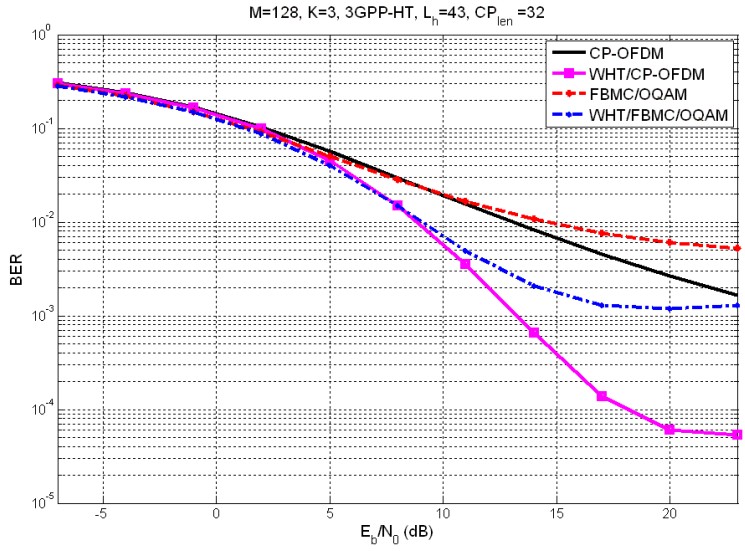

(b)

Fig. 4.2 Comparison of WHT-based schemes with conventional ones. Time-invariant *perfectly known* channels are assumed, following the (a) ITU-VehA and (b) 3GPP-HT models. Results of per-subcarrier *single*-tap MMSE equalization.

4.2 Adaptive equalization based on channel tracking

To cope with time varying channels, pilots are needed to be placed in the frame, in addition to a known preamble at its beginning. In this work, an LTE-compatible pilot configuration was used, as shown in Fig. 4.3 and Fig. 4.4 As shown in Fig. 4.3 , a frame consists of 10 subframes, each composed of 15 OFDM multicarrier symbols, for a total of 150 OFDM symbols in the frame payload. A preamble of 3 OFDM (equivalent to 6 FBMC) symbols is assumed to be transmitted in the beginning of the frame. Note that this is only *half as long* as the preamble proposed in the Milestone-4 (MS4) document. Results using a preamble of 6 OFDM (=12 FBMC) symbols will be provided in the next subsection.

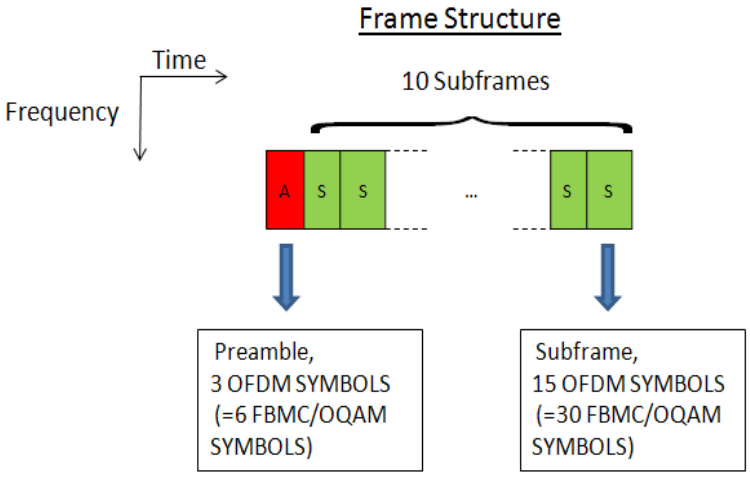

Fig. 4.3 LTE-based frame structure for the FBMC/OQAM system.

The pilots scattered in each subframe follow the *De-Modulation Reference Signal (DMRS antenna port 5)* LTE configuration. This is shown in Fig. 4.3 for the FBMC/OQAM system.

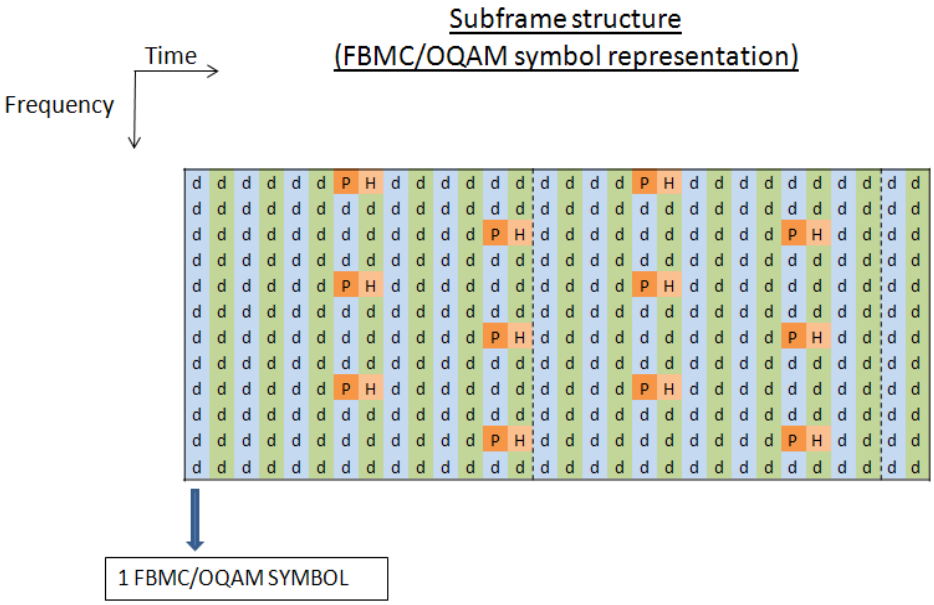

Fig. 4.4 LTE-based sub-frame structure, for the FBMC/OQAM system. “P” and “H” denote pilots and help (auxiliary) pilots, respectively. “d” stands for data.

The dashed lines in Fig. 4.3 denote the boundaries of LTE slots. Next to each *half-symbol* pilot ("P") there is an auxiliary (or help, "H") pilot. The latter is computed as usually in FBMC/OQAM to render the interference which is contributed to the pilot by its immediate neighbours equal to zero. This allows one to employ such pilots to compute estimates of the CFR. In this work, we have used these scattered pilots to aid tracking the channel. An initial estimate is provided by the preamble (in accordance to the methodologies presented in D3.1). In contrast to what we did in the PHYDYAS project (see [34] for the general MIMO case), namely using an LMS algorithm working in the decision-directed (DD) mode to track the channel[2] or employing linear interpolation in time for this task, we here follow a more straightforward approach which has been seen to be equally or even better performing. The channel impulse response (CIR) is estimated at each pilot symbol in much the same way as done for sparse preambles in the EMPhAtiC deliverable D3.1. This is possible thanks to the presence of the help pilots. The CIR estimate is then used to set a 3-tap equalizer (designed via frequency sampling as in [9]). This equalizer is used to recover the input data until the next pilot instant, where a new channel estimate is computed. In the period between two consecutive pilots instants, equal to 5 FBMC/OQAM symbols, the channel is assumed almost time invariant. Notice that this setup allows straightforward application of sparsity-aware channel estimation and equalizer initialization techniques in case the number of pilots available for estimation is smaller than the length of the CIR but larger than the number of significant CIR coefficients. Such a technique, based on the Orthogonal Matching Pursuit (OMP) algorithm, was also described and tested in D3.1. See [35, 36] for more on this aspect. In the experiments of this section, all subcarriers were assumed to be active, for the sake of simplicity. Sparse long CIRs can be taken care of in the presence of null spectrum edges (inactive subcarriers) via techniques like [37, 38, 39].

Some examples of the BER performance of the method described above are shown in Fig. 4.5

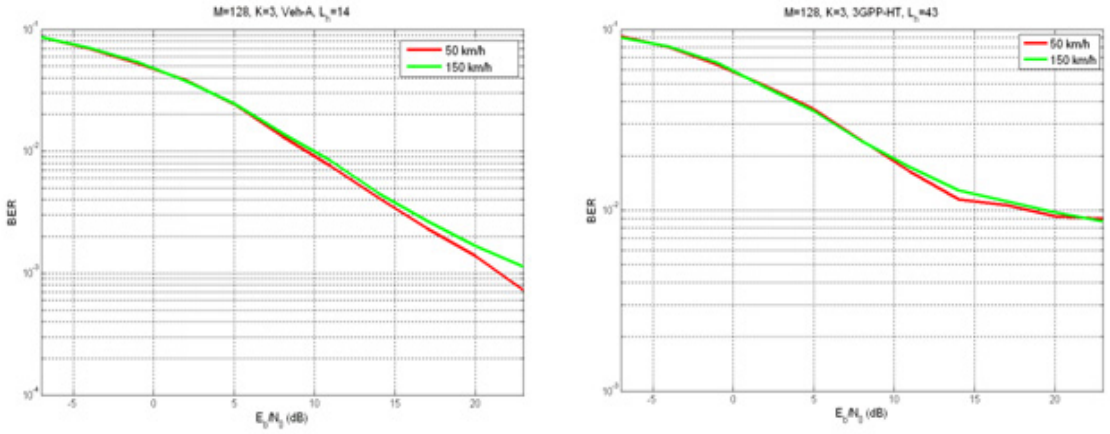

(a) (b)

Fig. 4.5 BER performance of ZF 3-tap equalizer [9] based on CIR tracking for (a) ITU-VehA and (b) 3GPP-HT channels, at vehicular speeds of 50 km/h and 150 km/h.

[2] Kalman filter-based tracking was also investigated in the PHYDYAS project. Analogous work, using *dual* Kalman filters to track both the channel model and its parameters, was recently reported in [52].

The same filter bank was adopted as previously, with the same subcarrier spacing. Two channel models, of moderate (a) and high (b) frequency selectivity were considered, at a medium (50 km/h) and a high (150 km/h) mobile speed. The carrier frequency was set to 400 MHz. One can see that the channel tracking-based equalizer is robust to mobility, especially at low and medium SNRs. It is of interest to remark that error floors appear in Fig. 4.5 (b) at high SNR values. This should not be unexpected in view of the high frequency selectivity of the channel which does not justify in this case calculating the help pilots in the usual, classical manner, relying on the assumption of flat subchannel CFRs.

4.3 Direct adaptive equalization – Sparsity promoting algorithm

The pilot configuration described above was also used to aid the adaptation of *direct* equalization algorithms, that is, not relying on estimates of the channel itself. Both linear (LE) and decision-feedback equalizers (DFE), following Tu's principle [5] as in [1, 29, 30], were tested. Normalized LMS (NLMS) adaptation was preferred due to its lower (than recursive least squares (RLS)) complexity and satisfactory tracking performance. Moreover, only results from LE are reported here, since – as also pointed out in [1] – DFEs showed no better performance than the LEs in this context.

In addition to the NLMS LE algorithms, a modified version of the NLMS recursion was also tested, which aims at facilitating the adaptation of *sparse* equalizer filters. It was shown – both experimentally and via theoretical arguments – at several places in the equalization literature (see, e.g., [40]) that the equalizer filters corresponding to sparse channel impulse responses are very often sparse as well. This allows the use of sparsity-aware (or sparsity-promoting) algorithms that take this structure into account in order to provide faster convergence and better equalization performance. A sparse CIR also leads to sparse subchannel impulse responses. An example is provided in Fig. 4.6, where the amplitude of a 3GPP-HT CIR is shown, along with the response of one of the resulting subchannels. Observe the sparse nature of both the broadband and narrowband CIRs.

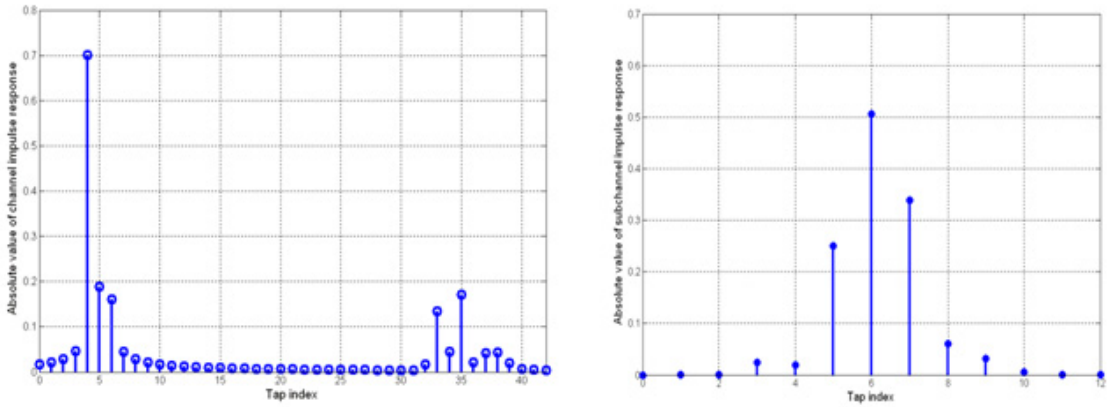

(a) (b)

Fig. 4.6 Amplitude of the impulse response of (a) a 3GPP-HT channel and (b) one of the corresponding FBMC/OQAM subchannels.

Hence gains from sparsity-aware equalization can also be attained through the adoption of such an algorithm on a per-subchannel basis. To keep things as simple as NLMS, a so called *improved proportionate NLMS (IPNLMS)* algorithm was adopted in our experiments, which is only a slightly modified version of conventional NLMS [41]]. The idea is to *adapt* the step size for each of the weights of the equalizer in such a way that more significant weights are allowed to converge faster than less significant ones ("proportionate" step size), allowing faster convergence for sparse equalizers. This has been applied so far in acoustics (for echo cancellation) and underwater communication problems, and shown to be quite successful in such applications. In fact, its underlying idea, though quite simple in its conception, can be shown to correspond to the use of the *natural* gradient instead of the conventional one, which can be shown to be a more suitable choice for filters that exhibit a sparse structure [42, 43]. The IPNLMS recursion for the k th-subcarrier equalizer of length L_{eq} is given by

$$\mathbf{w}_k(n) = \mathbf{w}_k(n-1) + \mu \frac{\mathbf{G}_k(n)\mathbf{y}_k(n)}{\mathbf{y}_k(n)^H \mathbf{G}_k(n)\mathbf{y}_k(n) + \delta} e_k^*(n)$$

where $\mathbf{y}_k(n)$ is the corresponding equalizer input (AFB output), μ denotes the NLMS step size, δ is a small positive constant aiming at preventing division by zero, and

$$e_k(n) = \breve{d}_k(n) - \widetilde{d}_k(n)$$

is the *a-priori* adaptation error, with

$$\widetilde{d}_k(n) = \Re\left\{\mathbf{w}_k(n-1)^H \mathbf{y}_k(n)\right\}$$

and

$$\breve{d}_k(n) = \begin{cases} d_k(n-\Delta), & (k, n-\Delta) \text{is a pilot position} \\ \text{dec}\left[\widetilde{d}_k(n)\right], & \text{otherwise} \end{cases},$$

where Δ is the equalization delay and dec[.] denotes the decision device (e.g., sign(.) for OQPSK) providing the desired output to the algorithm in its DD mode of operation. $\mathbf{G}_k(n)$ stands for a diagonal matrix with diagonal entries computed as

$$\left[\mathbf{G}_k(n)\right]_{i,i} = \frac{1-\alpha}{2L_{\text{eq}}} + \frac{1+\alpha}{2\left\|\mathbf{w}_k(n-1)\right\|_1 + \varepsilon}\left|\left[\mathbf{w}_k(n-1)\right]_i\right|, \; i = 1,2,\ldots,L_{\text{eq}}.$$

One can see that it consists of two parts: a constant one, which ensures a minimum speed of convergence, and a variable one, which is larger for larger weights. Notice the dependence of the above quantity on the ℓ_1-norm, known in sparse signal processing for its sparsity promoting effect. As previously, a small positive constant, ε, is employed to ensure that division by zero will be avoided. The principal role in this modified version of NLMS is played by the constant α, which is allowed to take values in [-1, 1]. The closer to -1 is this constant the less care is taken of sparsity. In fact, the algorithm reduces to the well known NLMS for $\alpha = -1$. On the other hand, sparsity is promoted for values of α closer to 1. IPNLMS is known to be robust to lack of sparsity, i.e., it will still offer a satisfactory performance even if the equalizer filter is far from being classified as sparse [41]. In the simulations to be reported below, α was set to 0.5. Moreover, $L_{\text{eq}} = 5$, $\Delta = 0$, and $\mu = 0.5$ were assumed. Unless stated otherwise, the same parameters as previously were employed,

namely PHYDYAS filter bank with $M = 128$ and $K = 3$, subcarrier spacing of $\Delta f = 15\,\text{kHz}$, carrier frequency 400 MHz, with a training preamble of 6 FBMC/OQAM symbols in the beginning of the frame. It must be emphasized that *no* help pilots were employed, since their presence (along with their rather *uncontrollable* values) was seen not to be beneficial for the direct adaptive equalization task. This means that the bandwidth efficiency of the FBMC/OQAM system in the following results is twice that of CP-OFDM, not counting of course the necessity of a CP in the latter. Moreover, unless stated otherwise, no boosting of the pilots was assumed.

Fig. 4.7 depicts the BER curves for NLMS and IPNLMS LEs for an FBMC/OQAM system as described above.

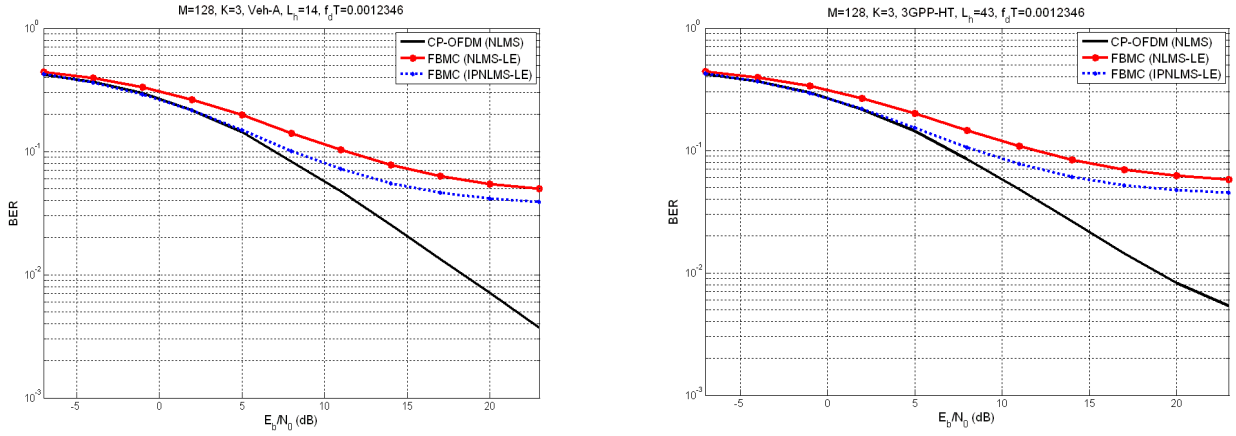

(a) (b)

Fig. 4.7 BER performance of NLMS and IPNLMS adaptive linear equalizers, for (a) ITU-VehA and (b) 3GPP-HT channels. Mobile speed: 50 km/h. *Half-symbol* pilots are used in FBMC/OQAM. *No* pilot boosting was assumed.

The performance of (single-tap) NLMS LE for CP-OFDM is included for comparison. CP duration was set to $M/4$. Two channel models, of medium (a) and high (b) frequency selectivity, were tested, at a medium speed, of 50 km/h. Analogous results for a speed of 150 km/h are given in Fig. 4.8. Observe the significant performance gain provided by the IPNLMS algorithm, especially at medium to high SNRs. The error floors exhibited by the FBMC/OQAM curves are not unexpected, and are due in part to the Doppler spread and in part to the residual intrinsic interference, as it is common in such systems. In all cases, CP-OFDM performs at least as well as FBMC/OQAM and the performance difference grows as noise gets weaker. (It is also of interest to note how CP-OFDM floors when the channel delay spread is significantly larger than the length of the CP employed.)

At high enough SNRs, one could not expect FBMC/OQAM to outperform CP-OFDM, for the reasons outlined above. However, one can do better for FBMC/OQAM over a much wider range of SNRs if the advantage of CP-OFDM in pilot density described above is taken away. This was tested in additional experiments, where the original help pilot positions were

occupied by pilots instead of data. Moreover, to make things more realistic, a boost of 2.5 dB was assumed for the pilots in both multicarrier systems. In order to put more emphasis on the propagation scenarios more common in PMR environments, our simulations focused more on the 3GPP-HT channel model, and at mobile speeds ranging from medium to very high. Thus, 50 km/h, 150 km/h, and 200 km/h were assumed in Fig. 4.9(a), (b), and (c), respectively. Case (c) was tested with 6 OFDM (=12 FBMC) symbols in the preamble, as allowed in the MS4 specifications. Observe that IPNLMS still provides significant gain over conventional NLMS. Moreover, it outperformed CP-OFDM NLMS-LE at low and medium SNRs, bringing FBMC/OQAM to be at least as good as CP-OFDM for at least up to 10 dB of SNR.

(a)

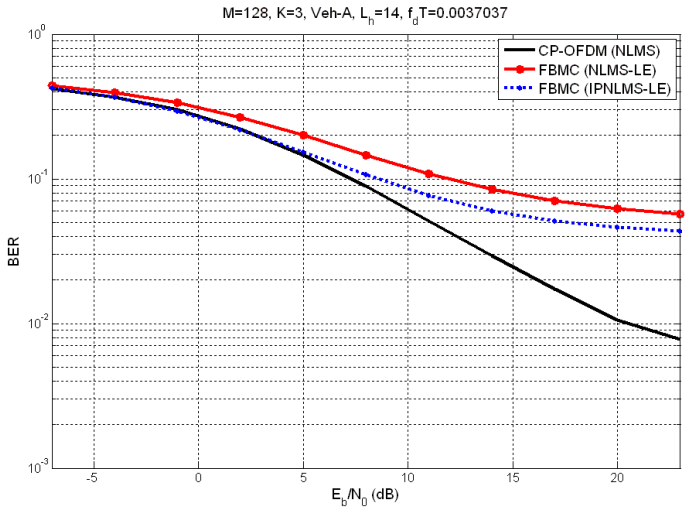

(b)

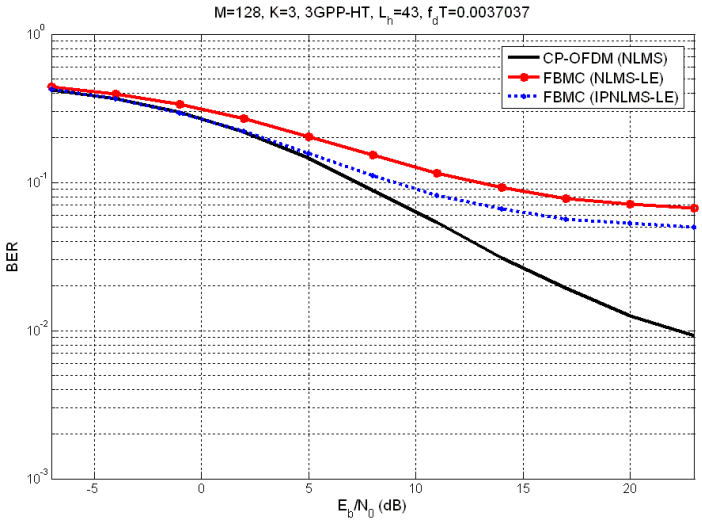

Fig. 4.8 As in Fig. 4.7, with mobile speed 150 km/h.

(a)

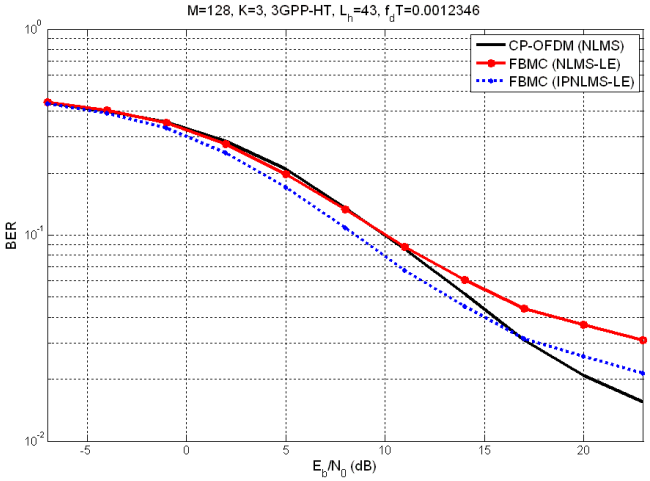

(b)

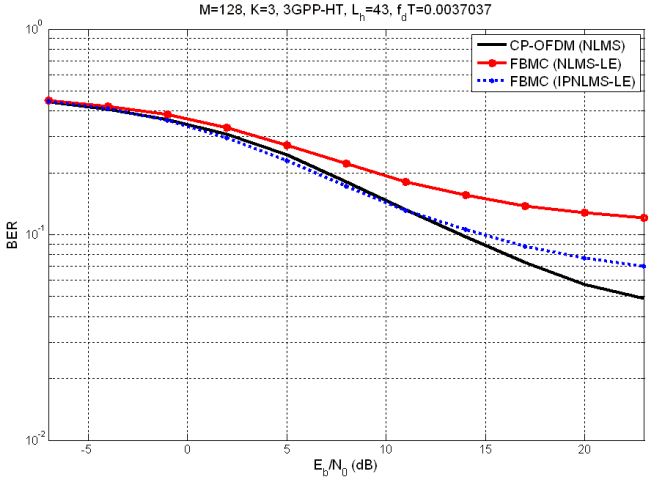

(c)

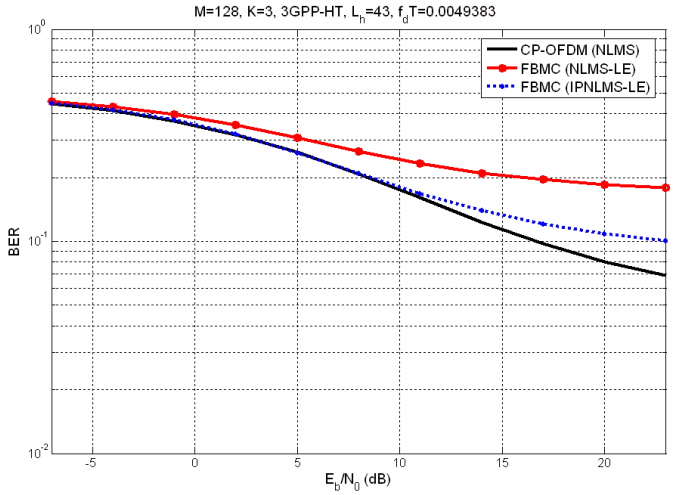

Fig. 4.9 BER performance of equalizing 3GPP-HT channels, at mobile speeds of (a) 50, (b) 150, and (c) 200 km/h. In (c), a preamble of 12 FBMC symbols (as suggested in MS4) was used. In all cases, the help pilot positions were occupied by independent pilots. Pilots were boosted by 2.5 dB.

4.3.1 Application in a PMR environment

The above algorithms were also tested in a setup compliant to a PMR environment. We have adopted the downlink frame for TEDS, as detailed in [15, 44]. As previously, no help pilots were used for FBMC/OQAM. Instead, pairs of OQAM pilots were placed at the QAM pilot positions of the TEDS frame. According to [15, 44], a preamble of 2 OFDM (= 4 FBMC) symbols was adopted in the beginning of the frame. The remaining system parameters were as follows: *M*=32 subcarriers (one of the options of TEDS), *K*=3 and subcarrier spacing equal to 2.7 kHz. Fig. 4.10 shows examples of the performance of the algorithms in such an environment, for the two propagation scenarios outlined in [15, 44]: GSM channels obeying the (a) Typical Urban (TU) and (b) Hilly Terrain (HT) models.

(a)

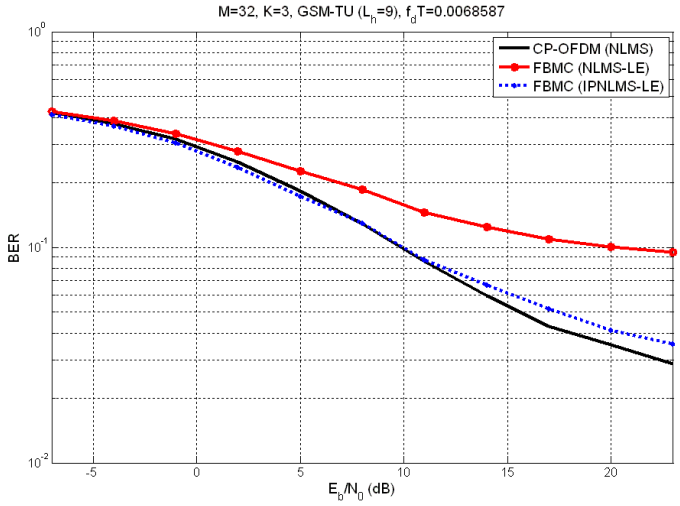

(b)

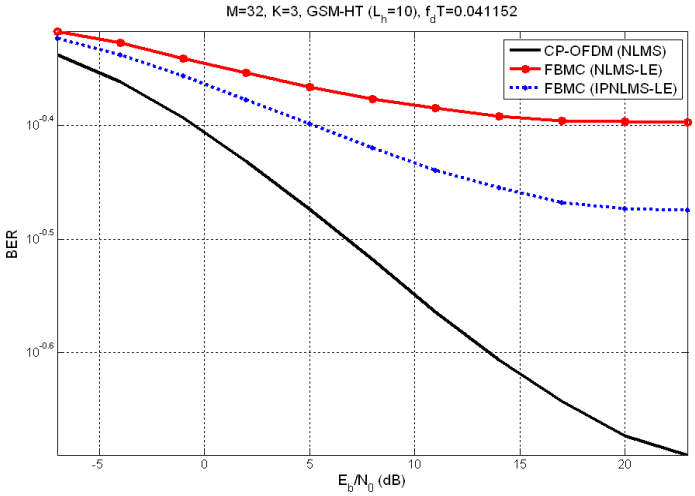

Fig. 4.10 BER performance of the adaptive equalization algorithms in a TEDS system, with GSM channels of type (a) TU and (b) HT. Mobile speeds were equal to (a) 50 km/h and (b) 150 km/h.

In (a), the carrier frequency was set to 400 MHz and a mobile speed of 50 km/h was assumed. The corresponding conditions for (b) were 800 MHz and 150 km/h, respectively. The equalizer length for FBMC/OQAM was set to 5 taps, with a zero equalization delay, while the NLMS step size was chosen as 0.5 and 0.8 for (a) and (b), respectively. In all cases, the proportionate weight for IPNLMS was set to 0.5 as previously. For CP-OFDM, the CP duration was M/4. It is observed that in both cases the sparsity-awareness *greatly* improves the performance of NLMS, especially at medium and high SNRs. It is seen in (a) that (as previously) CP-OFDM outperforms both FBMC/OQAM algorithms at high SNRs. However, IPNLMS achieves lower or at most equal BER at practical SNR values, below 10 dB. The error floor appearance of the CP-OFDM curves is due to the ICI resulting from a CP of insufficient length and, of course, the frequency dispersion effect of mobility. As it has also been noted elsewhere (for example, in the EMPhAtiC deliverable D3.1), the HT channel represents a great challenge for the algorithms, as clearly shown in Fig. 4.10(b). Possible solution approaches could include using a denser pilot placement format and/or adopting a sparsity-aware algorithm which exploits the *group sparse* structure of the HT channel more effectively than IPNLMS. These are subjects of on-going and future work.

One more example is given here, with a 3GPP Rural Area (RA) channel, run under the same conditions as those previously used with the TU channel. The results are plotted in Fig. 4.11. The performance here is similar to that for TU, albeit slightly worse. A more extensive study including a larger number of channel models is part of future work on this subject.

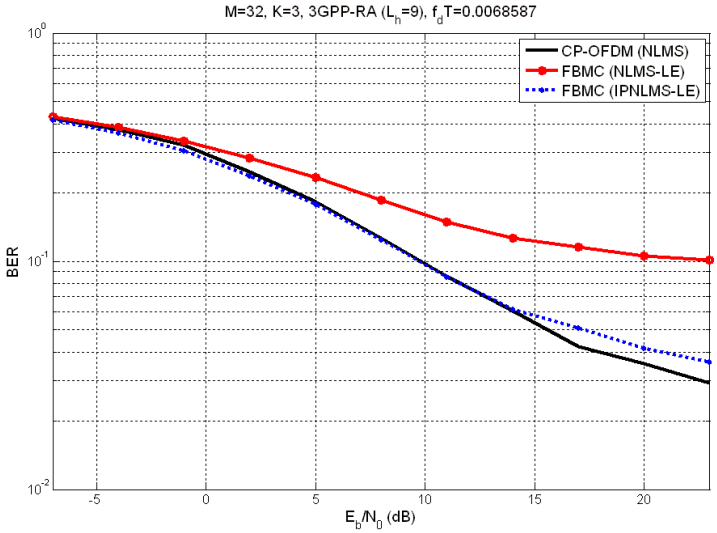

Fig. 4.11. As in Fig. 4.10(a), with 3GPP-RA channels.

4.4 Conclusion

Adaptive equalization of doubly dispersive channels in FBMC/OQAM systems was considered in this chapter. The contributions were split into three parts: (a) precoder-assisted equalization (using WHT for simplicity) for increasing frequency diversity, (b) equalization based on channel tracking, and (c) direct adaptive equalization algorithms, with (b)-(c) relying on pilots scattered throughout the frame. For the latter, an LTE-compatible

pilot format was adopbted, with and without pilot boosting, appropriately modified for use in an FBMC/OQAM system. This translates to inserting help (auxiliary) pilots next to the pilot positions when (almost) interference-free channel estimation is required (case (b)) or pairs of pilots at the positions occupied by QAM pilots in the OFDM LTE frame (case (c)). Specifically, the DMRS pilot configuration was adopted and implemented. In all three cases, channels of sufficiently high time dispersion to imply frequency selective subchannels were assumed, relaxing the commonly made assumption of flat subchannel responses and hence enhancing the practical value of these results in PMR environments. Both medium (Vehicular A) and high (Hilly Terrain) frequency selectivity channels were tested, at zero, medium, and high vehicular speeds. In particular, a PMR-specific experiment was also implemented, employing a pilot format appropriate for downlink transmission, and transmission parameters compatible to a TEDS system.

In all scenarios tested, FBMC/OQAM was seen to perform similarly or better than CP-OFDM, with the exception of high SNR values, where, as it is typically the case, the performance of FBMC floors due to un-equalized residual intrinsic interference. Error floors were also observed in some of the CP-OFDM curves, due to the inadequacy of the employed CP (according to LTE) in highly dispersive channels. Albeit only tested in a time-invariant transmission scenario, the WHT-based equalizers demonstrated considerable improvement over the classical ones. Adopting a simple channel tracking-based approach, with the equalizers being held fixed between two consecutive pilot multicarrier symbols, was shown to be quite effective in coping with demanding channels and robust to increased Doppler spread. In addition to the classical NLMS linear equalizer (and other equalizer structures and adaptive algorithms not reported here), a *sparsity-promoting* NLMS-type algorithm was extensively tested in the context of direct adaptive equalization of such systems. It was shown that the sparse adaptive filters are able to provide a significant performance gain over a conventional, sparsity-blind equalizer. Results favorable for FBMC/OQAM with the sparse algorithm were also obtained in the PMR (TEDS) scenarios, except for the particularly challenging case of a highly mobile GSM-HT channel, where all algorithms tested failed to provide satisfactory results. Difficulties in coping with HT channels have been already pointed out in earlier EMPhAtiC work, including the D3.1 deliverable. It must be emphasized that only a very short (much shorter than required in the EMPhAtiC milestone MS4) preamble was considered for initializing the equalizers. Directions for future research in order to address the questions and overcome the difficulties pointed out above will be discussed in Chapter 9.

5. Channel estimation

In this chapter, we revisit the problem of pilot-based channel estimation in FBMC/OQAM. Indeed, the received pilots in this modulation system are corrupted by the intrinsic interference, generated by the surrounded data symbols in the frequency-time domain. Solutions based on auxiliary symbols have been proposed [53], but these auxiliary symbols are data dependent and have to be calculated at the transmitter side. In this work, we address FBMC/OQAM channel estimation (without auxiliary pilots) in the Maximum Likelihood (ML) sense disregarding the complexity issue. First of all, we calculate the Cramer-Rao lower bound of the optimal estimator, and we show that if a Cramer-Rao estimator exists, it should offer the same performance as the ZF estimator does in OFDM. Then, we propose different estimators aiming to reach the optimal bound. The first one is the ML estimator maximizing the probability of the received pilot symbols given a channel coefficient. Since this probability is calculated based on the discrete probability of the intrinsic interference, the derivation is formidable and then the maximization is done numerically within a grid. The performance strongly depends on the grid step. The second proposed solution called "Individual Term Maximization" (ITM) is based on the fact that the interference term belongs to a finite set. For each possible value of the interference term, the most likely channel coefficient can be easily obtained. Hence, we get a finite set of the corresponding channel coefficients which are candidates, and we select the one that maximizes the probability of the received pilot symbols. This solution offers better performance than that offered by the first ML estimator. The last proposed solution is based on the assumption that the interference is Gaussian. This assumption allows us to obtain a closed form of the likelihood probability and makes the maximum derivation easier. The obtained performance is not limited by a grid step, but it offers worse performance compared to the ITM estimator.

5.1 Problem statement

We address the problem of pilot-based channel estimation in FBMC/OQAM using LTE configuration. We focus in this work on the case where the channel is not highly selective. In OFDM-based LTE, transmitted pilots are known at the receiver side and serve to observe the channel effect on a particular subcarrier. The pilot values are in general complex. When FBMC/OQAM modulation is used, the complex-valued pilots are split into two real-valued PAM symbols (real and imaginary parts) transmitted with a time shift of $T/2$. This modulation, called OQAM, causes an intrinsic interference since the prototype filter has a length of $K \times T$ with $K > 1$ being the overlapping factor. In our considered case, the overlapping factor is set to $K = 4$. One of the characteristics of the FBMC/OQAM modulation is the intrinsic interference, which is purely imaginary when the channel is low frequency selective. That is, the orthogonality condition is only satisfied in the real domain. The input-output model of the FBMC/OQAM transceiver for low frequency selective channels is given by

$$r_{k,n} = h_{k,n}\left(a_{k,n} + ju_{k,n}\right) + \gamma_{k,n} \tag{5.1}$$

where $a_{k,n}$ is the PAM data symbol transmitted at the k th subcarrier and the time index n, $u_{k,n}$ is the real intrinsic interference term, $h_{k,n}$ is the channel coefficient, $r_{k,n}$ is the received signal sample, and $\gamma_{k,n}$ is the Gaussian noise contribution. The intrinsic interference $u_{k,n}$ is generated from the transmitted symbols around the frequency-time position (k,n) and is given by

$$ju_{k,n} = \sum_{p,q} \alpha_{p,q} a_{k+p,n+q} \tag{5.2}$$

where the values of $\alpha_{p,q}$ are purely imaginary and depend on the prototype filter. In our case, we use the PHYDYAS prototype filter. Hence, the interference coefficients $\alpha_{p,q}$ are given in the following table

Table 5.1 Interference coefficients (main part) using PHYDYAS filter

	$n-3$	$n-2$	$n-1$	n	$n+1$	$n+2$	$n+3$
$k-1$	$0.043j$	$0.125j$	$0.206j$	$0.239j$	$0.206j$	$0.125j$	$0.043j$
k	$-0.067j$	0	$-0.564j$	0	$0.564j$	0	$0.067j$
$k+1$	$0.043j$	$-0.125j$	$0.206j$	$-0.239j$	$-0.206j$	$-0.125j$	$0.043j$

In the pilot configuration assumed here, two transmitted PAM symbols $p_{k,n}$ and $p_{k,n+1}$ are known at the receiver, and the objective is to obtain an estimate $\hat{h}_{k,n}$ of the channel coefficient $h_{k,n}$. Assuming that the channel is considered invariant in a certain neighborhood around the considered frequency-time position (k,n), we can write

$$\begin{cases} r_{k,n} = h_{k,n}\left(p_{k,n} + ju_{k,n}\right) + \gamma_{k,n} \\ r_{k,n+1} = h_{k,n}\left(p_{k,n+1} + ju_{k,n+1}\right) + \gamma_{k,n+1} \end{cases} \tag{5.3}$$

In matrix form, and without loss of generality, we can omit the indices and write the above equations as

$$\underbrace{\begin{bmatrix} r_1 \\ r_2 \end{bmatrix}}_{\mathrm{r}} = h \underbrace{\begin{bmatrix} p_1 + ju_1 \\ p_2 + ju_2 \end{bmatrix}}_{\mathrm{c=p+ju}} + \underbrace{\begin{bmatrix} \gamma_1 \\ \gamma_2 \end{bmatrix}}_{\gamma} \tag{5.4}$$

As reported in the deliverable D3.1, the noise at the demodulator output is correlated and the covariance matrix is given by

$$\mathrm{R} = \mathrm{E}\left\{\gamma\gamma^H\right\} = \sigma^2 \begin{bmatrix} 1 & -j\alpha \\ j\alpha & 1 \end{bmatrix} \tag{5.5}$$

where σ^2 is the noise power, and $j\alpha = \alpha_{0,1}$ is the FBMC/OQAM interference coefficient between the time-frequency position (k,n) and $(k,n+1)$. When the PHYDYAS filter is used, $\alpha = 0.564$. It is obvious from (5.2) that the interference vector u is a discrete random vector since the data symbols $a_{k,n}$ are also discrete. The power density function of the received vector r can be given as

$$p(\mathrm{y};h)=\frac{1}{\pi^2\det(\mathrm{R})}\sum_{\mathrm{u}\in\mathrm{U}}p_u(\mathrm{u})\exp\left\{-\left(\mathrm{y}-h\left(\mathrm{p}+j\mathrm{u}\right)\right)^H\mathrm{R}^{-1}(\mathrm{y}-h(\mathrm{p}+j\mathrm{u}))\right\} \quad (5.6)$$

where $p_u(\mathrm{u})$ is the discrete probability distribution of the interference vector u which can be obtained off-line, and U is the set of all possible interference vectors.

5.2 Cramer-Rao lower bound

In this section, we analyze the possibility of deriving an estimator of the parameter h that attains the Cramer-Rao lower bound. This bound alerts us to the impossibility of finding an unbiased estimator whose variance is less than the bound. The Cramer-Rao bound is expressed as

$$\mathrm{E}\left\{|\hat{h}-h|^2\right\}\geq\frac{-1}{\mathrm{E}\left\{\frac{\partial^2\ln\left[p(\mathrm{y};h)\right]}{\partial h_1^2}\right\}}-\frac{1}{\mathrm{E}\left\{\frac{\partial^2\ln\left[p(\mathrm{y};h)\right]}{\partial h_2^2}\right\}} \quad (5.7)$$

where h_1 and h_2 are the real and imaginary parts of h, respectively. Letting $E(h,\mathrm{u})=\left(\mathrm{y}-h\left(\mathrm{p}+j\mathrm{u}\right)\right)^H\mathrm{R}^{-1}(\mathrm{y}-h(\mathrm{p}+j\mathrm{u}))$, we can derive that

$$E(h,\mathrm{u})=\mathrm{y}^H\mathrm{R}^{-1}\mathrm{y}+|h|^2\,\mathrm{c}^H\mathrm{R}^{-1}\mathrm{c}-2h_1\mathrm{Re}\left\{\mathrm{y}^H\mathrm{R}^{-1}\mathrm{c}\right\}+2h_2\mathrm{Im}\left\{\mathrm{y}^H\mathrm{R}^{-1}\mathrm{c}\right\} \quad (5.8)$$

Hence, we can obtain the following partial derivatives

$$\frac{\partial E(h,\mathrm{u})}{\partial h_1}=2h_1\mathrm{c}^H\mathrm{R}^{-1}\mathrm{c}-2\mathrm{Re}\left\{\mathrm{y}^H\mathrm{R}^{-1}\mathrm{c}\right\} \quad (5.9)$$

$$\frac{\partial E(h,\mathrm{u})}{\partial h_2}=2h_2\mathrm{c}^H\mathrm{R}^{-1}\mathrm{c}+2\mathrm{Im}\left\{\mathrm{y}^H\mathrm{R}^{-1}\mathrm{c}\right\} \quad (5.10)$$

$$\frac{\partial^2E(h,\mathrm{u})}{\partial h_1^2}=\frac{\partial^2E(h,\mathrm{u})}{\partial h_2^2}=2\mathrm{c}^H\mathrm{R}^{-1}\mathrm{c} \quad (5.11)$$

We obtain

$$\frac{\partial\ln\left[p(\mathrm{y};h)\right]}{\partial h_i}=\frac{-\sum_{\mathrm{u}\in\mathrm{U}}p_u(\mathrm{u})(\partial E(h,\mathrm{u})/\partial h_i)\exp\left\{-E(h,\mathrm{u})\right\}}{\sum_{\mathrm{u}\in\mathrm{U}}p_u(\mathrm{u})\exp\left\{-E(h,\mathrm{u})\right\}} \quad (5.12)$$

The second derivatives will be

$$\frac{\partial^2\ln\left[p(\mathrm{y};h)\right]}{\partial h_i^2}=\frac{\sum_{\mathrm{u}\in\mathrm{U}}p_u(\mathrm{u})\left[(\partial E(h,\mathrm{u})/\partial h_i)^2-2\mathrm{c}^H\mathrm{R}^{-1}\mathrm{c}\right]\exp\left\{-E(h,\mathrm{u})\right\}}{\sum_{\mathrm{u}\in\mathrm{U}}p_u(\mathrm{u})\exp\left\{-E(h,\mathrm{u})\right\}}$$

$$-\left[\frac{\sum_{\mathrm{u}\in\mathrm{U}} p_u(\mathrm{u})(\partial E(h,\mathrm{u})/\partial h_i)\exp\{-E(h,\mathrm{u})\}}{\sum_{\mathrm{u}\in\mathrm{U}} p_u(\mathrm{u})\exp\{-E(h,\mathrm{u})\}}\right]^2 \tag{5.13}$$

We can observe that the second term of the right hand side of the above equation is the square of the first derivative $\partial \ln[p(\mathrm{y};h)]/\partial h_i$ given by equation (5.12). Therefore, we can write

$$\frac{\partial^2 \ln[p(\mathrm{y};h)]}{\partial h_i^2} = \frac{\sum_{\mathrm{u}\in\mathrm{U}} p_u(\mathrm{u})\left[(\partial E(h,\mathrm{u})/\partial h_i)^2 - 2\mathrm{c}^H \mathrm{R}^{-1}\mathrm{c}\right]\exp\{-E(h,\mathrm{u})\}}{\sum_{\mathrm{u}\in\mathrm{U}} p_u(\mathrm{u})\exp\{-E(h,\mathrm{u})\}} - \left[\frac{\partial \ln[p(\mathrm{y};h)]}{\partial h_i}\right]^2 \tag{5.14}$$

Finally, since

$$\mathrm{E}\left\{\frac{\partial^2 \ln[p(\mathrm{y};h)]}{\partial h_1^2}\right\} = -\mathrm{E}\left\{\left[\frac{\partial \ln[p(\mathrm{y};h)]}{\partial h_1}\right]^2\right\} \tag{5.15}$$

we have

$$\mathrm{E}\left\{\frac{\partial^2 \ln[p(\mathrm{y};h)]}{\partial h_1^2}\right\} = -\mathrm{E}\left\{\left[\frac{\sum_{\mathrm{u}\in\mathrm{U}} p_u(\mathrm{u})(\partial E(h,\mathrm{u})/\partial h_i)\exp\{-E(h,\mathrm{u})\}}{\sum_{\mathrm{u}\in\mathrm{U}} p_u(\mathrm{u})\exp\{-E(h,\mathrm{u})\}}\right]^2\right\} \tag{5.16}$$

Therefore,

$$\mathrm{E}\left\{|\hat{h}-h|^2\right\} \geq \sum_{i=1}^{2} \frac{1}{\mathrm{E}\left\{\left[\frac{\sum_{\mathrm{u}\in\mathrm{U}} p_u(\mathrm{u})(\partial E(h,\mathrm{u})/\partial h_i)\exp\{-E(h,\mathrm{u})\}}{\sum_{\mathrm{u}\in\mathrm{U}} p_u(\mathrm{u})\exp\{-E(h,\mathrm{u})\}}\right]^2\right\}} \tag{5.17}$$

We can evaluate the curve of the Cramer-Rao bound by numerical calculation of (5.17) using a Monte Carlo algorithm.

In OFDM, pilot-based channel estimation makes use of one complex pilot symbol. We can write for OFDM $r = hp + n$. We can easily show that the optimum estimator is the ZF one and reaches the Cramer-Rao bound, and it is given by $\hat{h} = y/p$. In Fig. 5.1, we show that the Cramer-Rao bound of FBMC/OQAM is almost the same as that for OFDM. The Cramer-Rao lower bound for FBMC/OQAM is plotted by making use of (5.17). The channel estimation error curve of OFDM-ZF is obtained by simulation by assuming flat fading channel.

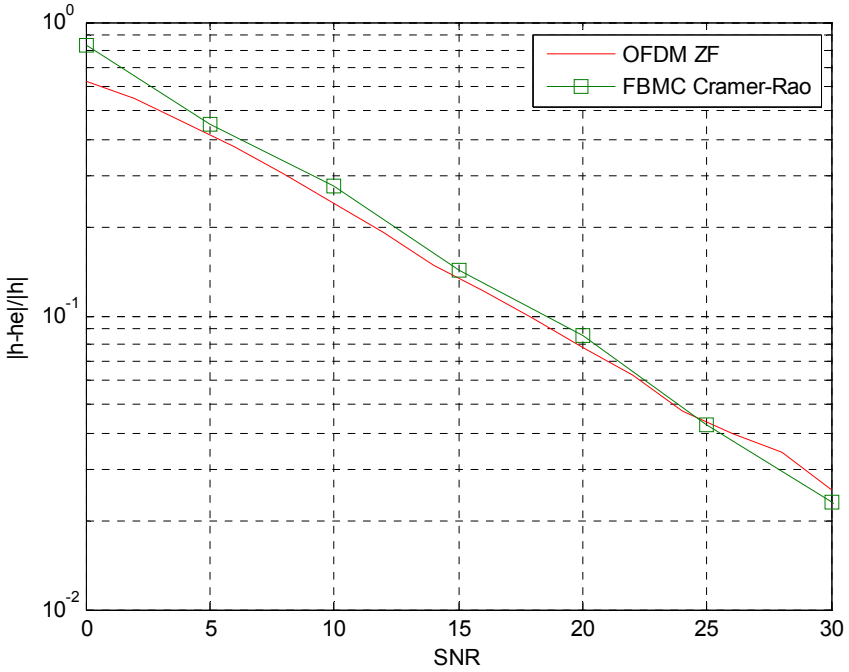

Fig. 5.1 Channel estimation Cramer-Rao lower bounds for FBMC/OQAM and OFDM.

5.3 Individual terms maximization

Let us consider (5.6). We know that the exact value of the interference vector u belongs to the vector set U ($\mathrm{u} \in \mathrm{U}$). Then, if we assume that u is known, the maximum likelihood estimate of h is the one that maximizes

$$p(\mathrm{y}/\mathrm{u};h) = \frac{1}{\pi^2 \det(\mathrm{R})} \exp\left\{-\left(\mathrm{y} - h\left(\mathrm{p} + j\mathrm{u}\right)\right)^H \mathrm{R}^{-1}(\mathrm{y} - h(\mathrm{p} + j\mathrm{u}))\right\} \tag{5.18}$$

By calculating the derivative with respect to h and set it to zero, we obtain:

$$\hat{h} = \frac{\mathrm{c}^H \mathrm{R}^{-1}\mathrm{y}}{\mathrm{c}^H \mathrm{R}^{-1}\mathrm{c}} \tag{5.19}$$

where $\mathrm{c} = \mathrm{p} + j\mathrm{u}$. Hence, we can determine a set of possible $\hat{h}$ that can maximize (5.18). Let us define

$$\mathrm{H} = \left\{ \hat{h} = \frac{(\mathrm{p} + j\mathrm{u})^H \mathrm{R}^{-1}\mathrm{y}}{(\mathrm{p} + j\mathrm{u})^H \mathrm{R}^{-1}(\mathrm{p} + j\mathrm{u})}; \mathrm{u} \in \mathrm{U} \right\} \tag{5.20}$$

Finally, the channel estimator is

$$\begin{aligned} \hat{h} &= \arg\max_{h \in \mathrm{H}} \{p(\mathrm{y};h)\} \\ &= \arg\max_{h \in \mathrm{H}} \left\{ \sum_{\mathrm{u} \in \mathrm{U}} p_u(\mathrm{u}) \exp\left\{-\left(\mathrm{y} - h\left(\mathrm{p} + j\mathrm{u}\right)\right)^H \mathrm{R}^{-1}(\mathrm{y} - h(\mathrm{p} + j\mathrm{u}))\right\} \right\} \end{aligned} \tag{5.21}$$

Fig. 5.2 depicts the performance curve of the proposed channel estimator.

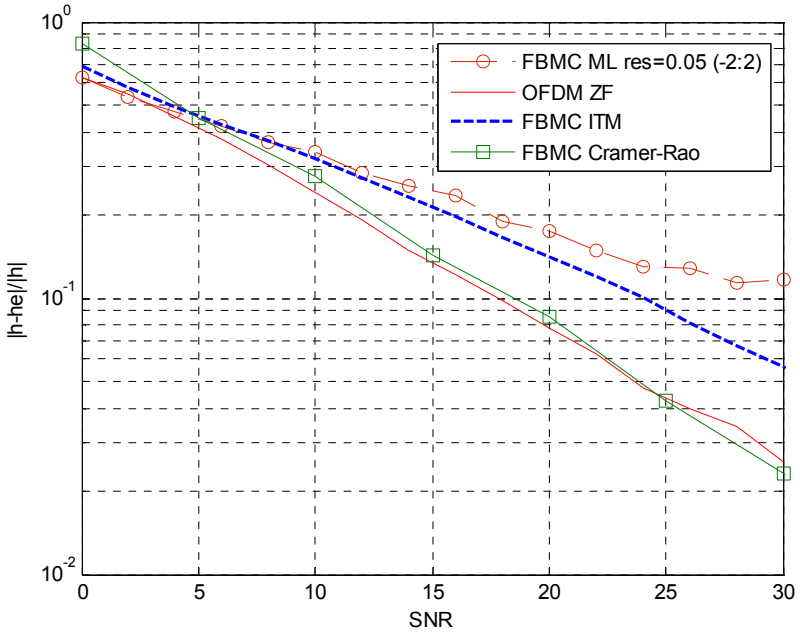

Fig. 5.2: Performance of ITM channel estimation.

5.4 Real part forcing estimator

Let $\beta = 1/\hat{h}$, and we set:

$$\begin{cases} \mathrm{Re}\{\beta y_1\} = p_1 \\ \mathrm{Re}\{\beta y_2\} = p_2 \end{cases} \tag{5.22}$$

Let β_1 and β_2 the real and imaginary parts of β, y_1^R and y_1^I the real and imaginary parts of y_1, and y_2^R and y_2^I the real and imaginary parts of y_2. We can write

$$\begin{cases} \beta_1 y_1^R - \beta_2 y_1^I = p_1 \\ \beta_1 y_2^R - \beta_2 y_2^I = p_2 \end{cases}, \tag{5.23}$$

which is equivalent to

$$\begin{bmatrix} y_1^R & -y_1^I \\ y_2^R & -y_2^I \end{bmatrix} \begin{bmatrix} \beta_1 \\ \beta_2 \end{bmatrix} = \begin{bmatrix} p_1 \\ p_2 \end{bmatrix} \tag{5.24}$$

Then, if the determinant of the matrix above is not zero, we have

$$\begin{bmatrix} \beta_1 \\ \beta_2 \end{bmatrix} = \frac{1}{y_1^I y_2^R - y_1^R y_2^I} \begin{bmatrix} -y_2^I & y_1^I \\ -y_2^R & y_1^R \end{bmatrix} \begin{bmatrix} p_1 \\ p_2 \end{bmatrix} \tag{5.25}$$

Therefore, we can calculate $\hat{h} = 1/\beta = 1/(\beta_1 + j\beta_2)$, and we obtain

$$\hat{h} = \frac{j\,\mathrm{Im}\{y_1 y_2^*\}}{p1 y_2^* - p2 y_1^*} \tag{5.26}$$

It must be noted that this estimator has been also studied in the PHYDYAS project.

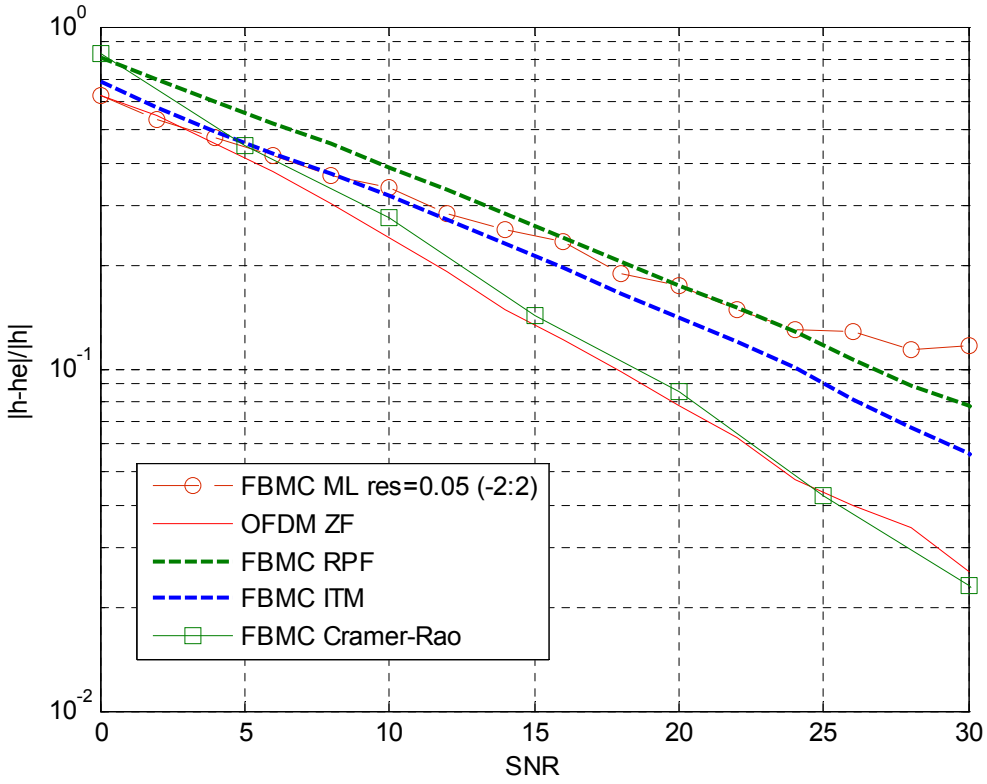

Fig. 5.3 Performance of channel estimation.

The normalized channel estimation error of the RPF estimator is depicted in Fig. 5.3. We have tested by simulation this proposed estimator and assessed the bit-error rate (BER) performance. Fig. 5.4 compares the FBMC performance to OFDM. The channel model is the time-invariant Ped-A channel. The sampling frequency is set to 1.92 MHz with 128 subcarriers. 16 pilot symbols are distributed uniformly among one multicarrier symbol (one pilot symbol for every 8 subcarriers). Then, the channel coefficient in each subcarrier is determined by using FFT interpolation. The figure shows that we obtain almost the same BER performance compared to OFDM.

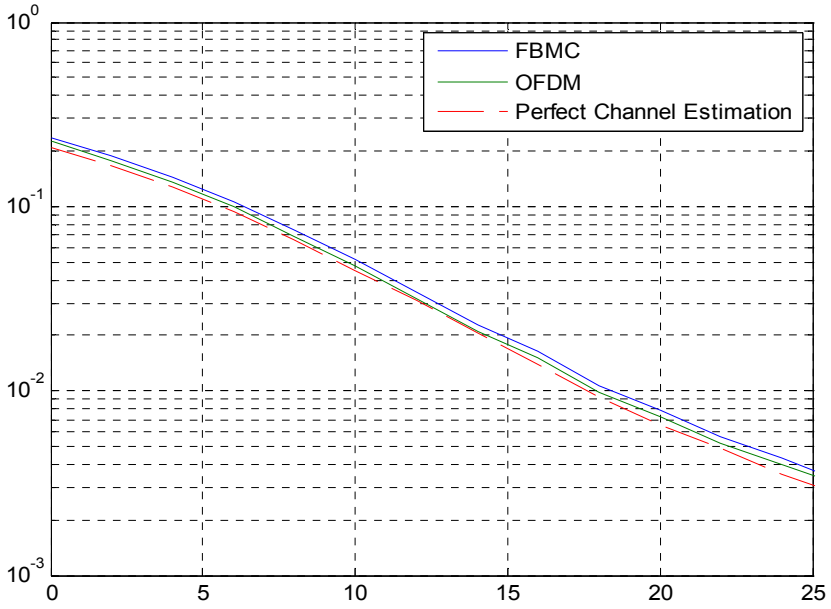

Fig. 5.4 BER performance after channel estimation in Ped-A channel.

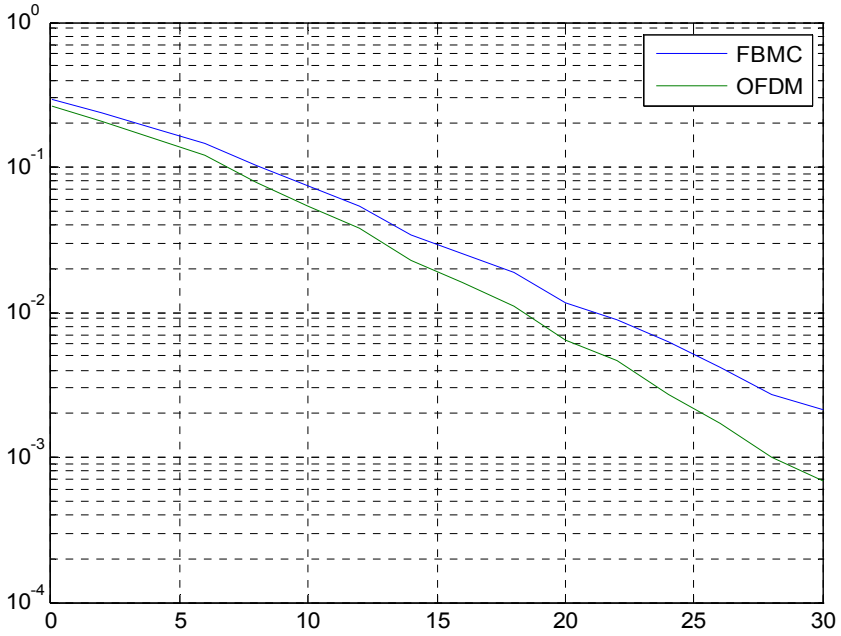

Fig. 5.5 BER performance after channel estimation in Veh-A channel.

We have also tested the estimator in a Veh-A channel model using the same previous simulation parameters. Fig. 5.5 shows that the situation is different, FBMC performance is worse than OFDM. The degradation can be explained by the fact that the channel is more frequency selective here.

5.5 Interference distribution approximation to Gaussian

In this section, we assume that the interference terms are Gaussian distributed. Then, we consider the extended vectors and rewrite (5.4) as

$$\underbrace{\begin{bmatrix} y_{1r} \\ y_{2r} \\ y_{1i} \\ y_{2i} \end{bmatrix}}_{\tilde{\mathrm{y}}} = \underbrace{\begin{bmatrix} h_r & 0 & -h_i & 0 \\ 0 & h_r & 0 & -h_i \\ h_i & 0 & h_r & 0 \\ 0 & h_i & 0 & h_r \end{bmatrix} \times \left(\begin{bmatrix} p_1 \\ p_2 \\ 0 \\ 0 \end{bmatrix} + \begin{bmatrix} 0 \\ 0 \\ u_1 \\ u_2 \end{bmatrix} \right) + \begin{bmatrix} \gamma_{1r} \\ \gamma_{2r} \\ \gamma_{1i} \\ \gamma_{2i} \end{bmatrix}}_{\tilde{\mathrm{H}} \times (\tilde{\mathrm{p}} + \tilde{\mathrm{u}}) + \tilde{\gamma}} \tag{5.27}$$

where h_r, y_{kr} and γ_{kr} denote the real parts of h, y_k and γ_k, and their imaginary parts are respectively denoted by h_i, y_{ki} and γ_{ki} with $k \in \{1,2\}$.

Since we have assumed that the interference terms u_1 and u_2 are Gaussian, the whole equivalent "interference plus noise" is also Gaussian. Therefore, we can write the likelihood function as

$$p(\tilde{\mathrm{y}}, h) = \frac{1}{4\pi^2 \sqrt{\det(\mathrm{R})}} \exp\left\{ -\frac{1}{2} \left(\tilde{\mathrm{y}} - \tilde{\mathrm{H}} \overline{\mathrm{p}}_u \right)^T \mathrm{R}^{-1} \left(\tilde{\mathrm{y}} - \tilde{\mathrm{H}} \overline{\mathrm{p}}_u \right) \right\} \tag{5.28}$$

where the vector $\overline{\mathrm{p}}_u$ is the expectation of the random vector $\tilde{\mathrm{p}} + \tilde{\mathrm{u}}$, and R is the covariance matrix defined as:

$$\begin{aligned} \mathrm{R} &= \mathrm{E}\left\{ \left(\tilde{\mathrm{y}} - \tilde{\mathrm{H}} \overline{\mathrm{p}}_u \right) \left(\tilde{\mathrm{y}} - \tilde{\mathrm{H}} \overline{\mathrm{p}}_u \right)^T \right\} \\ &= \tilde{\mathrm{H}} \times \underbrace{\mathrm{E}\left\{ (\tilde{\mathrm{u}} - \overline{\mathrm{u}})(\tilde{\mathrm{u}} - \overline{\mathrm{u}})^T \right\}}_{\mathrm{R}_u} \tilde{\mathrm{H}} + \underbrace{\mathrm{E}\left\{ \tilde{\gamma} \tilde{\gamma}^T \right\}}_{\mathrm{R}_n} \end{aligned} \tag{5.29}$$

where $\overline{\mathrm{u}} = \mathrm{E}\{\tilde{\mathrm{u}}\}$. Then, we have

$$\mathrm{R}_n = \frac{\sigma_n^2}{2} \begin{bmatrix} 1 & 0 & 0 & \alpha \\ 0 & 1 & -\alpha & 0 \\ 0 & -\alpha & 1 & 0 \\ \alpha & 0 & 0 & 1 \end{bmatrix} \tag{5.30}$$

$$\mathrm{R}_u = K_g \begin{bmatrix} 0 & 0 & 0 & 0 \\ 0 & 0 & 0 & 0 \\ 0 & 0 & 1 & 0 \\ 0 & 0 & 0 & 1 \end{bmatrix} \tag{5.31}$$

where K_g is positive real valued. According to the expressions above, we can write the covariance matrix R as

$$\mathrm{R}=\begin{bmatrix} \frac{\sigma_n^2}{2}+K_g h_i^2 & 0 & -K_g h_i h_r & \alpha\frac{\sigma_n^2}{2} \\ 0 & \frac{\sigma_n^2}{2}+K_g h_i^2 & -\alpha\frac{\sigma_n^2}{2} & -K_g h_i h_r \\ -K_g h_i h_r & -\alpha\frac{\sigma_n^2}{2} & \frac{\sigma_n^2}{2}+K_g h_r^2 & 0 \\ \alpha\frac{\sigma_n^2}{2} & -K_g h_i h_r & 0 & \frac{\sigma_n^2}{2}+K_g h_r^2 \end{bmatrix} \tag{5.32}$$

The determinant of the matrix R is

$$\det(\mathrm{R})=\frac{\sigma_n^4}{16}\left(2K_g\,|h|^2+\sigma_n^2\left(1-\alpha^2\right)\right)^2. \tag{5.33}$$

It is worth noticing that the determinant of R does not depend on the phase of the channel coefficient h. In order to maximize the likelihood function (5.28), we have to differentiate it with respect to the channel coefficient h and set the derivative to zero. However, finding the zeros of the derivative $\partial p(\tilde{\mathrm{y}},h)/\partial h$ is formidable. Since the determinant of R does not depend on the phase of h, it is worth differentiating (5.28) with respect to the phase of h. Let $h=|h|e^{j\Phi}$, we can simplify the maximization problem by calculating

$$\frac{\partial \ln\left(p(\tilde{\mathrm{y}},h)\right)}{\partial\Phi}=-\frac{\partial}{2\partial\Phi}\left[\left(\tilde{\mathrm{y}}-\tilde{\mathrm{H}}\overline{\mathrm{p}}_u\right)^T\mathrm{R}^{-1}\left(\tilde{\mathrm{y}}-\tilde{\mathrm{H}}\overline{\mathrm{p}}_u\right)\right] \tag{5.34}$$

We have:

$$\mathrm{R}^{-1}=\frac{1}{\sqrt{\det(\mathrm{R})}}\underbrace{\begin{bmatrix} \frac{\sigma_n^2}{2}+K_g h_r^2 & 0 & K_g h_i h_r & -\alpha\frac{\sigma_n^2}{2} \\ 0 & \frac{\sigma_n^2}{2}+K_g h_r^2 & \alpha\frac{\sigma_n^2}{2} & K_g h_i h_r \\ K_g h_i h_r & \alpha\frac{\sigma_n^2}{2} & \frac{\sigma_n^2}{2}+K_g h_i^2 & 0 \\ -\alpha\frac{\sigma_n^2}{2} & K_g h_i h_r & 0 & \frac{\sigma_n^2}{2}+K_g h_i^2 \end{bmatrix}}_{\mathrm{M}} \tag{5.35}$$

Therefore, equation (5.34) can yield

$$\frac{\partial \ln\left(p(\tilde{\mathrm{y}},h)\right)}{\partial\Phi}=\frac{1}{\sqrt{\det\mathrm{R}}}\left[\left(\frac{\partial\tilde{\mathrm{H}}\overline{\mathrm{p}}_u}{\partial\Phi}\right)^T\mathrm{M}\left(\tilde{\mathrm{y}}-\tilde{\mathrm{H}}\overline{\mathrm{p}}_u\right)-\frac{1}{2}\left(\tilde{\mathrm{y}}-\tilde{\mathrm{H}}\overline{\mathrm{p}}_u\right)^T\frac{\partial\mathrm{M}}{\partial\Phi}\left(\tilde{\mathrm{y}}-\tilde{\mathrm{H}}\overline{\mathrm{p}}_u\right)\right] \tag{5.36}$$

According to the value of $\tilde{\mathrm{H}}$ in equation (5.27), we have

$$\frac{\partial\tilde{\mathrm{H}}}{\partial\Phi}=|h|\begin{bmatrix} -\sin(\Phi) & 0 & -\cos(\Phi) & 0 \\ 0 & -\sin(\Phi) & 0 & -\cos(\Phi) \\ \cos(\Phi) & 0 & -\sin(\Phi) & 0 \\ 0 & \cos(\Phi) & 0 & -\sin(\Phi) \end{bmatrix} \tag{5.37}$$

According to the definition of the matrix M in (5.35), we have

$$\frac{\partial \mathrm{M}}{\partial \Phi} = K_g \mid h \mid^2 \begin{bmatrix} -2\cos(\Phi)\sin(\Phi) & 0 & \cos(\Phi)^2 - \sin(\Phi)^2 & 0 \\ 0 & -2\cos(\Phi)\sin(\Phi) & 0 & \cos(\Phi)^2 - \sin(\Phi)^2 \\ \cos(\Phi)^2 - \sin(\Phi)^2 & 0 & 2\cos(\Phi)\sin(\Phi) & 0 \\ 0 & \cos(\Phi)^2 - \sin(\Phi)^2 & 0 & 2\cos(\Phi)\sin(\Phi) \end{bmatrix} \quad (5.38)$$

Now, we set the expression given in (5.36) to zero, and we obtain:

$$\overline{\mathrm{p}}_u^T \frac{\partial \tilde{\mathrm{H}}^T}{\partial \Phi} \mathrm{M}\tilde{\mathrm{y}} - \overline{\mathrm{p}}_u^T \frac{\partial \tilde{\mathrm{H}}^T}{\partial \Phi} \mathrm{M}\tilde{\mathrm{H}}\overline{\mathrm{p}}_u - \frac{1}{2}\tilde{\mathrm{y}}^T \frac{\partial \mathrm{M}}{\partial \Phi}\tilde{\mathrm{y}} - \frac{1}{2}\overline{\mathrm{p}}_u^T \tilde{\mathrm{H}}^T \frac{\partial \mathrm{M}}{\partial \Phi}\tilde{\mathrm{H}}\overline{\mathrm{p}}_u + \tilde{\mathrm{y}}^T \frac{\partial \mathrm{M}}{\partial \Phi}\tilde{\mathrm{H}}\overline{\mathrm{p}}_u = 0 \quad (5.39)$$

We have

$$\overline{\mathrm{p}}_u^T \frac{\partial \tilde{\mathrm{H}}^T}{\partial \Phi} \mathrm{M}\tilde{\mathrm{H}}\overline{\mathrm{p}}_u + \frac{1}{2}\overline{\mathrm{p}}_u^T \tilde{\mathrm{H}}^T \frac{\partial \mathrm{M}}{\partial \Phi}\tilde{\mathrm{H}}\overline{\mathrm{p}}_u = 0 \quad (5.40)$$

Then, equation (5.39) becomes

$$\overline{\mathrm{p}}_u^T \frac{\partial \tilde{\mathrm{H}}^T}{\partial \Phi} \mathrm{M}\tilde{\mathrm{y}} - \frac{1}{2}\tilde{\mathrm{y}}^T \frac{\partial \mathrm{M}}{\partial \Phi}\tilde{\mathrm{y}} + \tilde{\mathrm{y}}^T \frac{\partial \mathrm{M}}{\partial \Phi}\tilde{\mathrm{H}}\overline{\mathrm{p}}_u = 0 \quad (5.41)$$

We have

$$\tilde{\mathrm{H}}^T \frac{\partial \mathrm{M}}{\partial \Phi}\tilde{\mathrm{H}} = K_g \mid h \mid^4 \begin{bmatrix} 0 & 0 & 1 & 0 \\ 0 & 0 & 0 & 1 \\ 1 & 0 & 0 & 0 \\ 0 & 1 & 0 & 0 \end{bmatrix} \quad (5.42)$$

$$\frac{\partial \mathrm{M}}{\partial \Phi}\tilde{\mathrm{H}} = K_g \mid h \mid^3 \begin{bmatrix} -\sin(\Phi) & 0 & \cos(\Phi) & 0 \\ 0 & -\sin(\Phi) & 0 & \cos(\Phi) \\ \cos(\Phi) & 0 & \sin(\Phi) & 0 \\ 0 & \cos(\Phi) & 0 & \sin(\Phi) \end{bmatrix} \quad (5.43)$$

$$\frac{\partial \tilde{\mathrm{H}}^T}{\partial \Phi} \mathrm{M} = \mid h \mid \begin{bmatrix} -\frac{\sigma_n^2}{2}\sin(\Phi) & \alpha\frac{\sigma_n^2}{2}\cos(\Phi) & \frac{\sigma_n^2}{2}\cos(\Phi) & \alpha\frac{\sigma_n^2}{2}\sin(\Phi) \\ -\alpha\frac{\sigma_n^2}{2}\cos(\Phi) & -\frac{\sigma_n^2}{2}\sin(\Phi) & -\alpha\frac{\sigma_n^2}{2}\sin(\Phi) & \frac{\sigma_n^2}{2}\cos(\Phi) \\ -K_g'\cos(\Phi) & -\alpha\frac{\sigma_n^2}{2}\sin(\Phi) & -K_g'\sin(\Phi) & \alpha\frac{\sigma_n^2}{2}\cos(\Phi) \\ \alpha\frac{\sigma_n^2}{2}\sin(\Phi) & -K_g'\cos(\Phi) & -\alpha\frac{\sigma_n^2}{2}\cos(\Phi) & -K_g'\sin(\Phi) \end{bmatrix} \quad (5.44)$$

with $K_g' = \left(K_g |h|^2 + \frac{\sigma_n^2}{2} \right)$. We have defined that $\bar{\mathrm{p}}_u = \mathrm{E}\{\tilde{\mathrm{p}} + \tilde{\mathrm{u}}\} = \tilde{\mathrm{p}} + \bar{\mathrm{u}}$. We can show that $\bar{\mathrm{u}} = [0 \quad 0 \quad -\alpha p_2 \quad \alpha p_1]^T$. Then, plugging $\bar{\mathrm{p}}_u = [p_1 \quad p_2 \quad -\alpha p_2 \quad \alpha p_1]^T$ into equation (5.41) and according to the expressions above, we can write

$$\underbrace{\left[\left(K_g |h|^2 + (1-\alpha^2)\frac{\sigma_n^2}{2} \right)\left(p_1 y_{1r} + p_2 y_{2r} \right) \right]}_{D} \sin(\Phi) + \underbrace{\left[\frac{1}{2} K_g |h| \left(y_{1i}^2 - y_{1r}^2 - y_{2r}^2 + y_{2i}^2 \right) \right]}_{B} \sin(2\Phi) +$$

$$\underbrace{\left[K_g |h| \left(y_{1i} y_{1r} + y_{2i} y_{2r} \right) \right]}_{A} \cos(2\Phi) + \underbrace{\left[\left((\alpha^2 - 1)\frac{\sigma_n^2}{2} - K_g |h|^2 \right)\left(p_1 y_{1i} + p_2 y_{2i} \right) \right]}_{C} \cos(\Phi) = 0 \quad (5.45)$$

Setting $X = \cos(\Phi)$, we can obtain

$$A(2X^2 - 1) + (2BX + D)\sqrt{1 - X^2} + CX = 0 \quad (5.46)$$

which can lead to the following polynomial equation

$$4(B^2 + A^2)X^4 + 4(BD + CA)X^3 + (D^2 - 4B^2 + C^2 - 4A^2)X^2$$
$$-(4BD + 2CA)X + (A^2 - D^2) = 0$$

where the coefficients A, B, C and D depend on the channel magnitude $|h|$ and defined as in equation (5.45). Hence, for a given value of $|h|$, we can numerically solve the equation above and obtain 4 different solutions X_i $(i = 1, \ldots, 4)$. Since $X = \cos(\Phi)$, then we only keep the real solutions $X_i \in [-1, 1]$. After that, we choose among the selected solutions $\Phi_i = \pm \arccos(X_i)$ the one that maximizes the likelihood function (5.28). Because the selected solution Φ_0 still depends on $|h|$, we can make use of a grid of $|h|$ values with a sufficiently small step.

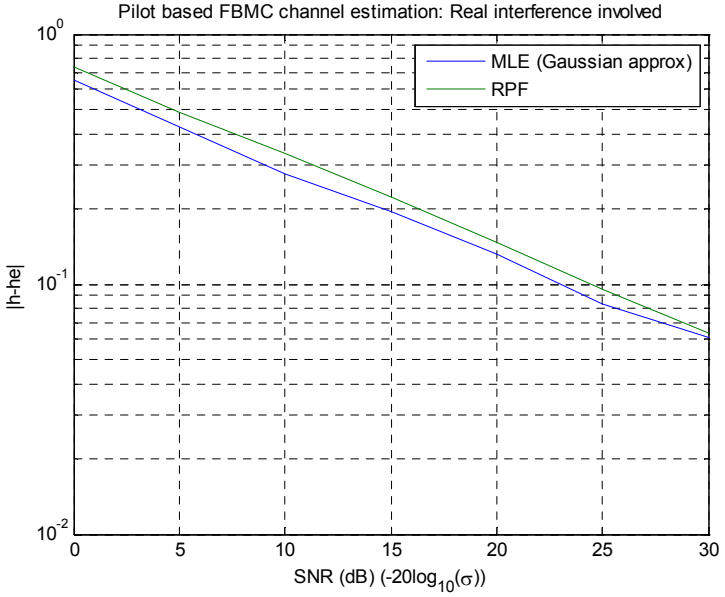

Fig. 5.6: Performance comparison between channel estimation algorithms in flat fading channel.

We show in Fig. 5.6 the obtained channel estimation performance using the maximum likelihood estimation, and we compare with the RPF estimator. We can notice that maximum likelihood estimator slightly outperforms the RPF one but with much higher computational complexity.

5.6 Conclusion

We have attempted to propose optimum FBMC/OQAM channel estimation and analyze the obtained performance. This study does not take into account the complexity issues. In terms of mean estimation error performance, the ITM estimator and the ML estimator with Gaussian approximation offer the best performance, but their performance is still far from the simple OFDM-ZF estimator. Since the ITM estimator has to enumerate all the interference terms, the MLE with Gaussian approximation is relatively less complicated. Nevertheless, since an exhaustive search within a one-dimensional grid is needed, the complexity of such an estimator is still high. The least complicated estimator is the « Real Part Forcing » (RPF) one. Simulation results show that the BER performance of the RPF estimator is almost the same as OFDM-ZF's performance when the channel is not highly selective (Ped-A channel model). However, when the channel is highly selective, the BER performance of the RPF estimator is considerably degraded.

6. Real-domain based soft self-interference cancellation framework

In this section we return to the problem of compensation of linear distortions and elaborate on successive interference cancellation as a viable alternative to linear equalizer or DFE. At the same time, this is accomplished by relying entirely on the real-valued formulation of the system model, as it was presented under 3.2.1 above. The sufficiency of statistics regarding the detection capability is indirectly demonstrated through the simulated BER performance matching the theoretical ones. Furthermore, while the real-domain formulation essentially assumes use of only the in-phase component of the received base-band signal, the use of the quadrature component becomes also possible, because of the redundancy it carries regarding the information content, and actually represents the complex-notation term known as intrinsic interference pertinent to the FBMC systems, generally considered as an obstacle towards conventional complex-domain detection procedures, notably for MIMO.

However, by the mere fact that the noise components on the two quadrature components are independent one can think of a certain form of diversity-like combining of the data samples independently estimated on the two branches. (An additional independency might come from the influence of multipath fading transmission channel as well.) Having this in mind we made an attempt to demonstrate certain (theoretically 3 dB) SNR gain based on that. Moreover, since the noise samples in the complex-domain are mutually correlated due to the AWGN filtering by the AFB subchannel filters, there comes to mind to consider the prediction and cancellation of the predicted noise samples within the SIC framework.

6.1 Self-interference cancellation using only the in-phase subchannel signal component

The soft inter-symbol and inter-subchannel interference cancelation procedure combined with the turbo-like interaction with the soft-input/soft-output decoder of a convolutional code is shown in the following figure, in which the SIC decoder acts as a kind of inner-code.

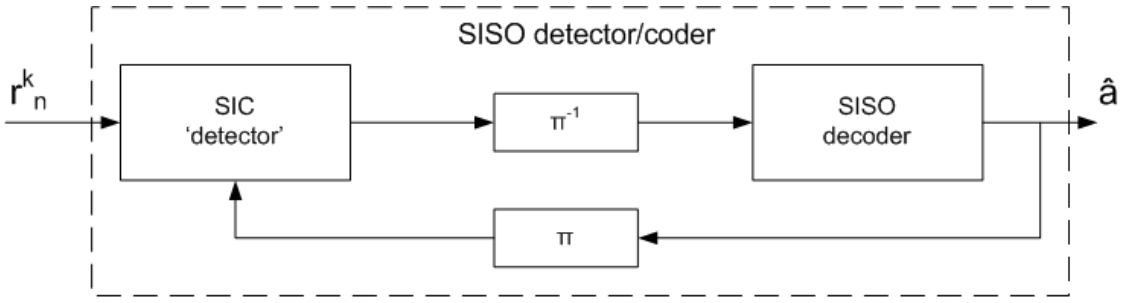

Fig. 6.1 Turbo-mode configuration for estimation of subchannel data within the SISO FBMC.

The main idea in interference cancellation is to suppress the interferences coming from all other symbols, except the symbol for the time-frequency bin of the current interest, by using an estimation of their conditional expectation $\hat{d}_n^k = E\left\{d_n^k \left| r' \right.\right\}$, where *r'* is the received signal after suppression of the interferences produced by all symbols except d_n^k, that is, in accordance with the real-domain system model formulation (2.21)

$$r'^{k+k'}_{n+n'} = r^{k+k'}_{n+n'} - \sum_{k''=-1}^{1} \sum_{n''=-L}^{L} \hat{d}^{k+k'+k''}_{n+n'-n''} \hat{h}^{k+k',k''}_{n''} \quad , \tag{6.1}$$

for $k'+k'' \neq 0$, $n'-n'' \neq 0$, $k' = -1,0,1$ and $n' = -L,\ldots,0,\ldots L$ where ^ denotes an estimate – or, by replacing the received samples by (2.21) and at the same time adding and subtracting the contribution of the very (n,k) -th bin data symbol d^k_n

$$r'^{k+k'}_{n+n'} = \sum_{k''=-1}^{1} \sum_{n''=-L}^{L} \left(d^{k+k'-k''}_{n+n'-n''} - \hat{d}^{k+k'-k''}_{n+n'-n''} \right) \hat{h}^{k+k',k''}_{n''} + \left(\hat{d}^{k}_{n} \right) \hat{h}^{k+k',k'}_{n'} + b^{k+k'}_{n+n'} \tag{6.2}$$

where for the double sum applies also $n'-n'' = 0$ and $k'+k'' = 0$ and the second one represents the contribution of the estimated d^k_n to all the surounding bins in the time-frequency grid.

The next step, in order to provide an expression which furnishes the extrinsic probability of the data symbol d^k_n as the apposteriory probability of the received signal under condition that that particular data symbol had been sent [45], $P\left(\{r'^k_n\}, d^k_n\right)$ as an important simplification compared to the general maximum a posteriori probability (MAP) formulation, is to assume that the first term on the right side of the equation (6.2) is zero, to then have

$$r'^{k+k'}_{n+n'} = \left(\hat{d}^{k}_{n} \right) \hat{h}^{k+k',k'}_{n'} + b^{k+k'}_{n+n'} \, . \tag{6.3}$$

From this it follows, as the probability density function of Gaussian noise having the average value given by the the first summand in (6.3)

$$P\left(\{r'^k_n\}, d^k_n\right) \approx \exp\left(- \frac{(r'^k_n - d^k_n \hat{h}^{k,0}_0)^2}{2\sigma^2_k} \right). \tag{6.4}$$

Since this is based on just one sample, in order to involve the other samples to which the particular data symbol has contribution, one option would be to calculate the a-posteriori probability by multiplication of values in (6.4) for each of the "affected" time-frequency bins, to produce

$$P(\{r'^k_n\}, d^k_n) \approx \exp\left(- \frac{\sum_{k'=-1}^{1} \sum_{n'=-L}^{L} \left(r'^{k+k'}_{n+n'} - d^k_n \hat{h}^{k,k'}_{n'} \right)^2}{2\sigma^2_k} \right). \tag{6.5}$$

By applying the squaring operation of the sum in the exponent's numerator results in a term that represents the matched filtering step with the output

$$f^k_n = \sum_{k'=-1}^{1} \sum_{n'=-L}^{L} \left(r'^{k+k'}_{n+n'} h^{k,k'}_{n'} \right), \tag{6.6}$$

so that, by neglecting the term that comes from the signal sample itself as a normalization,

$$P\left(\{r'^k_n\}, d^k_n\right) \approx \exp\left(- \frac{d^k_n f^k_n - (d^k_n)^2 (E^k_s / 2)}{2\sigma^2_k} \right). \tag{6.7}$$

Alternatively, by upfront accounting for the mached-filter operation and its use in the conditional probability expression (6.4)one gets

$$P\left(r''^{k}_{n} \mid d^{k}_{n}\right) \approx \exp\left(-\frac{(f^{k}_{n} - d^{k}_{n}E^{k}_{s})^{2}}{2\sigma^{2}_{k}}\right), \tag{6.8}$$

whereby the pertaining Gaussian process average value is now given by the data symbol value multiplied by the received signal energy

$$E^{k}_{s} = \sum\nolimits_{k'=-1}^{1} \sum\nolimits_{n'=-L}^{L} \left(h^{k,k'}_{n'}\right)^{2}. \tag{6.9}$$

As further simplification, the sum of residual interference and the AWGN term, r'', can be used so that

$$r''^{k+k'}_{n+n'} = \hat{d}^{k+k'}_{n+n'} E^{k+k'}_{s} + r''^{k+k'}_{n+n'} \tag{6.10}$$

and the matched filter output is redefined as the sum of the filtered residual and the previously estimated data sample as

$$f^{k}_{n} = \sum\nolimits_{k'=-1}^{1} \sum\nolimits_{n'=-L}^{L} \left(r''^{k+k'}_{n+n'} h^{k,k'}_{n'}\right) + \hat{d}^{k}_{n} E^{k}_{s} \tag{6.11}$$

We proceed with denoting the use of the interference residuals and reconstructing the filtered signal samples through (6.11), and utilization of the residual in (6.1) along with (6.6) will be called the full-fledged one, for the possible differences in performance, in particular for the MIMO cases. In the simplified case in all the iterations firstly interference is entirely cancelled based on initial and subsequently updated soft data symbols decisions, and the two-dimensional matched filtering (MF) operation for each time-frequency bin is conducted on the matrix of the residuals $r''^{k+k'}_{n+n'}$, with subsequent augmenting by the previously estimated data symbols of that particular bin. In the full-fledged case, the MF is performed on the matrix of the received signal samples produced by cancelling of only the interference terms coming from other neighbouring bins. The visualization of the related interference cancelation and MF operations is provided in the Fig. 6.2.

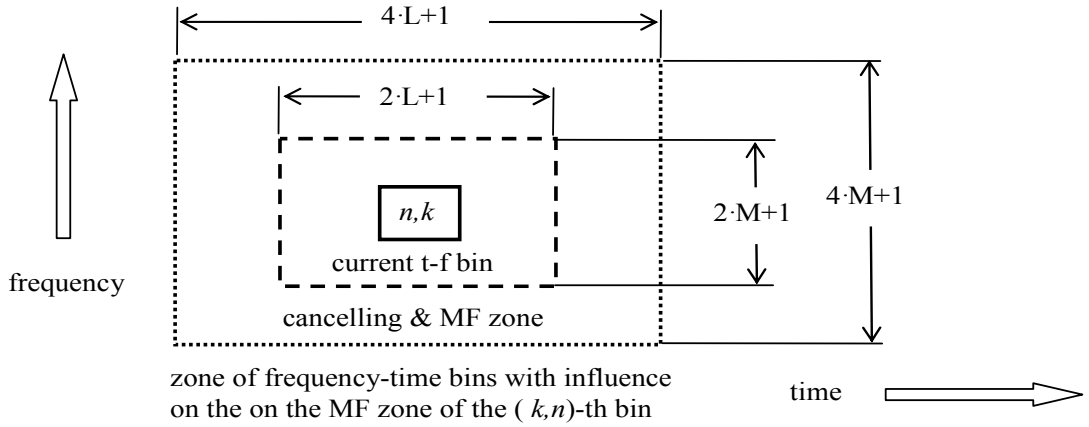

Fig. 6.2 Illustration of partitioning between time-frequency bins which are contributing to the samples which are supposed to be evaluated by the matched filtering for (n,k)-th bin.

Within each iteration, sequentially, bin-by-bin, the following operations are performed: cancelling the influence of all bins from the time-frequency neighbourhood in accordance

with the estimated impulse response lengths (L) and the number of sub-channels that significantly spectrally overlap with the currently considered bin; performing two-dimensional matched filtering within the zone spanned by the currently considered bin; re-loading the samples from the input (receive) signal samples within the zone of bins the cancellation operation was applied upon; incrementing bin location; and so on. This has been repeated for all active bins, taking into account also the corresponding time-frequency segment of the training 'block' and dummy (zero) samples augmented above, below and to the right of the samples of the received packet.

The interference cancellation algorithms are based on message passing over bipartite graphs, as shown on Fig. 6.3. In the bipartite graph, the variable nodes are the observations r_n^k, and the modulated symbols d_n^k nodes, while the control nodes are defined from the observation equation(6.10) . A control node η_n^k is associated with each set of variable nodes $\{r'^k_{n'}\}; d_n^k$. The joint probability of this set is defined by

$$P\left(\{r'^k_{n'}\}, d_n^k\right) = P\left(r'^k_n \mid d_n^k\right) \cdot P_{api}\left(d_n^k\right). \tag{6.12}$$

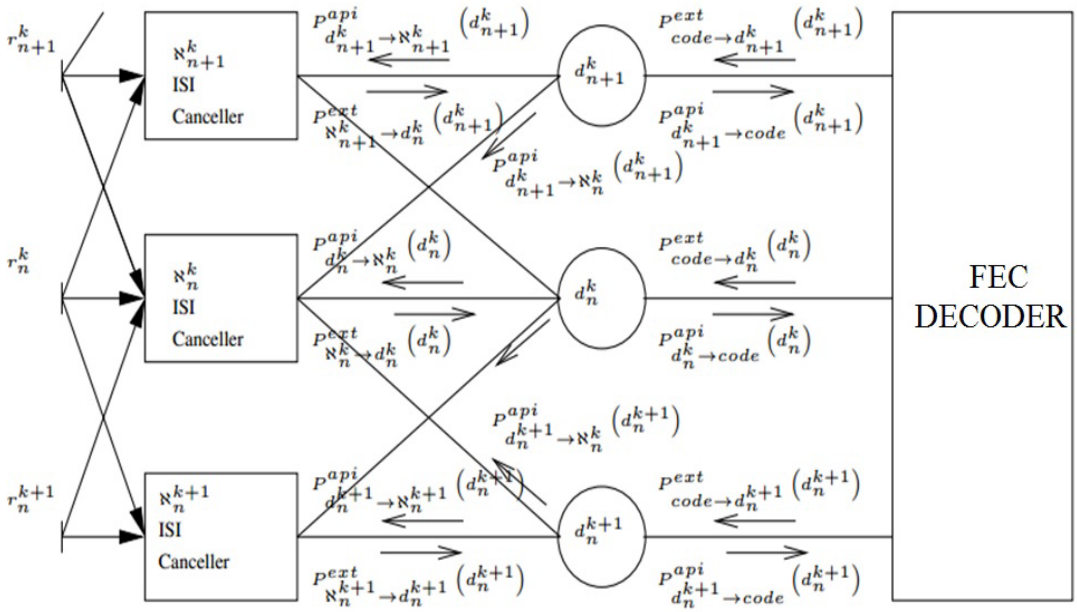

Fig. 6.3 Belief propagation between ISI canceller nodes and FEC decoder.

The a posteriori probability itself is proportional to the joint probability

$$P\left(\{r'^k_{n'}\}, d_n^k\right) = P\left(d_n^k \mid r'^k_n\right) \cdot P\left(r'^k_n\right), \tag{6.13}$$

which by Bayesian rule has also the form and from

$$P\left(\{r'^k_{n'}\}, d_n^k\right) = P\left(r'^k_n \mid d_n^k\right) \cdot P\left(d_n^k\right). \tag{6.14}$$

From the equality between the right-hand sides of the two equations above, since the *a posteriori* probability of a random variable is the product of its *a priori* probability and its *extrinsic* probability, from the equality between the right-hand sides of the two equations

above it follows that the *extrinsic* probability of a data symbol d_n^k is proportional to the *a posteriori* probability of its related signal sample, that is to $P\left(r'^k_n \mid d_n^k\right)$.

The resulting extrinsic probabilities from (6.8), produced by an additional normalization, are denoted with $P^{ext}_{\eta_n^k \to d_n^k}(d_n^k)$ in Fig. 6.3. To compute the intermediary received signal samples $r'^{k+k'}_{n+n'}$, as per (6.2), through the subtraction of the samples of the "re-modulated" signal produced by the data estimates, the node η_n^k uses the a priori probabilities $P^{api}_{d_n^k \to \eta_n^k}(d_{n'}^{k'})$ for $n \neq n'$ and $k \neq k'$ in computing conditional data symbols expectation by

$$\hat{d}_n^k = E\{d_n^k \mid r\} = \sum_{\{d_n^k\}} d_n^k P^{api}_{d_n^k \to \eta_n^k}(d_n^k). \tag{6.15}$$

Since in the case without coding or with decoupled decoder iterations only one edge terminates at the variable node d_n^k the a priori probability $P^{api}_{d_n^k \to \eta_n^k}(d_{n'}^{k'})$ is equal to the extrinsic probability $P^{ext}_{\eta_n^k \to d_n^k}(d_n^k)$.

If an error correcting code is used, the variable node d_n^k is connected to the control node defined by the transformation of QAM symbols into bits, a deinterleaver, and a soft input soft output FEC decoder. The message passed from the FEC decoder to the variable node d_n^k is defined by $P^{ext}_{cod \to d_n^k}\left(d_n^k\right)$

$$P^{api}_{d_{n+1}^k \to \eta_n^k}(d_{n+1}^k) = P^{ext}_{\eta_{n+1}^k \to d_{n+1}^k}(d_{n+1}^k) \cdot P^{ext}_{cod \to d_{n+1}^k}(d_{n+1}^k). \tag{6.16}$$

In combination with coding, the output of FEC decoder is used as intrinsic information to calculate the new soft symbols.

Further details regarding the interface between the SIC detector and FEC decoder parts are illustrated by the following figure for the 16-QAM constellation case, with the pertinent expressions given in the sequel.

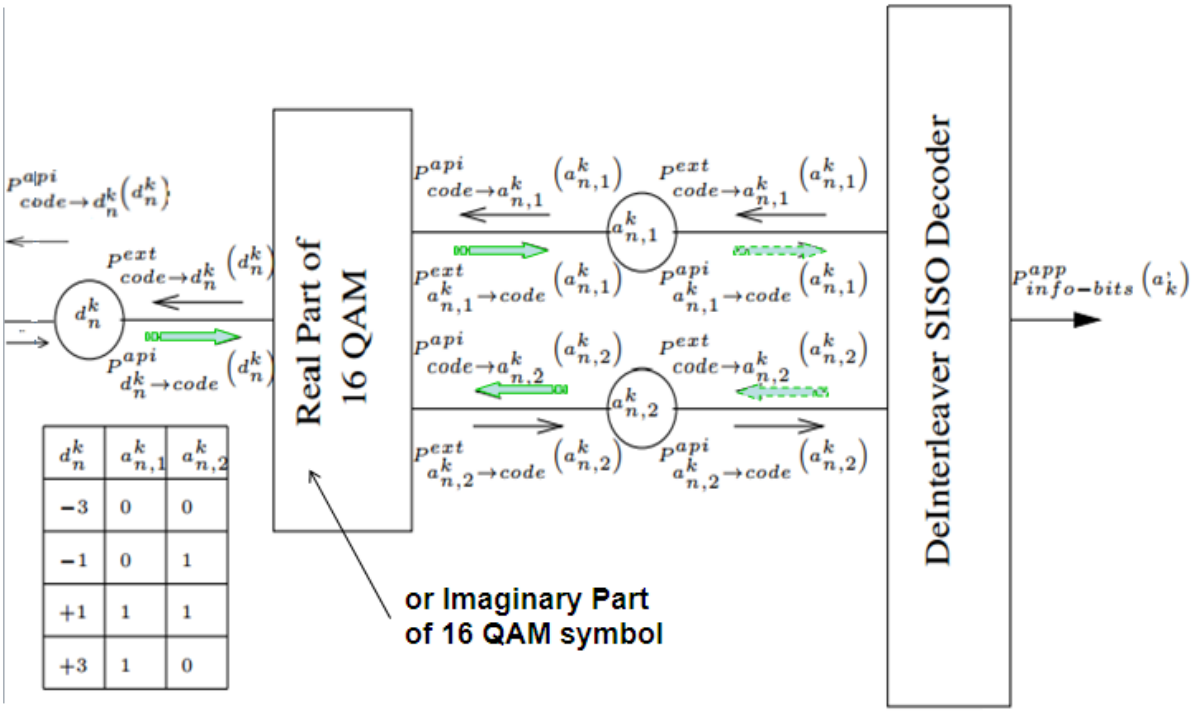

d_n^k	$a_{n,1}^k$	$a_{n,2}^k$
−3	0	0
−1	0	1
+1	1	1
+3	1	0

Fig. 6.4 Interfacing SIC detector and FEC decoder.

The convolutional code is decoded by using a forward-backward. The inputs of the FEC decoder are the a priori probabilities of the coded bits, $P^{api}_{a^k_{n,j}\to code}\left(a^k_{n,j}\right)$, while its outputs are the a posteriori probabilities of the information bits for the sink $P^{app}_{ifrmbit}(a'^k_{n,j})$ and the extrinsic probabilities of the coded bits $P^{ext}_{code\to a^k_{n,j}}\left(a^k_{n,j}\right)$. For the 16-QAM modulation, the two bits $a^k_{n,1}, a^k_{n,2}$ are associated with the quaternary symbol d^k_n with a mapping indicated in the table shown in the figure above.

A third group of control nodes represents the AM modulation, the real or imaginary component of a QAM modulation. In the case of a multidimensional QAM modulation, a 32 QAM, or an 8-dimensional coded modulations, these modulation nodes represent the coded modulation mapping. For a 16-QAM, i.e. a 4-AM modulation for each of the quadrature components, the control node AM is connected to the variable nodes d^k_n, $a^k_{n,1}$ and $a^k_{n,2}$. The corresponding a priori probabilities are defined by using the variable nodes input-output relations defined as follows:

$$P^{api}_{a^k_{n,j}\to PAM^k_n}(a^k_{n.j}) = P^{ext}_{code\to a^k_{n,j}}(a^k_{n.j}), \tag{6.17}$$

and

$$P^{api}_{d^k_n\to \eta^k_n}(d^k_n) = P^{ext}_{code\to d^k_n}(d^k_n). \tag{6.18}$$

The message passing is divided in two directions. The forward direction from the ISI canceller to the decoder, and the backward direction from the decoder to the ISI canceller. The relations are

$$P^{ext}_{code\to a^k_{n,j}}\left(a^k_{n,1}=0\right)=\left\{\begin{matrix} P^{ext}_{code\to a^k_{n,2}}\left(a^k_{n,2}=0\right)P^{api}_{d^k_n\to code}\left(d^k_n=-3\right)+ \\ P^{ext}_{code\to a^k_{n,2}}\left(a^k_{n,2}=1\right)P^{api}_{d^k_n\to code}\left(d^k_n=-1\right) \end{matrix}\right\} \tag{6.19}$$

$$P^{ext}_{code\to a^k_{n,j}}\left(a^k_{n,1}=1\right)=\begin{Bmatrix}P^{ext}_{code\to a^k_{n,2}}\left(a^k_{n,2}=0\right)P^{api}_{d^k_n\to code}\left(d^k_n=3\right)+\\ P^{ext}_{code\to a^k_{n,2}}\left(a^k_{n,2}=1\right)P^{api}_{d^k_n\to code}\left(d^k_n=1\right)\end{Bmatrix}, \tag{6.20}$$

and similar definitions apply for the second bit $a^k_{n,2}$.

The backward relations are given by

$$P^{api}_{code\to d^k_n}(d^k_n=-3)=P^{api}_{code\to a^k_{n,1}}(a^k_{n,1}=0)P^{api}_{code\to a^k_{n,2}}(a^k_{n,2}=0) \tag{6.21}$$

$$P^{api}_{code\to d^k_n}(d^k_n=-1)=P^{api}_{code\to a^k_{n,1}}(a^k_{n,1}=0)P^{api}_{code\to a^k_{n,2}}(a^k_{n,2}=1), \tag{6.22}$$

etc., for dibits 11 and 10 with respective PAM levels 1 and 3.

For basic reference, further are provided simulation results for the SISO case with AWGN and the frequency flat, Rayleigh fading channel and the multi-tap channel impulse response with the power profile given by the table below (with the channel bandwidth spanned with 7 out of 8 FBMC subchannels, as it was considered in the in the Chapter 3:

Table 6.1 The power profile for multi-tap channel used in simulation

Delay [ns]	**Power [dB]**
0	0
100	-5.4287
200	-2.5162
300	-5.8905
400	-9.1603
500	-12.5105
600	-15,6126
700	-18,7147
800	-21.8168

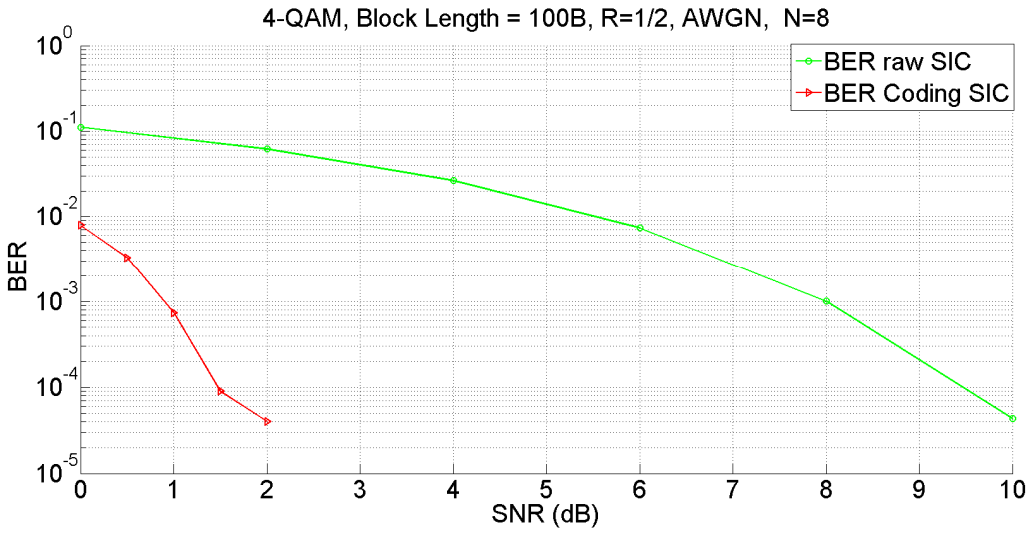

Fig. 6.5 SISO SIC AWGN BER curves.

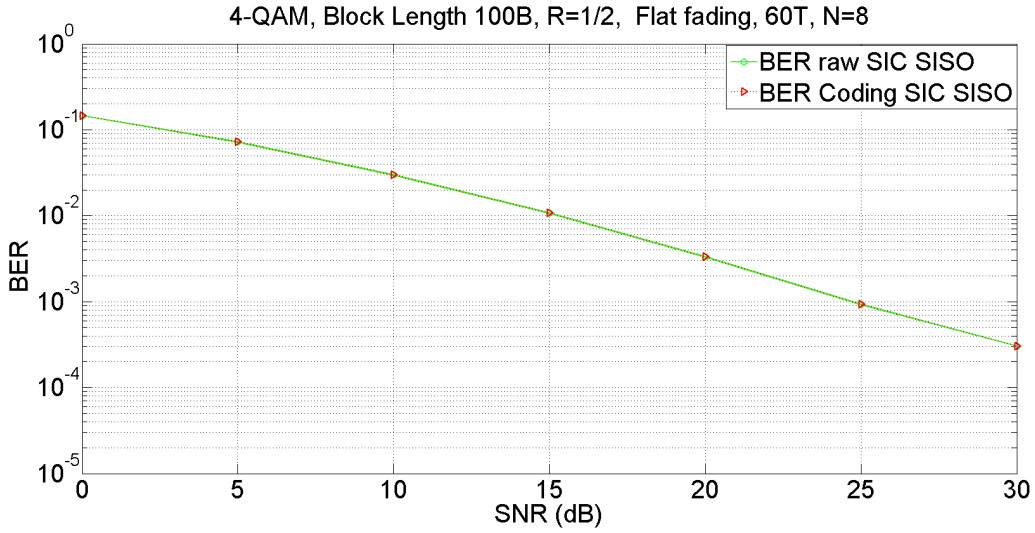

Fig. 6.6 SISO SIC BER curves for Rayleigh flat fading distributed channel.

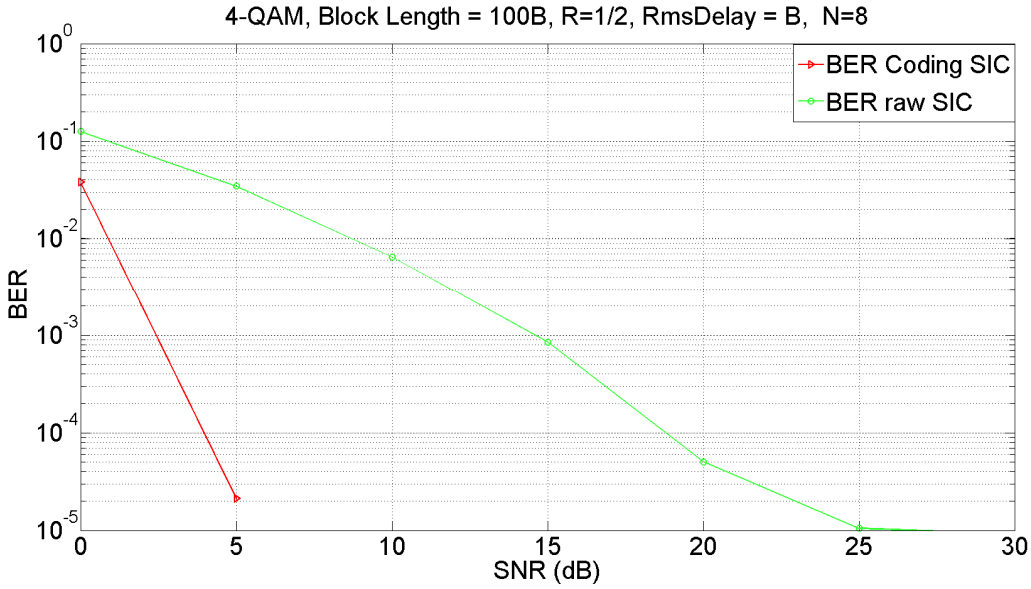

Fig. 6.7 SISO SIC BER curves for multipath channel.

6.1.1 Log likelihood ratio formulation

In this subsection we will give the brief description of traversing into the conventional log likelihood ratio (LLR) formulation which has been shown to be much more advantageous for the extensions towards MIMO configuration, in particular the 2x1 one.

Starting from (6.8) the LLR ratio of the two extrinsic probabilities in 4-QAM (or QPSK) is defined as

$$L_{extr}(r_n^k \mid d_n^k) = \ln\left(\frac{P(r_n^k \mid d_n^k = +1)}{P(r_n^k \mid d_n^k = -1)}\right). \tag{6.23}$$

The $L_{extr}(r_n^k \mid d_n^k)$ matched with the $P^{ext}_{\eta_n^k \to d_n^k}(d_n^k)$ in the previous section. By denoting the feedback from the decoder as $L_{api}(r_n^k \mid d_n^k)$, which is defined similarly, the data symbols estimates now take the form

$$\hat{d}_n^k = (\tanh(L_{app}(d_n^k \mid r_n^k)/2))/\sqrt{2}, \tag{6.24}$$

where the $L_{app}(d_n^k \mid r_n^k)$ is represented by sum of the two previously calculated LLRs, that is

$$L_{app}(d_n^k \mid r_n^k) = L_{extr}(r_n^k \mid d_n^k) + L_{apri}(r_n^k \mid d_n^k). \tag{6.25}$$

6.2 Diversity-like combination of in-phase and quadrature components

Rather than considering the "intrinsic interference" as a problem, we attempt its constructive use, primarily through independence of the noise components present on the in-phase and quadrature branches, with possibly further benefitting from at least certain independence among even the in-phase and quadrature branches of fading channels impulse responses. The block diagram of such a configuration, with incorporation of the prediction and cancellation of the noise part coloured by the receiver-end filter-bank is

hinted in Fig. 6.8 to the right of the vertical dashed line, demarcation between the complex- and real-domain processing, whereby the FEC decoder part to the tight has been omitted.

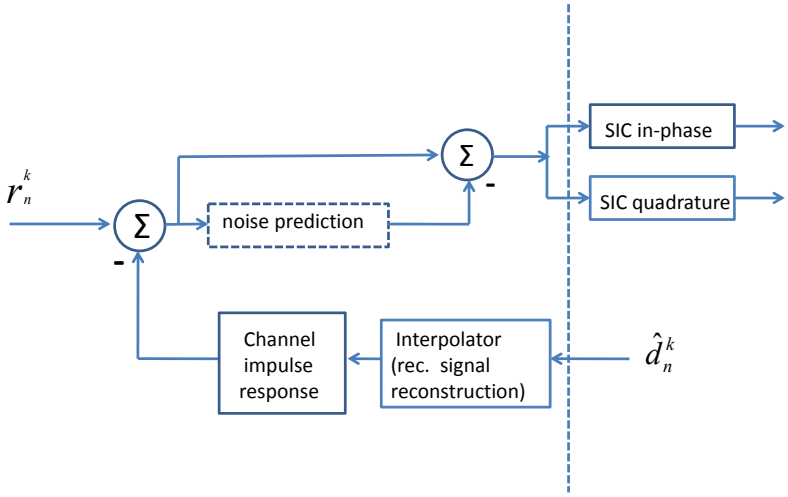

Fig. 6.8 Block-diagram of I/Q combining, with noise prediction and cancellation part to be considered later.

As in (2.21) we involve the imaginary component of received signal in the following manner

$$r_n^k imag = \mathrm{Im}\left\{\int_{-L_gT}^{L_gT}\sum_{k'=k_1}^{k_2}\sum_{n'=0}^{2M-1} j^{k'+n'} d_{n'}^{k'} g_{k'}\left(t+(m-n')T/2\right)\cdot e^{j2\pi k'\frac{t+(m-n')T/2}{T}} j^{-k-m} g(t)\cdot e^{-j2\pi k\frac{t}{T}} dt\right\}, \quad (6.26)$$

with estimation of the corresponding set of impulse responses as in the in-phase branch.

After producing the matched filter outputs within the process of the independent SIC detectors applied to the two signal quadrature components in a turbo-like interaction with the one FEC decoder, the question arises as to how to perform the combination of the two extrinsic probabilities to perform the data symbols estimation without or with combination with the FEC.

Derivation of I/Q diversity configuration

In line with the joint (bivariate) distribution of two Gaussian processes (*X* and *Y*), i.e. the respective variables *x* and *y*, with respective average values μ_x and μ_y in the form

$$f(x,y) = \frac{1}{2\pi\sigma_x\sigma_y\sqrt{1-\rho^2}}\exp\left(-\frac{1}{2(1-\rho^2)}\left[\frac{(x-\mu_x)^2}{\sigma_x^{\,2}}+\frac{(y-\mu_y)^2}{\sigma_y^{\,2}}-\frac{2\rho(x-\mu_x)(y-\mu_y)}{\sigma_x\sigma_y}\right]\right), \quad (6.27)$$

where correlation coefficient is $\rho = \dfrac{E(XY)}{\sigma_x\sigma_y}$, by taking the outputs of the matched filter outputs for these two variables along the corresponding average values (assuming same energies of the Re and Im branches, the produced exponent part becomes

$$\frac{(f_n^k[Re]-d_n^k E_s^k[Re])^2+(f_n^k[Im]-d_n^k E_s^k[Im])^2}{\sigma_k^{\,2}} - \frac{2\rho(f_n^k[Re]-d_n^k E_s^k[Re])(f_n^k[Im]-d_n^k E_s^k[Im])}{\sigma_k^{\,2}} \quad (6.28)$$

For independent noise, the two random processes are uncorrelated, and the above expression (with reinserting the previously omitted factor in the exponent) now becomes

$$\frac{(f_n^k[Re] - d_n^k E_s^k[Re])^2 + (f_n^k[Im] - d_n^k E_s^k[Im])^2}{2 \cdot \sigma_k^{\ 2}} \tag{6.29}$$

meaning that the effective extrinsic probability would be a product of extrinsic probabilities of two branches, that is

$$P_{ext}^{eff} = P_{ext}^{[Re]} \cdot P_{ext}^{[Im]}, \tag{6.30}$$

where the superscripts are added to differentiate between the two branches. This becomes conceptually quite appealing, in that the product of the two probability density functions (with the same average values and the same variances) reveals narrowed shape compared with any one of them, implying (by the product of two numbers smaller than 1 is smaller than either one of them) the reduction of the overall variance, that is the effective SNR, which lies in the essence of the maximal-ratio combining of the two (diversity) branches.

Another option would be to combine the outputs of matched filters which are calculated separately according to (6.11). After that, we use the following equation to calculate the extrinsic probability:

$$P\left(r'^k_n, r'^k_n\, imag \mid d_n^k\right) \approx \exp\left(-\frac{(f_n^k + f_n^k imag - 2 \cdot d_n^k E_s^k)^2}{2(\sigma_k^2 + \sigma_k^2 imag)}\right). \tag{6.31}$$

When we introduce the imaginary branch we also get a better signal to noise (SNR) ratio but we still don't have a gain in comparison to the processing only real branch as in standard SIC SISO mode.

6.3 Conclusion

Neither of these two options has yet produced the expected diversity effect, and we will continue with these explorations for some time. The Q-branch otherwise works as the I one, and the noise samples had been checked to be independent, so there must be a "way out".

7. Noise prediction and cancellation for FBMC

The presence of coloured noise at the input of data signal detection stage has been traditionally considered as an obstacle toward achievement of optimal performance of the ML, i.e. MLSE (maximum likelihood sequence estimation) detection procedures, and its whitening has been attempted by the mere redistribution of the input noise spectral density, at the expense of introducing the additional linear distortions, which are then coped with through the adequately defined target impulse response. The result is that the power of noise remains essentially unchanged, but only redistributed is its frequency content.

However, since the noise coloration at least in principle allows for the possibility of its prediction and the subsequent cancellation (subtraction, thus reduction of the effective noise power, along its whitening) of the predicted part from the overall signal entering the detector stage, it appears reasonable to attempt such a procedure in particular within the MLSE and/or the block-level detection/decoding as is the SIC method, optionally interacting with a FEC decoder. Indeed, in line with the in last decade or two well established trellis-embedding of per-path DFE structures [46], in [47] has been elaborated the incorporation of noise prediction and cancellation structures within the trellis-search of the partial-response class IV [48], applied in the frequency-domain, consistently with the Hanning-windowed CP-OFDM receive signal.

A rather thorough analysis of the noise correlation at the output of the analysis filter-bank in the context of FBMC (FBMC/OQAM) format has been conducted in [1], where the goal was to demonstrate the independence of noise samples pertinent to the I and Q at subsequent T/2 instants (within one subchannel) along with the generalization to the situation when a per-subchannel equalizer or other form of filtering is taking place. Therein it has been shown and adequately illustrated that, while being mutually independent, both the real (in-phase) and the imaginary (quadrature) components have strong correlation, with the factor around 0.5, at T/2 time-lag. This allows for the candidate noise samples pertaining to the "intrinsic interference" terms, along those that directly correspond to the data-bearing samples, be produced by subtracting from the received (complex) signal its re-modulated version based on the data samples estimated within the previous SIC iteration. Those noise samples, now available at T/2 instants, can then be used to make prediction of the noise samples for the subsequent time instant and to subtract them before filtering the residual signal.

7.1 Integration of the NPC functionality into the soft interference cancellation framework

The complex-domain FBMC signal reconstruction, in line with (2.11), is based on soft data samples estimates and has the form

$$\widetilde{x}_n^k = \sum_{k=k_1}^{k_2} \sum_{m=0}^{2M-1} j^{k+m} \widehat{d}_n^k \cdot g(n - mT/2) e^{j2\pi k \frac{t-mT/2}{T}} . \qquad (7.1)$$

The predicted noise samples in complex-domain, $\{\overline{x_n^k - \widetilde{x}_n^k}\}$, produced based on the difference between the actual and interpolated complex receive samples, x_n^k and $\widetilde{x}_n^k$, that is

their (Re and Im) parts corresponding tob the information bearing T/2 instants, $\tilde{b}_n^k$, are further subtracted from the corresponding components of the received complex signal used in the real-domain SIC, i.e.

$$r'^{k+k'}_{n+n'} = \hat{d}_n^k \hat{h}_{n'}^{k+k',k'} + r''^{k+k'}_{n+n'} - \tilde{b}_{n+n'}^{k+k'}, \tag{7.2}$$

for $k'+k'' \neq 0$, $n'-n'' \neq 0$, $k' = -1,0,1$, and $n' = -L,\ldots,0,\ldots L$.

The prediction coefficients are produced by spectral decomposition, and for the case of the FBMC referent impulse response

$$c = [0\ 0.0008\ -0.0260\ 0.0245\ 0.9996\ 0.9992\ 0.0243\ -0.0259\ 0.0008\ 0] \tag{7.3}$$

designed by the procedure proposed in [2], the prediction coefficients calculated by the standard procedure, in particular using the Levison-Durbin algorithm (MATLAB function *levison*), in case of selected order 8, are

$$p = [-0.9691\quad 0.8869\quad -0.8383\quad 0.6716\quad -0.5250\quad 0.3750\quad -0.2650\quad 0.1268]. \tag{7.4}$$

For illustration, in Fig. 7.1 are shown spectra of the FBMC subchannel noise, its predicted, and the residual parts.

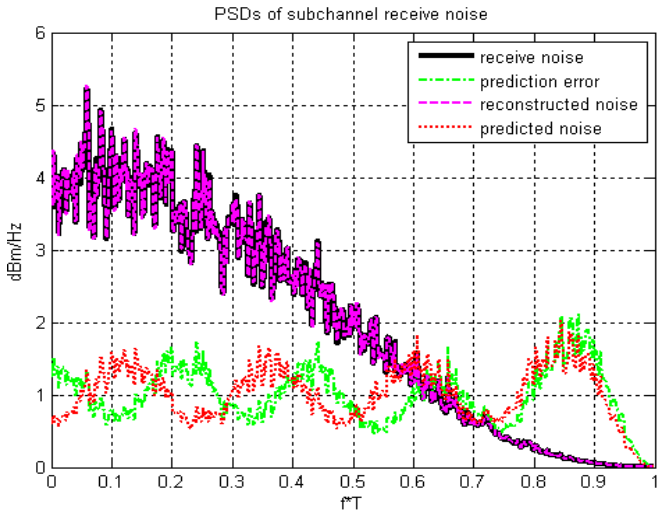

Fig. 7.1 Spectra of the FBMC subchannel noise, its predicted, and the residual parts.

Fig. 7.2 shows the factual and predicted noise samples for the one of quadrature components. By roughly counting the number of squares under the PSD plots for the total and the predicted noise signals, it comes out that the effective noise power would be reduced by about 3dB if the sufficiently reliable soft decisions could be made in the process of block-level SIC-detector/SISO-decoder iterations.

It could be expected that the SIC and noise prediction/cancellation passes might aid each other, but it might be necessary to find best strategy in order not to rely on insufficiently accurate data symbol expectations for the noise prediction/cancellation steps. In the following several options are explored, without looking for the possibly best strategies, but more for the testing purpose.

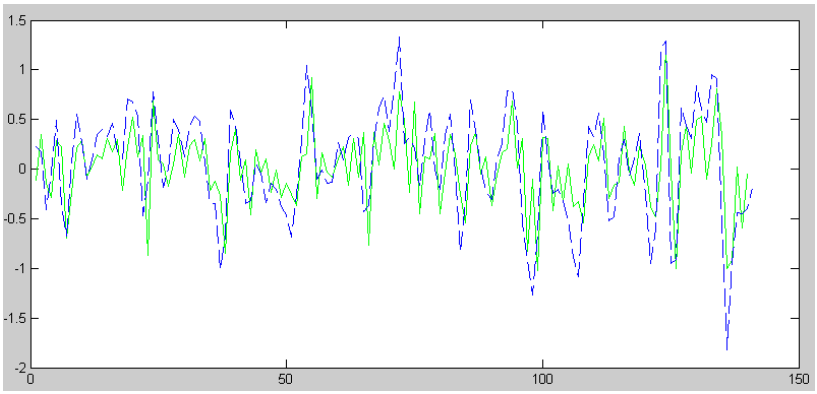

Fig. 7.2 The factual and the predicted noise samples for the one of quadrature components.

The structure is shown in Fig. 7.3, no I/Q combining takes place, but only the SIC on the in-phase branch is involved. (With the inclusion of the quadrature branch as per the method proposed in the previous section, the SNR gains from both methods individually can be expected to be combined to certain level.) Simulation results for AWGN channel are given in Fig. 7.4.

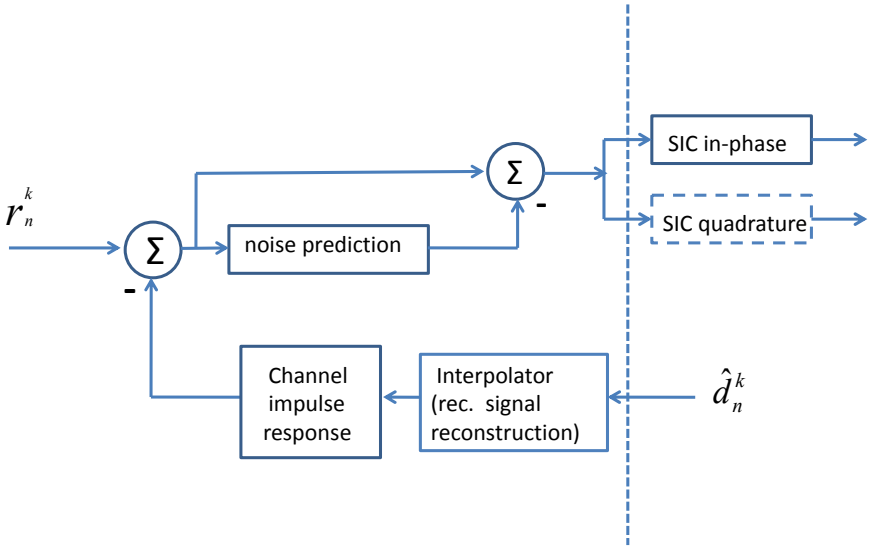

Fig. 7.3 Block-diagram of noise prediction and cancellation

Noise cancellation by direct cancellation subtraction of estimated residuals

Since in block-level processing, all the soft data symbols along their interpolated values can be available, the (estimated) total noise term components are available, too, and question arises why one should at all do the prediction?! Furthermore, in such situation the interpolation procedure would not be needed.

Cancellation of the predicted noise part

The use of noise prediction and subtraction of only the predicted noise part during the SIC-detector/SISO-decoder iterations was the initial intent, in line with the previously conceived procedure for the MLSE framework.

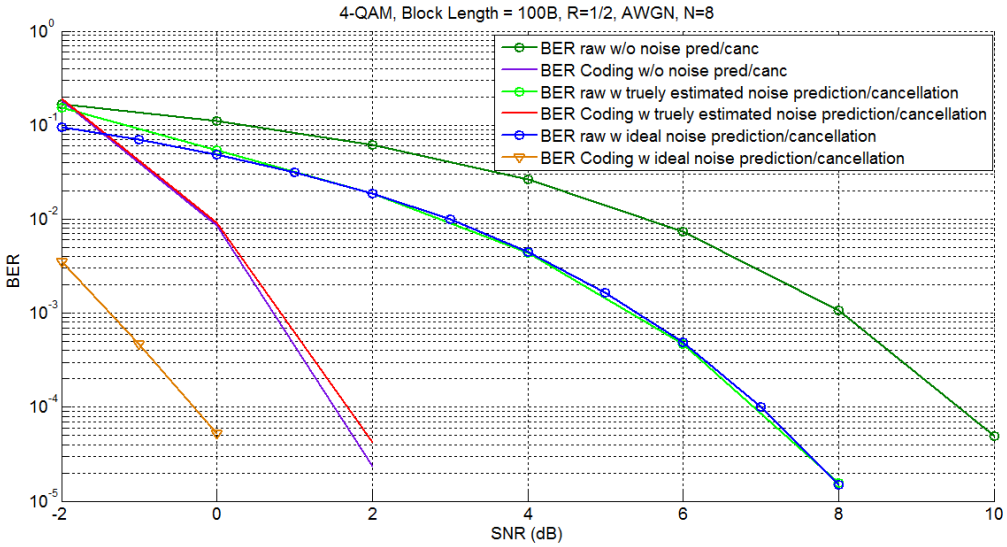

Fig. 7.4 Simulation results for the cases without and with noise suppression for the AWGN channel.

Simulation results

In Fig. 7.4 above are shown simulation results for the option with cancellation of the predicted noise, including the use of the ideally estimated noise part. While in the latter case the effect of noise suppression is clearly visible, when realistically estimated noise samples are used in prediction, only the uncoded BER performance becomes significantly improved, for even more that 3dB, while the coded performance remains unchanged with respect to the case without noise suppression. This behaviour needs to be further explored.

7.2 Conclusion

These results were produced in turbo-mode interaction between SIC detector and the convolutional FEC decoder, and the noticeable SNR gain in produced by hard-decision of the soft data estimates, although corresponding exactly to the expected 3dB then becomes irrelevant, since coded BER performance is still better than un-coded. It might be possible, though, that the soft-input-soft-output FEC decoder used may be sensitive to the particular coloration of the residual noise. The simulations have to be performed with fully decoupled SI detector and FEC decoder to resolve this situation. By all means, when the noise samples are correctly estimated and then used in prediction, the coded performance becomes improved, while the “uncoded” remains the same as when noise samples are realistically extracted by subtraction of the received samples from soft-estimates the interpolated data bearing samples.

8. Progress with the unified frequency-domain synchronization concept

One of the main targets of the synchronization studies under EMPhAtiC WP3 is to move the time and frequency synchronization functions from the time-domain processing side to frequency domain, to be implemented through subcarrier processing. This is important in fragmented spectrum use scenarios, i.e., in non-contiguous multicarrier systems, because otherwise it is difficult to manage the strong interfering spectral components which may be dynamically allocated between the used portions of the received spectrum. Furthermore, the fast-convolution filter bank (FC-FB) processing structure is able to support simultaneous processing of non-synchronized signals from different users. In this respect, our goal is to support asynchronous operation in cellular uplink or ad-hoc scenarios, such that only coarse frequency synchronization is required to be achieved outside the subcarrier processing functions of the receiver.

Earlier we have reported in EMPhAtiC deliverable D3.1 FC-FB based timing offset and frequency offset estimation algorithms, as well as timing offset compensation methods fulfilling the mentioned requirements. The timing adjustment method is capable of compensating relative timing offsets between non-overlapping groups of subcarriers which are well beyond the subcarrier OQAM symbol interval.

8.1 CFO compensation

In this section we complete the picture by introducing carrier frequency offset (CFO) compensation methods implemented through subcarrier processing utilising the FC-FB ideas. Earlier the idea of shifting the FFT-domain subchannel weight mask by an integer number of FFT bins has been mentioned as a way to compensate CFO's up to ± 0.5 times the FFT bin spacing. In the EMPhAtiC demonstrator configuration, the subcarrier spacing is 8 FFT bins, so the residual CFO is within ±0.0625 times the subcarrier spacing. Clearly this is too much for obtaining reasonable link performance.

Our approach for fine CFO compensation is to shift the subchannel weight mask by a fraction of the FFT bin spacing. Similar approach was used in [49] for fine CFO compensation in the context of polyphase FBMC/OQAM implementation. The weight mask shift can be achieved, e.g., by sampling the square root raised cosine function with the desired frequency offset. Alternatively, it would be possible to optimize different sets of weight masks, with sufficient number of fractional frequency shifts using the methods presented in deliverable D2.1. Another approach is to interpolate the weight mask for the target frequency shift from the basic weight mask. Actually, it will be seen that linear interpolation is likely to be sufficient for most practical needs. The general idea is illustrated in Fig. 8.1(a). In the case of linear interpolation, the mask is first shifted by integer number of FFT bins such that the residual CFO $\delta_{CFO} \in (-1, 0]$. Here, δ_{CFO} is the CFO value normalized to FFT bin spacing. Then, the new weight values are interpolated as follows:

$$\hat{w}_k = (1 - \delta_{CFO}) w_k + \delta_{CFO} w_{k+1} . \quad (8.1)$$

Interpolation methods, and linear interpolation in particular, can be applied in flexible ways. After re-calculating the weights, they can be used for processing longer sequences of data samples, as long as the CFO value remains constant. But this is equivalent to weighting the

FFT bins by the original weight factors and interpolating the data samples between FFT-bins afterwards.

In addition to the weight mask shifting, it is necessary to use I/Q mixing after the IFFT of the receiver analysis bank, to shift the subcarrier spectrum to the right position as shown in Fig. 8.1(b). In other words, the shifted weight mask implements the subchannel filtering in a proper way, and the mixing brings the subchannel to the correct spectral position.

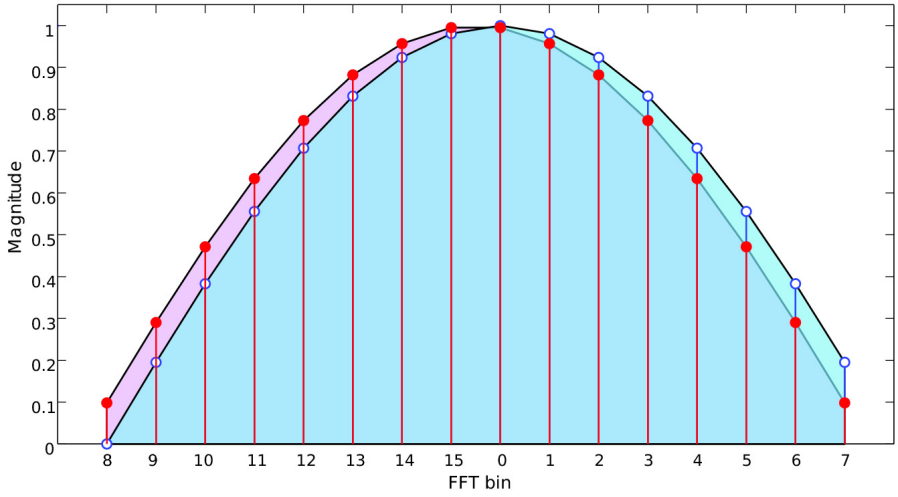

(a)

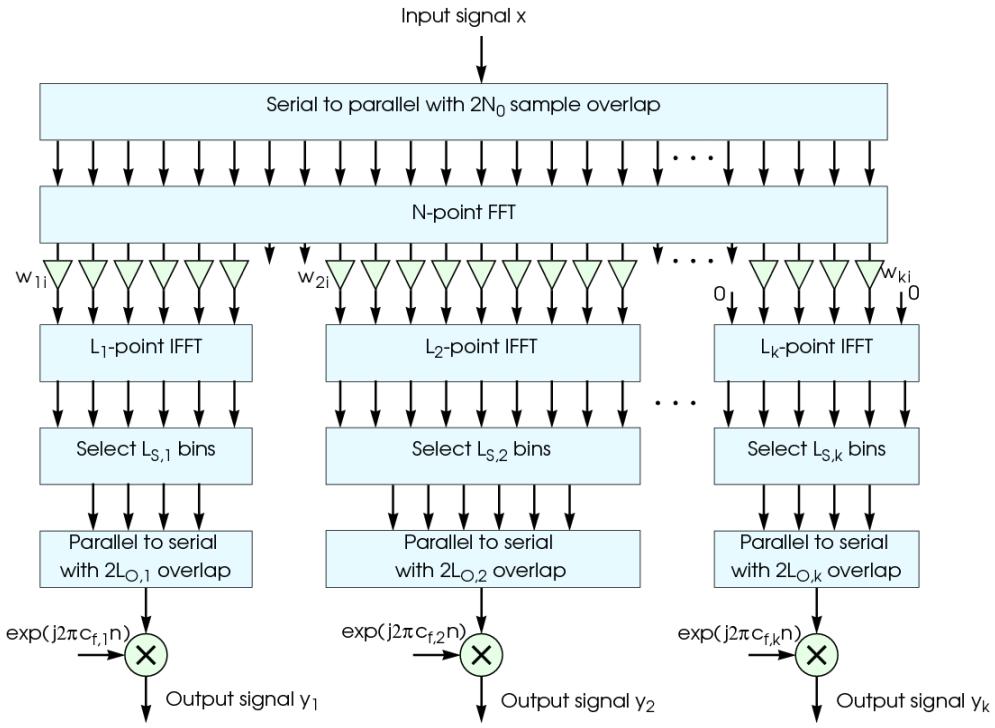

(b)

Fig. 8.1 (a) FFT weight mask shifting for CFO compensation. (b) FC-AFB structure including I/Q modulation based frequency shifting as another element of the CFO compensation idea.

The CFO compensation can also be realized by interpolating the FFT bins directly in frequency-domain by means of circular convolution [50, 51]. In this case, the FFT weight mask shifting and I/Q modulation can be avoided. However, in general, the complexity of the circular convolution is higher than the aforementioned technique. Future work is devoted on analysing the performance and implementation complexities of these two alternative ways of performing the CFO compensation.

8.2 Numerical example

The following numerical example is based on the EMPhAtiC demonstrator parameterization for 1.4 MHz 3GPP LTE like scenario (sampling rate of 1.92 MHz, 72 active subcarriers out of 128). The fast-convolution based analysis filter bank (FC-AFB) for FBMC/OQAM waveform is based on FFT length of 1024 and short transform length of 16, such that the subcarrier spacing is 8 FFT bins. The overlapping factor is 6/16, i.e., each FFT block carries 5 OQAM subcarrier symbols. The real coefficient optimized weight mask is used.

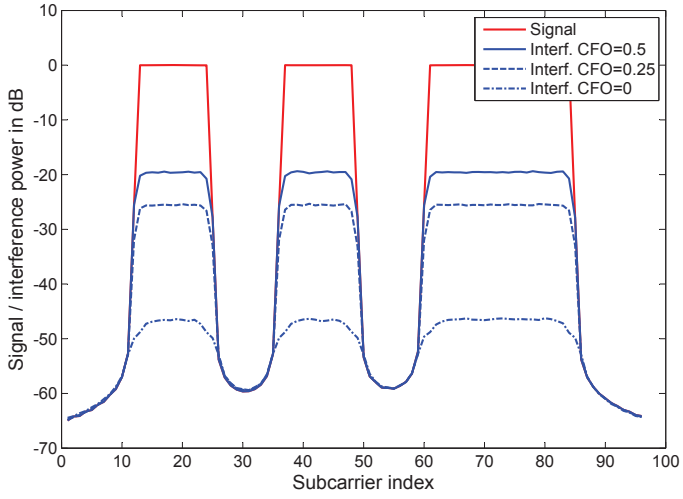

(a)

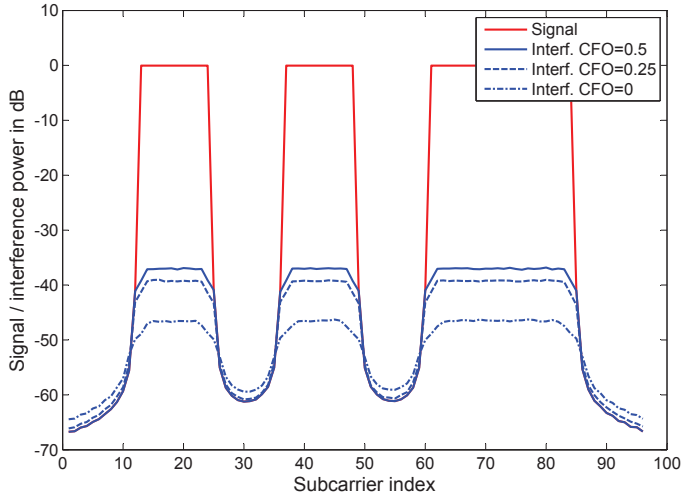

(b)

Fig. 8.2 Interference levels with CFO compensation for FBMC/OQAM waveform: (a) Subchannel weight mask not shifted. (b) Weight mask shifted through linear interpolation.

Fig. 8.2 shows the spectra, measured through the subcarrier power levels, for a case where two gaps of 1 resource block width (12 subcarriers) are placed in the middle of active subcarriers. It can be seen that without properly shifted subchannel filtering, the interference levels are greatly increased in case of plain I/Q-modulation based CFO compensation. With linear interpolation based shifting, the interference level is below –35 dB with respect to the subcarrier power levels, even with the worst-case CFO of 0.5 FFT bins.

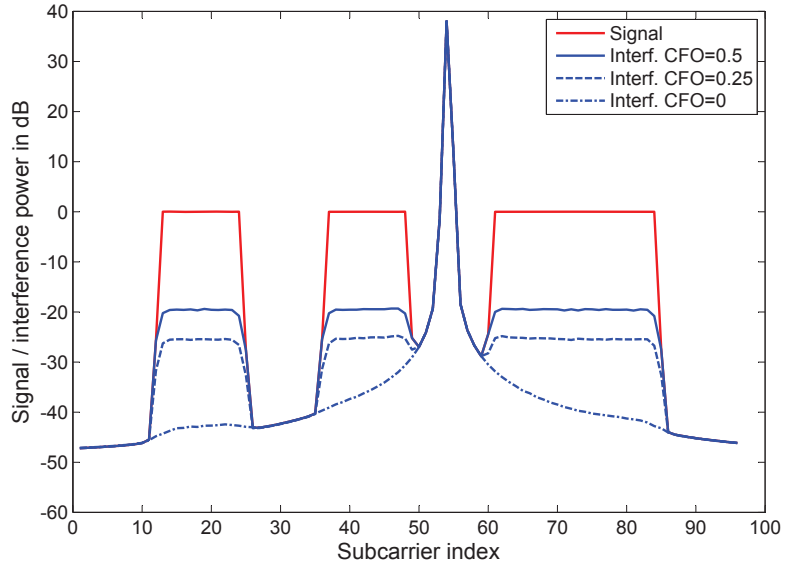

(a)

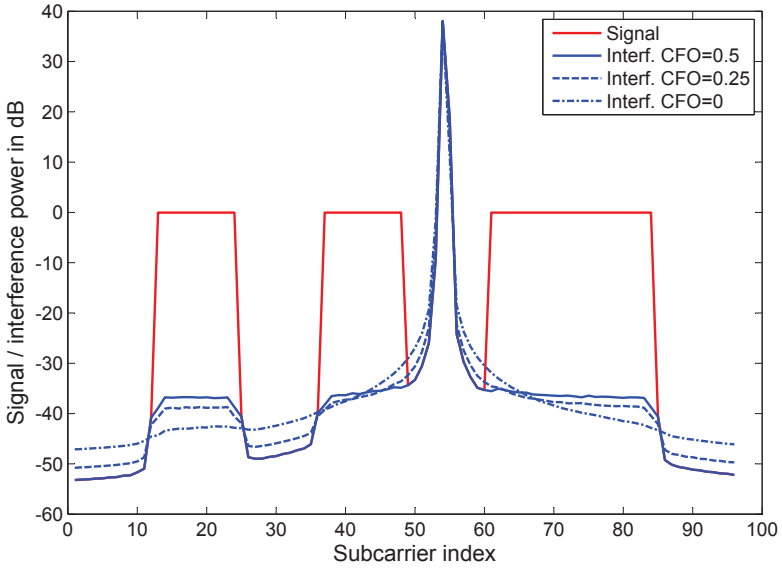

(b)

Fig. 8.3 Interference levels with CFO compensation for FBMC/OQAM waveform in the presence of strong narrowband interference: (a) Subchannel weight mask not shifted. (b) Weight mask shifted through linear interpolation.

Fig. 8.3 shows another case where a strong narrowband interference appears in one of the spectral gaps. The interference power is 40 dB above the active subcarrier power level. It can be seen that the interference remains at a tolerable level also in such a scenario.

8.3 Conclusion

A method for fine CFO compensation was developed utilizing the fast-convolution filter bank structure. Very good CFO compensation performance was demonstrated for any CFO in the range of (–1,0] subcarrier spacings. This method can be combined with the basic idea that CFO's of integer multiples of the subcarrier spacing can be compensated simply through the selection of FFT bins to the subcarrier weighting process. This combination makes it possible to compensate basically any CFO with high quality and low computational complexity. This method is especially valuable for supporting frequency-domain multiplexing of different users' transmissions without the needed for precise synchronization between them.

9. Conclusions

Besides equalization and successive interference cancellation to cope with the linear distortions induced by the multipath fading transmission channel, we paid attention to the recently actualized WLF-based equalization approach and explored it for the suppression of co-channel interference coming from a signal of the same type. For excessive multipath, and in particular the propagation conditions where the channel impulse response taps are partially concentrated (i.e. the impulse response exhibits sparseness), several methods have been developed to efficiently compensate for the resulting linear distortions, also coping with time varying channels.

We presented a comprehensive treatment of the co-channel interference resilience inherent to the FBMC/OQAM format by the use of MMSE WLF to clearly indicate a certain gain in comparison with the strictly linear MMSE equalization approach. Since the pseudocorrelation matrix with essentially 100% roll-off subchannels' spectra is zero, in the simulations conducted the non-zero pseudocorrelation was emulated by taking only every second subchannel as active. Otherwise, with all the subchannels active, the whole range of the second order statistics going from the mere circularity to the "full" non-circularity can be produced with roll-off factors from 100% to (non-realistic) 0% roll-off. This brings about the need to revisit the classical FBMC/OQAM waveforms from this perspective and offers a motivation for exploiting the use of the FMT subchannels configuration with I/Q staggering (essentially the 2G wireless GMSK standard with the trivial extension towards multi-level modulation in its linearized form), or particularly the fully overlapped TLO FB-MC subchannels (documented in D2.1) offering an appealing trade-off between spectral efficiency and the transmission latency. For future work, before we start including the feed-back parts to work with the DFE configuration and possibly have some additional degrees of freedom over the conventional FBMC/OQAM, we will be exploring the impact of spectral overlapping of subchannels with roll-off factors smaller than one, as well as the case where subchannels overlap among several consecutive subchannels, as it is the case in the TLO multi-carrier waveform case, including also the non-overlapping (FMT) subchannels with relatively small roll-off factors to trade-off spectral efficiency and the sub-channel interference suppression capability.

The contribution on equalization of doubly dispersive channels was split into three parts: (a) precoder-assisted equalization (using WHT for simplicity) for increasing frequency diversity, (b) equalization based on channel tracking, and (c) direct adaptive equalization algorithms, with (b)-(c) relying on pilots scattered throughout the frame. In all three cases, channels of sufficiently high time dispersion to imply frequency selective subchannels were assumed, relaxing the commonly made assumption of flat subchannel responses and hence enhancing the practical value of these results in PMR environments. Both medium and high frequency selectivity channels were tested, at zero, medium, and high vehicular speeds. In particular, a PMR-specific experiment was also implemented, employing a pilot format appropriate for downlink transmission, and transmission parameters compatible to a TEDS system. In all scenarios tested, FBMC/OQAM was seen to perform similarly or better than CP-OFDM, with the exception of high SNR values, where, as it is typically the case, the performance of FBMC floors due to un-equalized residual intrinsic interference. Error floors were also observed in some of the CP-OFDM curves, due to the inadequacy of the employed CP (according to LTE) in highly dispersive channels. Albeit only tested in a time-invariant transmission scenario,

the WHT-based equalizers demonstrated considerable improvement over the classical ones. These results suggest that further investigation of such schemes, where the precoder could also be selected in an adaptive (e.g., channel-dependent) manner, is worthwhile. Adopting a simple channel tracking-based approach, with the equalizers being held fixed between two consecutive pilot multicarrier symbols, was shown to be quite effective in coping with demanding channels and robust to increased Doppler spread. Further research in this part will be directed towards a more extensive study of *sparsity-aware* channel tracking techniques for coping with channels of a very large delay spread and/or additional pilot formats, denser in the frequency axis, which could probably facilitate the task for such channels. In addition to the classical NLMS linear equalizer (and other equalizer structures and adaptive algorithms not reported here), a *sparsity-promoting* NLMS-type algorithm was extensively tested in the context of direct adaptive equalization of such systems. It was shown that the sparse adaptive filters are able to provide a significant performance gain over a conventional, sparsity-blind equalizer. Results favorable for FBMC/OQAM with the sparse algorithm were also obtained in the PMR (TEDS) scenarios, except for the particularly challenging case of a highly mobile GSM-HT channel, where all algorithms tested failed to provide satisfactory results. Difficulties in coping with HT channels have been already pointed out in earlier EMPhAtiC work, including the D3.1 deliverable. Possible ways to overcome these challenges include employing a denser pilot configuration, enhancing the adaptive algorithm by incorporating the *group sparsity* characteristic found in this type of channels and/or using more effective means of coping with the intrinsic interference, that would better take the double selectivity of the subchannels into account. It must be emphasized that only a very short (much shorter than required in the EMPhAtiC milestone MS4) preamble was considered for initializing the equalizers. A seemingly promising alternative approach could be to combine channel tracking (as in case (b)) with direct adaptive equalization (as in case (c)), with the equalizers being (re-)initialized on the basis of updated channel estimates. Such an approach has been recently successfully adopted in the EMPhAtiC deliverable D4.2, for adaptive MIMO-FBMC/OQAM DFE equalization.

While SIC has been demonstrated to possess sufficient statistics and to be a viable alternative to the complex-domain non-linear MAP and/or MLSE methods, the potentials that naturally arise from the essentially redundant quadrature components and the fact that noise samples at the output of receiver filters are correlated have not been demonstrated clearly yet, and our work in this direction is to be continued.

A method of estimating the channel transfer function coefficients which overcomes the problem of intrinsic interference in the complex domain has been successfully elaborated in various forms of optimization and provides a more efficient method than those having been developed earlier. Optimum FBMC/OQAM channel estimation options have been developed and the obtained performance analyzed. This study did not take into account the complexity issues and it was focused on the case of low frequency selective channels. In terms of mean estimation error performance, the ITM estimator and the MLE one with Gaussian approximation offer the best performance, but their performance is still far from the simple OFDM-ZF estimator. Since the ITM estimator has to enumerate all the interference terms, MLE with Gaussian approximation is relatively less complicated. Nevertheless, since an exhaustive search within a one-dimensional grid is needed, the complexity of such an estimator is still high. The least complicated estimator is the “Real Part Forcing” (RPF) one.

Simulation results show that the BER performance of the RPF estimator is almost the same as OFDM-ZF performance when the channel is not highly selective (Ped-A channel model). However, RPF's performance is considerably degraded with highly selective channels.

The feasibility of carrier frequency offset compensation in the FC-FB framework has been confirmed at a preliminary stage. Very good CFO compensation performance was demonstrated for any CFO in the range of (–1, 0) subcarrier spacings. This method can be combined with the basic idea that CFOs of integer multiples of the subcarrier spacing can be compensated simply through the selection of FFT bins to the subcarrier weighting process. This combination makes it possible to compensate basically any CFO, with high quality and low computational complexity. This method is especially valuable for supporting frequency-domain multiplexing of different users' transmissions without the need for precise synchronization among them.

10. References

[1] D. S. Waldhauser, *Multicarrier systems based on filter banks*, Ph.D. dissertation, Aachen, 2009.

[2] A. Vahlin and N. Holte, "Optimal finite duration pulses for OFDM," *Communications, IEEE Transactions on*, vol. 44, no. 1, pp. 10–14, 1996. [Online]. Available: http://-ieeexplore.ieee.org/xpls/abs_all.jsp?arnumber=476088

[3] B. Hirosaki, "An analysis of automatic equalizers for orthogonally multiplexed QAM systems," *Communications, IEEE Transactions on*, vol. 28, no. 1, pp. 73–83, 1980. [Online]. Available: http://ieeexplore.ieee.org/xpls/abs_all.jsp?arnumber=1094576

[4] P. A. Bello and K. Pahlavan, "Adaptive equalization for SQPSK and SQPR over frequency selective microwave LOS channels," *Communications, IEEE Transactions on*, vol. 32, no. 5, pp. 609–615, 1984. [Online]. Available: http://ieeexplore.ieee.org/xpls/-abs_all.jsp?arnumber=1096100

[5] J. C. Tu, "Optimum MMSE equalization for staggered modulation," in *Signals, Systems and Computers, 1993. 1993 Conference Record of The Twenty-Seventh Asilomar Conference on*. IEEE, 1993, pp. 1401–1406. [Online]. Available: http://-ieeexplore.ieee.org/xpls/abs_all.jsp?arnumber=342310

[6] S. Nedic, "An unified approach to equalization and echo cancellation in OQAM-based multi-carrier data transmission," in *Global Telecommunications Conference, 1997. GLOBECOM'97., IEEE*, vol. 3. IEEE, 1997, pp. 1519–1523. [Online]. Available: http://-ieeexplore.ieee.org/xpls/abs_all.jsp?arnumber=644388

[7] S. Nedic and N. Popovic, "Per-bin DFE for advanced OQAM-based multi-carrier wireless data transmission systems," in *Broadband Communications, 2002. Access, Transmission, Networking. 2002 International Zurich Seminar on*. IEEE, 2002, pp. 38–1. [Online]. Available: http://ieeexplore.ieee.org/xpls/abs_all.jsp?arnumber=991781

[8] D. S. Waldhauser, L. G. Baltar, and J. Nossek, "MMSE subcarrier equalization for filter bank based multicarrier systems," in *Signal Processing Advances in Wireless Communications, 2008. SPAWC 2008. IEEE 9th Workshop on*. IEEE, 2008, pp. 525–529. [Online]. Available: http://ieeexplore.ieee.org/xpls/abs_all.jsp?arnumber=4641663

[9] T. Ihalainen, T. Hidalgo Stitz, M. Rinne, and M. Renfors, "Channel equalization in filter bank based multicarrier modulation for wireless communications," *EURASIP Journal on Advances in Signal Processing*, vol. 2007, 2006, article ID 49389.

[10] P. Chevalier and F. Pipon, "New insights into optimal widely linear array receivers for the demodulation of BPSK, MSK, and GMSK signals corrupted by noncircular interferences-application to SAIC," *Signal Processing, IEEE Transactions on*, vol. 54, no. 3, pp. 870–883, 2006. [Online]. Available: http://ieeexplore.ieee.org/xpls/-abs_all.jsp?arnumber=1597554

[11] K. K. Kuchi, "Generalization of widely linear filtering concepts for equalization and interference suppression in PAM/QAM systems," 2007. [Online]. Available: http://-dspace.uta.edu/handle/10106/71

[12] F. Sterle, D. Mattera, and L. Paura, “Two nonequivalent structures for widely-linear decision-feedback MMSE equalization over MIMO channels,” in *EUSIPCO 2006*, Florence, Italy, September 4–8, 2006.

[13] M. Lipardi, *Widely linear filtering in modern MIMO transceivers*, h.D. dissertation, Università degli Studi di Napoli Federico II, 2009. [Online]. Available: http://-www.fedoa.unina.it/3905/

[14] G. Cherubini, E. Eleftheriou, S. Oker, and J. M. Cioffi, “Filter bank modulation techniques for very high speed digital subscriber lines,” *Communications Magazine, IEEE*, vol. 38, no. 5, pp. 98–104, 2000. [Online]. Available: http://ieeexplore.ieee.org/-xpls/abs_all.jsp?arnumber=841832

[15] M. Nouri, V. Lottici, R. Reggiannini, D. Ball, and M. Rayne, “TEDS: A high speed digital mobile communication air interface for professional users,” *Vehicular Technology Magazine, IEEE*, vol. 1, no. 4, pp. 32–42, 2006. [Online]. Available: http://-ieeexplore.ieee.org/xpls/abs_all.jsp?arnumber=4149624

[16] B. Hirosaki, “A maximum likelihood receiver for an orthogonally multiplexed QAM system,” *Selected Areas in Communications, IEEE Journal on*, vol. 2, no. 5, pp. 757–764, 1984. [Online]. Available: http://ieeexplore.ieee.org/xpls/-abs_all.jsp?arnumber=1146108 b

[17] T. Wiegand and N. J. Fliege, “Equalizers for transmultiplexers in orthogonal multiple carrier data transmission,” in *Proc. EUSIPCO-1996*, Sept. 1996, pp. 10–13. [Online]. Available: http://link.springer.com/article/10.1007/BF03001048

[18] T. Hunziker and D. Dahlhaus, “Iterative detection for multicarrier transmission employing time-frequency concentrated pulses,” *Communications, IEEE Transactions on*, vol. 51, no. 4, pp. 641–651, 2003. [Online]. Available: http://ieeexplore.ieee.org/-xpls/abs_all.jsp?arnumber=1199290

[19] Z. Kollár, G. Péceli, and P. Horváth, “Iterative decision feedback equalization for FBMC systems,” in *Proceedings of IEEE First International Conference on Advances in Cognitive Radio,(COCORA 2011)*, 2011.

[20] G. Lin, L. Lundheim, and N. Holte, “On efficient equalization for OFDM/OQAM systems,” in *Proc. 10th International OFDM-Workshop*, Hamburg, Germany, 31 Aug. - 1 Sept. 2005.

[21] B. Mongol, T. Yamazato, H. Okada, and M. Katayama, “MIMO zero-forcing equalizer for BFDM/OQAM systems in the highly mobile environments.” in *GLOBECOM*, 2006.

[22] N. Holte, “MMSE equalization of OFDM/OQAM systems for channels with time and frequency dispersion,” in *Wireless Communications & Signal Processing, 2009. WCSP 2009. International Conference on*. IEEE, 2009, pp. 1–5. [Online]. Available: http://-ieeexplore.ieee.org/xpls/abs_all.jsp?arnumber=5371391

[23] G. Ndo, H. Lin, and P. Siohan, “FBMC/OQAM equalization: Exploiting the imaginary interference,” in *Personal Indoor and Mobile Radio Communications (PIMRC), 2012 IEEE 23rd International Symposium on*. IEEE, 2012, pp. 2359–2364. [Online]. Available: http://ieeexplore.ieee.org/xpls/abs_all.jsp?arnumber=6362751

[24] C. Faria da Rocha and M. G. Bellanger, “Sub-channel equalizer design based on geometric interpolation for FBMC/OQAM systems,” in *Circuits and Systems (ISCAS), 2011 IEEE International Symposium on*. IEEE, 2011, pp. 1279–1282. [Online]. Available: http://ieeexplore.ieee.org/xpls/abs_all.jsp?arnumber=5937804

[25] L. G. Baltar, D. S. Waldhauser, and J. A. Nossek, “MMSE subchannel decision feedback equalization for filter bank based multicarrier systems,” in *Circuits and Systems, 2009. ISCAS 2009. IEEE International Symposium on*. IEEE, 2009, pp. 2802–2805. [Online]. Available: http://ieeexplore.ieee.org/xpls/abs_all.jsp?arnumber=5118384

[26] A. Ikhlef and J. Louveaux, “An enhanced MMSE per subchannel equalizer for highly frequency selective channels for FBMC/OQAM systems,” in *Signal Processing Advances in Wireless Communications, 2009. SPAWC’09. IEEE 10th Workshop on*. IEEE, 2009, pp. 186–190. [Online]. Available: http://ieeexplore.ieee.org/xpls/-abs_all.jsp?arnumber=5161772

[27] L. G. Baltar, A. Mezghani, and J. A. Nossek, “MLSE and MMSE subchannel equalization for filter bank based multicarrier systems: Coded and uncoded results,” in *Proceedings of the 18th European Signal Processing Conference (EUSIPCO-2010), Aalborg, Denmark*, 2010, pp. 2186–2190.

[28] R. Nour, P. Pedrosa, J. Louveaux, and F. Horlin, “Frequency selective channel equalization for filter bank multi-carriers modulation,” in *Proc. WICSP-2011*, Brussels, Belgium, 10-11 May 2011.

[29] D. S. Waldhauser, L. G. Baltar, and J. A. Nossek, “Adaptive equalization for filter bank based multicarrier systems,” in *Circuits and Systems, 2008. ISCAS 2008. IEEE International Symposium on*. IEEE, 2008, pp. 3098–3101. [Online]. Available: http://-ieeexplore.ieee.org/xpls/abs_all.jsp?arnumber=4542113

[30] ——, “Adaptive decision feedback equalization for filter bank based multicarrier systems,” in *Circuits and Systems, 2009. ISCAS 2009. IEEE International Symposium on*. IEEE, 2009, pp. 2794–2797. [Online]. Available: http://ieeexplore.ieee.org/xpls/-abs_all.jsp?arnumber=5118382

[31] M. Al Tarayrah and Q. A. Al-Haija, “LMS-based equalization in filter bank multicarrier wireless communication systems,” in *The International Conference on Digital Information Processing, E-Business and Cloud Computing (DIPECC2013)*. The Society of Digital Information and Wireless Communication, 2013, pp. 87–93. [Online]. Available: http://sdiwc.net/digital-library/lmsbased-equalization-in-filter-bank-multicarrier-wireless-communication-systems

[32] Z. Dlugaszewski and K. Wesolowski, “WHT/OFDM-an improved OFDM transmission method for selective fading channels,” in *Proc. Symposium on Communications and Vehicular Technology*, vol. 19, Leuven, Belgium, 19 Oct. 2000, pp. 144–149.

[33] M. Al-Attraqchi, S. Boussakta, and S. Le Goff, “An enhanced OFDM/OQAM system exploiting Walsh-Hadamard transform,” in *Vehicular Technology Conference (VTC Spring), 2011 IEEE 73rd*. IEEE, 2011, pp. 1–5. [Online]. Available: http://-ieeexplore.ieee.org/xpls/abs_all.jsp?arnumber=5956311

[34] M. Najar, “MIMO techniques and beamforming, deliverable 4.2,” FP7-ICT PHYDYAS-PHYsical layer for DYnamic AccesS and cognitive radio, Tech. Rep., 2010. [Online]. Available: http://www.ict-phydyas.org/delivrables/PHYDYAS-D4-2.pdf/view

[35] S. Cotter and B. Rao, “The adaptive matching pursuit algorithm for estimation and equalization of sparse time-varying channels,” in *Signals, Systems and Computers, 2000. Conference Record of the Thirty-Fourth Asilomar Conference on*, vol. 2. IEEE, 2000, pp. 1772–1776. [Online]. Available: http://ieeexplore.ieee.org/xpls/-abs_all.jsp?arnumber=911292

[36] S. F. Cotter and B. Rao, “Matching pursuit based decision-feedback equalizers,” in *Acoustics, Speech, and Signal Processing, 2000. ICASSP’00. Proceedings. 2000 IEEE International Conference on*, vol. 5. IEEE, 2000, pp. 2713–2716. [Online]. Available: http://ieeexplore.ieee.org/xpls/abs_all.jsp?arnumber=861049

[37] M. Belotserkovsky, “An equalizer initialization algorithm for OFDM receivers,” in *International conference on consumer electronics*, 2002, pp. 372–373. [Online]. Available: http://cat.inist.fr/?aModele=afficheN&cpsidt=15670053

[38] J. Siew, R. Piechocki, A. Nix, and S. Armour, “A channel estimation method for MIMO-OFDM systems,” in *Proc. London Communications Symp. 2002-UCL*, 9-10 Sept. 2002, pp. 101–104.

[39] M. Soltanolkotabi, M. Soltanalian, A. Amini, and F. Marvasti, “A practical sparse channel estimation for current ofdm standards,” in *Telecommunications, 2009. ICT’09. International Conference on*. IEEE, May 2009, pp. 217–222. [Online]. Available: http://-ieeexplore.ieee.org/xpls/abs_all.jsp?arnumber=5158647

[40] E. Vlachos, A. S. Lalos, and K. Berberidis, “Stochastic gradient pursuit for adaptive equalization of sparse multipath channels,” *Emerging and Selected Topics in Circuits and Systems, IEEE Journal on*, vol. 2, no. 3, pp. 413–423, 2012. [Online]. Available: http://ieeexplore.ieee.org/xpls/abs_all.jsp?arnumber=6303838

[41] K. Pelekanakis and M. Chitre, “Comparison of sparse adaptive filters for underwater acoustic channel equalization/estimation,” in *Communication Systems (ICCS), 2010 IEEE International Conference on*. IEEE, 2010, pp. 395–399. [Online]. Available: http://-ieeexplore.ieee.org/xpls/abs_all.jsp?arnumber=5686514

[42] S. L. Gay and S. C. Douglas, “Normalized natural gradient adaptive filtering for sparse and non-sparse systems,” in *Acoustics, Speech, and Signal Processing (ICASSP), 2002 IEEE International Conference on*, vol. 2. IEEE, 2002, pp. II–1405. [Online]. Available: http://ieeexplore.ieee.org/xpls/abs_all.jsp?arnumber=5745815

[43] K. Pelekanakis and M. Chitre, “New sparse adaptive algorithms based on the natural gradient and the L_0 norm,” *Oceanic Engineering, IEEE Journal of*, vol. 38, no. 2, pp. 323–332, 2013. b

[44] M. Nouri, D. Ball, M. Rayne, V. Lottici, R. Reggiannini, and M. Carta, “TEDS: a high speed digital mobile communication air interface for professional users part I: Overview of physical layer,” in *Vehicular Technology Conference, 2007. VTC2007-Spring. IEEE 65th*. IEEE, 2007, pp. 959–963. [Online]. Available: http://-ieeexplore.ieee.org/xpls/abs_all.jsp?arnumber=4212634

[45] M. Aoude, R. Vallet, and S. Nedic, “Interference cancellation in coded OFDM/OQAM,” in *Wireless Communication Systems (ISWCS), 2012 International Symposium on*. IEEE, 2012, pp. 181–185. [Online]. Available: http://ieeexplore.ieee.org/xpls/-abs_all.jsp?arnumber=6328354

[46] A. Duel-Hallen and C. Heegard, “Delayed decision-feedback sequence estimation,” *IEEE Transactions on Communications*, vol. 37, pp. 428–436, 1989. [Online]. Available: http://adsabs.harvard.edu/abs/1989ITCom.37.428D

[47] S. Nedic, “MLSE decoding of PRS type inter-bin interference in receiver-end windowed DMT system,” US Patent 7,058,141, Jun. 6, 2006. [Online]. Available: http://-www.google.com/patents/US7058141

[48] H. Kobayashi, “Correlative level coding and maximum-likelihood decoding,” *Information Theory, IEEE Transactions on*, vol. 17, no. 5, pp. 586–594, 1971. [Online]. Available: http://ieeexplore.ieee.org/xpls/abs_all.jsp?arnumber=1054689

[49] T. H. Stitz, T. Ihalainen, A. Viholainen, M. Renfors, and P. Siohan, “Pilot-based synchronization and equalization in filter bank multicarrier communications,” *EURASIP Journal on Advances in Signal Processing*, vol. 2010, p. 45, 2009, article ID 741429.

[50] M. Makundi, T. I. Laakso, and A. Hjørungnes, “Generalized symbol synchronization using variable IIR and FIR fractional-delay filters with arbitrary oversampling ratios,” in *Proc. IEEE ICASSP’04*, vol. 2, 2004, pp. 17–21.

[51] J.-W. Kim, Y.-J. Won, J.-W. Suh, and B.-S. Seo, “Adaptive carrier frequency offset compensation for OFDMA systems,” in *Instrumentation and Measurement Technology Conference (I2MTC), 2012 IEEE International*. Graz, Austria: IEEE, May 2012, pp. 2212–2215. [Online]. Available: http://ieeexplore.ieee.org/xpls/-abs_all.jsp?arnumber=6229693

[52] M. Aldababseh and A. Jamoos, “Estimation of FBMC/OQAM fading channels using dual Kalman filters,” *The Scientific World Journal*, Jan. 2014.

[53] J.-P. Javaudin, D. Lacroix, A. Rouxel, "Pilot-aided channel estimation for OFDM/OQAM," *Vehicular Technology Conference, 2003. VTC 2003-Spring. The 57th IEEE Semiannual* , vol.3, no., pp. 1581-1585, vol. 3, 22-25 April 2003.

Glossary and Definitions

Acronym	Meaning
AFB	Analysis Filter Bank
AWGN	Additive White Gaussian Noise
BER	Bit Error Rate
CFO	Carrier Frequency Offset
CFR	Channel Frequency Response
CIR	Channel Impulse Response
CP	Cyclic Prefix
DFE	Decision Feedback Equalizer
DMRS	De-Modulation Reference Signals
DWHT	Discrete WHT
FBMC/OQAM	Filter Bank Multi-Carrier based on OQAM
FBF	Feed-Back Filter
FFF	Feed-Forward Filter
FFT	Fast Fourier Transform
FEC	Forward Error Correction
FIR	Finite Impulse Response
FMT	Filtered Multi-Tone
GMSK	Gaussian Minimum Shift Keying
ICI	Inter-Carrier Interference
IPNLMS	Improved Proportionate NLMS
ISI	Inter-Symbol Interference
ITU	International Telecommunications Union
ITM	Individual Term Maximization
LE	Linear Equalizer
LLR	Log-Likelihood Ratio
LMS	Least Mean Squares
LTE	Long Term Evolution
MAP	Maximum A Posteriori
MF	Matched Filtering
MLSE	Maximum Likely-hood Sequence Estimation
MMSE	Minimum Mean Squared Error
NBI	Narrow-Band Interference

Acronym	Meaning
(N)LMS	(Normalized) Least Mean Squares
OFDM	Orthogonal Frequency Division Multiplexing
OMP	Orthogonal Matching Pursuit
OQAM	Offset Quadrature Amplitude Modulation
PAM	Pulse Amplitude Modulations
PMR	Professional Mobile Radio
QPSK	Quadrature Phase-Shift Keying
RLS	Recursive Least Squares
RPF	Real Part Forcing
SFB	Synthesis Filter Bank
SIC	Successive self-Interference Cancellation
SIR	Signal-to-Interference Ratio
SNR	Signal-to-Noise Ratio
TEDS	TETRA Enhanced Data Service
TLO	Time-Limited Orthogonal
WLF	Widely Linear Filtering
WHT	Walsh-Hadamard Transform
ZF	Zero Forcing
3GPP	3rd-Generation Partnership Programme